AEDC-TR-71-61

ELECTRON BEAM PROBE FOR A LOW DENSITY HYPERSONIC WIND TUNNEL

W. D. Williams, J. O. Hornkohl, and J. W. L. Lewis
ARO, Inc.

July 1971

VON KÁRMÁN GAS DYNAMICS FACILITY
ARNOLD ENGINEERING DEVELOPMENT CENTER
AIR FORCE SYSTEMS COMMAND
ARNOLD AIR FORCE STATION, TENNESSEE

NOTICES

When U. S. Government drawings specifications, or other data are used for any purpose other than a definitely related Government procurement operation, the Government thereby incurs no responsibility nor any obligation whatsoever, and the fact that the Government may have formulated, furnished, or in any way supplied the said drawings, specifications, or other data, is not to be regarded by implication or otherwise, or in any manner licensing the holder or any other person or corporation, or conveying any rights or permission to manufacture, use, or sell any patented invention that may in any way be related thereto.

Qualified users may obtain copies of this report from the Defense Documentation Center.

References to named commercial products in this report are not to be considered in any sense as an endorsement of the product by the United States Air Force or the Government.

ELECTRON BEAM PROBE FOR A LOW DENSITY HYPERSONIC WIND TUNNEL

W. D. Williams, J. O. Hornkohl, and J. W. L. Lewis
ARO, Inc.

FOREWORD

The work reported herein was sponsored by the Arnold Engineering Development Center (AEDC), Air Force Systems Command (AFSC), Arnold Air Force Station, Tennessee, under Program Element 64719F.

The results of research presented were obtained by ARO, Inc. (a subsidiary of Sverdrup & Parcel and Associates, Inc.), contract operator of AEDC, AFSC, under Contract F40600-72-C-0003. The work was conducted under ARO Project No. VM5915 from December 1, 1968, to June 30, 1969, and under ARO Project No. VM5068 from April 1 to June 30, 1970. The manuscript was submitted for publication on November 12, 1970.

Sincere thanks are due J. L. Potter for his most helpful discussions of the aerodynamic considerations of the investigated flow fields and his support of this experimental study, A. D. Killian for his invaluable technical skill, and R. F. Armstrong and R. L. Beavers for their operation of Tunnels L and M.

This technical report has been reviewed and is approved.

William G. Moretti, Jr.
Major, USAF
Research and Development Division
Directorate of Technology

Harry L. Maynard
Colonel, USAF
Director of Technology

ABSTRACT

The purpose of the experiments and calculations reported herein was to use the electron beam technique for rotational and vibrational temperature and density measurements in the free stream of low density, hypersonic flows of nitrogen. Beam energy was varied from 10 to 20 kev with currents of 1.0 to 4.0 ma. Free-stream rotational temperatures were in the range from 30 to 200°K, and vibrational temperatures varied from 300 to 3100°K, and free-stream densities were on the order of 10^{-8} to 10^{-7} gm/cm^3. The variation in the flow parameters was obtained through the use of four different nozzles; each was operated at two different conditions. The electron beam was injected through the flow, and the resulting spontaneous emission of light was spectroscopically analyzed. Light intensity measurements were made photoelectrically, and signal amplification and averaging were accomplished with a lock-in amplifier. Vibrational band intensities were measured by electronic integration of the rotational line structure. The results of the rotational temperature measurements are in good agreement with the free-stream temperature values predicted on the basis of conventional aerodynamic calibration except for the case of the Tunnel L 10 N_2 nozzle for which there is an approximately 24-percent discrepancey. Measured values of gas density are within 15 percent of the theoretical predictions, and the results of vibrational temperature determinations are consistently on the order of 10 percent higher than the expected values.

CONTENTS

APPENDIXES

I. ILLUSTRATIONS

Figure

NOMENCLATURE

B_o	Rotational constant corresponding to the $v_1' = 0$ vibrational level
c	Speed of light
d*	Throat diameter of nozzle
ERTP	Nitrogen (N_2) density expressed in pressure units for a temperature of 298°K
$(G)_o$	Muntz G-factor
$G(v_1'')$	Term value for the v_1'' vibrational level
H_o	Reservoir and total enthalpy
h	Planck's constant
$I_{v', K'}$ $v_2'', K'-1$	Intensity of radiation from the v', K' to the v_2'', K' -1 transition
$I(v', v_2'')$	Intensity of radiation from the v' to v_2'' transition

K'	Rotational quantum number of N_2^+ B $^2\Sigma$ state
$\bar{K}$	Quenching rate constant
k	Boltzmann constant
M_∞	Mach number
$\dot{m}_1$, $\dot{m}_2$	Mass flow rate
N_O, N_T	Nitrogen molecule number density
$N_2^+ [1^-]$	First negative system of nitrogen
$N_2 [2^+]$	Second positive system of nitrogen
N_2^+ B $^2\Sigma$	Upper electronic state of nitrogen ion
N_2^+ X $^2\Sigma$	Ground state of nitrogen ion
N_2 X $^1\Sigma$	Ground state of nitrogen molecule
p_o	Stagnation pressure
p_T	Test cabin pressure
p'_o	Impact pressure
p*	Sonic pressure
p_∞	Free-stream pressure
$p(v', v_2'')$	Vibrational strength factor of the v' to v_2'' transition
$p(v', v_1'')$	Vibrational strength factor of the v_1'' to v' transition
$(p.f.)_v$	Partition function for vibrational mode
$q(v', v_1'')$	Franck-Condon factor for the v_1'' to v' transition
q_∞	Dynamic pressure
Re_∞	Unit Reynolds number
$R_e(\bar{r}_{v',v''})$	Electronic transition moment
$\bar{r}(v', v'')$	Matrix element of internuclear distance
T_o	Stagnation temperature
T*	Sonic temperature
T_∞	Free-stream temperature
T_R	Rotational temperature

T_v	Vibrational temperature
$\frac{\bar{T}_R}{T_\infty}$	Weighted average of T_R/T_∞
U_∞	Free-stream velocity
v_1''	Vibrational quantum number referring to a vibrational level of the N_2 X $^1\Sigma$
v_2''	Vibrational quantum number referring to a vibrational level of the N_2^+ X $^2\Sigma$
v'	Vibrational quantum number referring to a vibrational level of the N_2^+ B $^2\Sigma$ state
(v', v_2'')	Vibrational band designation
w_i	Square of the normalized standard deviation
x	$K'(K' + 1)$
x'	Distance downstream from nozzle exit
λ	Wavelength
$\lambda_{v', K' \; v_2'', K' - 1}$	Wavelength of v', K' to v_2'', $K' - 1$ emission
λ'	Mean free path
γ	Ratio of specific heats
ρ_∞	Free-stream density
σ_i	Standard deviation of measured rotational temperature for the ith spectral scan
$\tau_{v'}$	Radiative lifetime of v' level

SECTION I
INTRODUCTION

1.1 TUNNEL DESCRIPTIONS

Low Density Hypersonic Wind Tunnels (L) and (M) are continuous flow, low density, hypervelocity wind tunnels (Figs. 1 and 2, Appendix I), and thorough descriptions of these facilities are contained in Refs. 1 and 2. Briefly, each tunnel consists of a direct-current electric arc heater, a stilling chamber, an expansion nozzle, a test section with probe traversing mechanism, a vacuum pumping system, and necessary instrumentation. Tunnel L may also be operated in a cold-flow condition, i. e., without the arc heater. Normal tunnel operating conditions of the two tunnels are within the following ranges:

Parameter	Engineering Units (U. S.)	MKS Units
Working fluid	Nitrogen (N_2)	---
Total temperature	540 to 7200°R	300 to 4000°K
Mach number	4 to 18	---
Stagnation enthalpy	130 to 2140 Btu/lbm	72 to 1189 kgm cal/kgm
Velocity	2000 to 8500 ft/sec	610 to 2590 m/s
Static pressure	0.006 to 0.095 torr	---
Static density	3×10^{-6} to 4×10^{-5} lbm/ft^3	4.8×10^{-5} to 6.4×10^{-4} kgm/m^3
Unit Reynolds number	40 to 200 per in.	1575 to 7874/m
Diameter of uniform core	0.5 to 10 in.	0.0125 to 0.254 m

Both tunnels are facilities for investigating the simulation of flight at extreme altitudes and are able to provide aerodynamic coefficients for lifting and ballistic bodies in the hypersonic, cold-wall condition at simulated altitudes above 300,000 ft.

1.2 GENERAL EXPLANATION OF THE ELECTRON BEAM TECHNIQUE

A method for directly measuring nitrogen rotational and vibrational temperatures and number density in wind tunnel flows is the electron

beam technique pioneered by E. P. Muntz (Refs. 3, 4, 5, and 6). This technique involves the ionization and excitation of nitrogen molecules with a beam of moderately energetic electrons (10 to 100 kev). The resulting spontaneous emission in the spectral region from 3500 to 5000 Å at low nitrogen density is predominately that of the first negative system of nitrogen ($N_2^+ [1^-]$). The intensity distribution of this system's vibrational bands can be related to an effective vibrational temperature of nitrogen, and the rotational structure of the vibrational bands has an intensity distribution that can be related to an effective rotational temperature of nitrogen. Additionally, the intensity of any one vibrational band can be related to the density of nitrogen molecules.

At low gas densities the beam is spatially well defined; therefore, observation of emission at different positions along the beam allows point temperature measurements.

By photoelectric, spectroscopic measurement of the rotational line intensities of a vibrational band, a rotational temperature can be determined. Vibrational band intensities can be measured by electronic integration of the rotational line intensities of a vibrational band. Usually the intensities of two bands are used to form a ratio which can be compared to a theoretical prediction of the ratio versus vibrational temperature.

For the density range of interest the intensity of a vibrational band is a linear function of density. Therefore, determination of the intensity of a vibrational band at some unknown density relative to the intensity at a condition of known density and temperature allows the gas density to be determined provided the vibrational temperature is known.

SECTION II
TUNNEL INSTRUMENTATION AND OPERATING PROCEDURE

2.1 INSTRUMENTATION

Figure 3 indicates the measurements that were necessary to ensure that proper flow conditions were obtained in the tunnels. Mass flow rates $\dot{m}_1$ and $\dot{m}_2$ were obtained from pressure readings from P^2B transducers. The input temperature of the nitrogen flow (TC_1) was obtained from a copper-constantan thermocouple reading. The stilling chamber pressure (p_o) was read using a P^2B transducer. Centerline impact pressure (p_o') was monitored with a ±0.15 psid transducer in Tunnel L and with a 30-mm Baratron® pressure gage in

Tunnel M. Normally the stagnation probe was at a position of 1.5 in. from the nozzle exit in Tunnel L and 14.25 in. from the nozzle exit in Tunnel M. The test cabin ambient pressure of Tunnel L was monitored with the ±0.15 psid transducer and with an Equibar® pressure gage; that of Tunnel M was monitored with a 3-mm Baratron pressure gage. Arc heater current, I, and voltage, E, were monitored with standard meters. More detailed discussion of the tunnel instrumentation may be found in Ref. 2.

2.2 OPERATING PROCEDURE

Before beginning each tunnel operation the pressure transducer readouts and amplifiers were balanced, and for Tunnel L the ±0.15 psid transducer was calibrated over the range of expected p_o' and p_T values using a micromanometer to read the calibration pressure. Mass flow rates $\dot{m}_1$ and $\dot{m}_2$ were then set to the required values and p_o, TC_1, $\dot{m}_1$, and $\dot{m}_2$ were read.

For arc-heated flow the heater was then started, and the power setting adjusted to obtain the required p_o. Values of E, I, p_o', and p_T were then read to ensure proper flow conditions.

SECTION III
ELECTRON BEAM SYSTEMS

3.1 VACUUM SYSTEM

In order to inject the electron beam, emitted by the electron gun at a pressure of less than 1.0×10^{-4} torr, into the higher free-stream pressures of both tunnels, a dynamic pumping system was used. Schematic diagrams of the system are shown in Figs. 4, 5, and 6. The system consisted of a 4-in. oil diffusion pump with a blank-off speed of approximately 700 liters/sec and a mechanical forepump with a maximum pumping speed of 140 liters/min. An additional mechanical pump with 70-liters/min pumping speed was used for rough-pumping the system. The electron gun section was separated by an orifice from the tunnel free stream into which the beam was injected. The orifice diameter was nominally 0.040 in. and the orifice length was 0.25 in. Pressures in the electron gun section were normally maintained by this system at less than 2×10^{-5} torr as measured with an ion gage.

As shown in Figs. 5 and 6 the electron gun was mounted in a housing inside the tunnel test cabin. Atmospheric pressure was always maintained inside the gun housing to prevent high voltage arcing. The gun housing was bolted to a traversing mechanism that allowed axial positioning of the electron beam along the tunnel free stream. In order to prevent accidental overpressuring of the electron gun which would shorten considerably the gun lifetime, an electrically operated, pneumatic gate valve was included between the orifice and the electron gun.

3.2 ELECTRON GUN AND RECEIVER CUP

The electron guns were television-type, oxide cathode models modified for a maximum of 50-kv operation. The accelerator grid of these guns was also modified by having its opening enlarged to 3/16-in. diameter. Magnetic focusing and deflection were used and the filament was battery powered at 6 to 18 v.

The electron gun high voltage power supply provided 0 to 50 kv, 0.01-percent ripple voltage, at 0 to 5 ma. The high voltage supplied to the guns was always negative with respect to the anode which was at ground potential.

The electron gun system was capable of injecting up to a 4.5-ma beam at 10 to 30 kv across the tunnel free stream to a beam receiver. The electron beam receiver cup for Tunnel L is shown in Fig. 7. Basically it was a 12-in. length of 1-3/4-in.-diam, water-cooled, stainless steel tubing capped with a stainless steel plate. The double grid structure added another inch to the cup. The grids were 1/16-in. mesh made of 0.02-in.-diam brass wire. The entrance diameter of both grids was 1 in.

The interior, or second, grid was negatively biased at 25 to 30 v to prevent the ejected secondary electrons from leaving the cup interior, which was carbon coated. The outer grid and cup are electrically connected, and the entire cup was electrically isolated from the tunnel floor by two sheets of Mylar® film.

Beam current measurement in Tunnel M presented more of a problem. A receiver cup of the type used in Tunnel L would have its entrance 3-1/2 ft from the orifice, which presented the problem of collecting the entire beam. For vibrational and rotational temperature measurements a precise value of the current is unimportant, and, for all temperature data, was a nominal value as registered by an aluminum flat-plate collector of approximate dimensions 12 by 18 in. located on

the tunnel floor, approximately 4 ft from the orifice. The accuracy of such a measurement is indeed questionable because of both boundary layer and secondary ejected electron effects; however, the value of current was constantly monitored to ensure minimum current fluctuations and drift, thereby decreasing the imprecision of the temperature measurements. As shown later, knowledge of the value of the beam current is critical for an accurate density measurement, and for that reason it was deemed essential that an additional current measurement be made in Tunnel M, specifically at the point of injection of the beam into the flow, thereby minimizing the errors attributable to beam spreading. To do this a collector was mounted onto a traversing mechanism. Before obtaining an absolute density data point, this collector was traversed axially until it was located directly beneath the gun orifice (Fig. 6). The current at the injection point was measured, and the auxiliary collector was withdrawn to allow the electron beam to traverse the tunnel flow. Figure 8 is a photograph of the auxiliary collector which was constructed of a 2-in. copper elbow with a reflecting plane attached to give an effective increase in the length-to-diameter ratio, thereby minimizing the loss of ejected secondary electrons. The location of this current measurement point was approximately 24 in. above the tunnel centerline. The individual values of current from each of the two collectors in Tunnel M were read from a digital voltmeter.

3.3 SPECTROSCOPIC INSTRUMENTATION

Schematic drawings of the spectrometer setups for Tunnels L and M are shown in Figs. 9 and 10, respectively. In the Tunnel L setup a 14-in.-focal length lens focused the optical radiation produced as a result of electron beam excitation onto the spectrometer slit. The f/numbers of the lens and spectrometer were matched at f/8.7. When band integration measurements were made, a dove prism was placed between the lens and spectrometer slit to rotate the beam image perpendicular to the entrance slit. A chopping disk was located near the entrance slit for modulating the light input at 400 Hz. For the Tunnel M setup the optical radiation was gathered by an f/12, 48-in.-focal length lens, and the chopping disk operated at 340 Hz.

The spectrometer for both setups was a 1-meter Jarrell-Ash Czerny-Turner combination scanning spectrometer-spectrograph. The 102- by 102-mm diffraction grating used had 1180 grooves/mm and was blazed at 5000 Å. With a 20-micron slit width the resolution in the first order was 0.29 Å, which, although by no means the maximum attainable

resolution, was sufficient for resolution of the R-branch lines for most of the prominent N_2^+ [1⁻] bands. Scanning speeds were 2.5 Å/min for rotational spectra and 25 Å/min for vibrational band integration.

A photomultiplier tube mounted at the exit slit of the spectrometer was used as the detection element. The photo-cathode voltage applied to the tube was normally -1700 vdc, and a load resistance of 500 kilohms was used on the photomultiplier output; output signals were processed by a lock-in amplifier. For the Tunnel L system the reference signal to the lock-in amplifier was provided by a small 6-v light bulb and photomultiplier tube. For the Tunnel M system the reference signal to the lock-in amplifier was supplied by the 340-Hz chopping wheel assembly.

In both tunnels the output of the lock-in amplifier was recorded by a strip-chart recorder for rotational spectra scans. In Tunnel L for band intensity measurements the output of the lock-in amplifier was fed to an active electronic integrator (Fig. 11) with an accuracy of ±1 percent provided the integration time was no longer than about 200 sec. The integrator output was recorded by the strip-chart recorder. In Tunnel M the lock-in amplifier output was fed to a different integrator (Fig. 12) with the output displayed on a digital voltmeter. Because the amplifier of the Tunnel M integrator had a factor of 300 increase in gain and a factor of 100 drift decrease, the Tunnel M integrator was more accurate than the one used in Tunnel L.

The relative sensitivity of the optical systems as a function of wavelength was measured using a calibrated, tungsten-strip standard lamp. Sensitivity curves for the optical systems are shown in Figs. 13 and 14.

Because of the small uniform flow core diameter in Tunnel L, radial scanning of the flow field was not performed, and all measurements were made on the free-stream centerline. Optical alignment was accomplished by positioning a small light source on the tunnel centerline at the desired axial position and focusing the light source image onto the spectrometer slit. In Tunnel M radial scanning was performed by mounting the lens and spectrometer on a welding table which was capable of being raised or lowered, thus moving the spectrometer and optics system along the radial direction of the beam. To ensure that the electron beam intersected the tunnel centerline, an object was located on the centerline and focused into view using a leveling telescope on the side of the tunnel opposite to the spectrometer (Fig. 10). A plumb bob was then suspended from the electron beam orifice, and the beam mount was rotated until the plumb bob intersected the centerline, which was indicated by the image in the level. The lens was then adjusted until

the entrance slit of the spectrometer came into focus with the level, and at that point it was certain that (1) neglecting magnetic field effects which were small, the electron beam intersected the centerline, and (2) the spectrometer entrance slit was focused onto the beam. The radial position of observation was determined by mounting a scale on the spectrometer table; using the level, a centerline reference position was determined on the scale, which had a 1-mm least count, and the table was raised until, as observed through the level, a change of position of predetermined magnitude had occurred. After the magnetic field coil was turned on during tunnel operation, a final optimizing adjustment of the axial and angular position of the beam was required, but the change was always small and did not require refocusing; both tunnels required this adjustment.

SECTION IV
ELECTRON BEAM TECHNIQUE

4.1 INTENSITY EQUATIONS

On the basis of Muntz's excitation theory the intensity equation for the rotational lines in the R branch of a $N_2^+ [1^-]$ system vibrational band excited by an electron beam may be written as

$$\ell n \left(\frac{I_{v',K'} \quad \lambda^4_{v',K'}}{v''_2, K'-1 \quad v''_2, K'-1} \right) = -B_o K'(K'+1) \frac{hc}{kT_R} + \text{constant} \qquad (1)$$

in which

$$(G)_o = \frac{(K'+1)e^{-2B_oK'(K'+1)hc/kT_R} + (K')e^{+2B_oK'hc/kT_R}}{2K'+1} \qquad (2)$$

Collisional deexcitation effects on rotational line intensity have been neglected in the development of Eq. (1). Furthermore, it has been assumed that the vibrational temperature, T_V, is sufficiently low to allow the neglect of all ground electronic state vibrational levels except the lowest ($v_1'' = 0$).

For the density range of both tunnels the first assumption should be valid, but the second assumption is not strictly valid under the high vibrational temperature conditions of both tunnels. However, calculations have shown that even for T_V = 3100°K the measured rotational temperature differs by only -2 to -3°K over the T_R range from

50 to 300°K from those values of T_R obtained assuming T_V = 500°K or less, thereby justifying the neglect of T_V effects on T_R measurements.

As shown in Ref. 7 the intensity of a vibrational band is

$$I_{(v',v_2'')} = \frac{(\text{const.})\, N_T}{(\text{p.f.})_v} \frac{p(v',v_2'')}{\lambda^4_{v',v_2''}} \frac{\sum_{v_1''=0}^{\infty} p(v_1'v_1'')e^{-G(v_1'')hc/kT_v}}{\sum_{v_2''=0}^{\infty} \frac{p(v',v_2'')}{\lambda^3_{v',v_2''}}} \tag{3}$$

Then the intensity ratio of two bands $(a_{v'}, b_{v_2^*})$ and $(c_{v'}, d_{v_2^*})$ is

$$\frac{I(a_{v'}, b_{v_2''})}{I(c_{v'}, d_{v_2''})} = \left(\frac{\lambda_{cd}}{\lambda_{ab}}\right)^4 \frac{p(a_{v'}, b_{v_2''})}{p(c_{v'}\, d_{v_2''})} \frac{\sum_{v_1''=0}^{\infty} p(a_{v'}, v_1'')e^{-G(v_1'')\, hc/kT_v}}{\sum_{v_1''=0}^{\infty} p(c_{v'}, v_1'')e^{-G(v_1'')hc/kT_V}}$$

$$\times \left[\frac{\sum_{v_2''=0}^{\infty} p(c_{v'}, v_2'')/\lambda^3_{c_{v'}, v_2''}}{\sum_{v_2''=0}^{\infty} p(a_{v'}, v_2'')/\lambda^3_{a_{v'}, v_2''}}\right] \tag{4}$$

Here again collisional deexcitation effects have been neglected.

4.2 ROTATIONAL TEMPERATURE MEASUREMENT

From a rotational spectral scan the peak heights of the spectral lines are measured and used as the relative intensity values of the rotational lines, $I^{v',K'}_{v_2^*,\ K'-1}$; using these values and the known values of $\lambda_{v',\ K'}$, Eq. (1) may be solved for rotational temperature by an
$v_2^*,\ K'-1$
iterative machine calculation. The program (Program TROT) for the computer is shown in Table I, Appendix II. The data deck requires input data cards for the following: spectral scan number and designation, total number of spectral lines in a scan, and the relative intensity value of each line. The intensities of even-numbered rotational lines (K' = 2, 4, ...) are doubled before input to account for the influence of nuclear spin statistics.

Letting

$$y = \ell n \left[\frac{I_{v',K'} \quad \lambda^4_{v',K'}}{v''_2,K'-1 \quad v''_2,K'-1} \right] \qquad (5)$$

$$K'(G)_o$$

and

$$x = K'(K' + 1) \qquad (6)$$

the machine calculation performs a least-squares fit of the y values to the straight line given by Eq. (1). As shown from Eq. (1) the slope of this straight line is hcB_o/kT_R; hence, a rotational temperature can be calculated from the slope of the straight line. A rotational temperature of 200°K is assumed for the calculation of $(G)_o$ in the first step of the iteration process, and a straight line is then fitted to the y values, the slope of which yields a new value of the rotational temperature. If this calculated value of rotational temperature is not within 0.01 percent of the assumed value of rotational temperature, the calculated value is used as the assumed value of rotational temperature for the calculation of a new set of $(G)_o$ values, and the least-squares fit of the intensity data according to Eq. (1) is repeated until the prescribed iteration accuracy of 0.01 percent is achieved.

As observed by Williams (Ref. 7) and Ashkenas (Ref. 8) only for temperatures near 200°K (pure nitrogen gas, equilibrium conditions) is the plot of y values versus $x = K'(K' + 1)$ a good straight line; that is, only with these restrictions is the temperature determined from the slope of the line not a function of the number of rotational lines used. For this reason a temperature $T_R(K_{max})$ defined by the maximum number of spectral lines (K_{max}) is first calculated by the iterative procedure described in the preceding paragraph. Then the entire process is repeated for $K'_{max}-1$ lines; and this gives another rotational temperature value $T_R(K'_{max}-1)$. This process is repeated i times through $K'_{max}-i+1 = 6$. Only if the variation of T_R with the number of rotational lines used is relatively small can a single, well-defined temperature be obtained. The standard deviation of the temperature is printed in °K for each $(K_{max}-i+1)$ data set. This value is computed using formulae from Beers (Ref. 9).

For a given tunnel condition four to six spectral scans are taken to comprise one temperature determination, and these scans are averaged within Program TROT. The output of this averaging process is presented as an average ratio of rotational temperature to predicted free-stream temperature ($\bar{T}_R/T_\infty$) and average standard deviation, $\bar{\sigma}$, for a

given value of the number of spectral lines used in calculating a T_R in a fixed set of data. Each individual value of T_R/T_∞ used in the calculation of the average value of $\overline{T}_R/T_\infty$ is weighted according to its standard deviation, σ, as given by

$$\frac{\overline{T}_R}{T_\infty} \equiv \overline{y} = \left(\sum_{i=1}^{s} \frac{y_i}{\sigma_i^2}\right) \Bigg/ \left(\sum_{i=1}^{s} \frac{1}{\sigma_i^2}\right) \tag{7}$$

which is by definition a weighted average (Ref. 9), where

$$\begin{aligned} \sigma_i &= \text{the standard deviation of the ith spectral scan} \\ y_i = \left(\frac{T_R}{T_\infty}\right)_i &= \text{the determined rotational temperature divided by the free-stream temperature for the ith spectral scan} \\ s &= \text{the number of spectral scans for a given tunnel condition (normally 4 to 6).} \end{aligned} \tag{8}$$

By definition (Ref. 9) the standard deviation of the average value of a set of experimental data is

$$\overline{\sigma} = \left[\left(\sum_{i=1}^{s} w_i^2 \sigma_i\right) \Bigg/ \left(\sum_{i=1}^{s} w_i\right)^2\right]^{1/2} \tag{9}$$

where

$$w_i = \left(\frac{\sigma_1}{\sigma_i}\right)^2 \tag{10}$$

It has been observed (Refs. 7 and 8) that the degree of nonlinearity of a Boltzmann plot of rotational line intensities and also the discrepancy between measured rotational temperature and known temperatures in laboratory conditions is a function of the density and temperature of the gas into which the electron beam is injected. Therefore, it is necessary to empirically correct the rotational temperature values determined from Program TROT, the magnitude of the empirical correction being density and temperature dependent, and this is accomplished through knowledge of the approximate density and temperature of the tunnel flow and from data from laboratory experiments.

4.3 VIBRATIONAL TEMPERATURE AND DENSITY MEASUREMENT

As shown in Ref. 10 the proper equation for the band intensity ratio of two vibrational bands neglecting quenching effects is Eq. (4).

As pointed out in Ref. 10 the last factor of Eq. (4) is identically equal to the ratio of the lifetimes of the $a_{v'}$ and $c_{v'}$ vibrational levels. Hence, Eq. (4) may be written

$$\frac{I(a_{v'}, b_{v_2''})}{I(c_{v'}, d_{v_2''})} = \left(\frac{\lambda_{cd}}{\lambda_{ab}}\right)^4 \left[\frac{p(a_{v'}, b_{v_2''})}{p(c_{v'}, d_{v_2''})}\right] \left(\frac{\tau_{a_{v'}}}{\tau_{c_{v'}}}\right) \frac{\sum_{v_1''=0}^{\infty} p(a_{v'}, v_1'')e^{-G(v_1'')hc/kT_v}}{\sum_{v_1''=0}^{\infty} p(c_{v'}, v_1'')e^{-G(v_1'')hc/kT_v}} \quad (11)$$

in which

$$p(v', v_2'') = q(v', v_2'') R_e^2[\bar{r}_{v'}, v_2''] \quad (12)$$

and

$$p(v', v_1'') = q(v', v_1'') R_e^2[\bar{r}_{v'}, v_1''] \quad (13)$$

Calculations by Hornkohl have yielded values for $q(v', v_2'')$ and $q(v', v_1'')$, and experimental data and calculations by Williams, Lewis, and Hornkohl have determined values of $p(v', v_2'')$. These parameters are listed in Tables II, III, and IV. The same experimental data also yielded values for $\tau_{v'=0}$, $\tau_{v'=1}$, $\tau_{v'=2}$ of 6.58×10^{-8}, 6.49×10^{-8}, and 6.43×10^{-8} sec, respectively. Since the values of $p(v', v_2'')$ are experimentally determined with concomitant errors it is considered prudent to minimize such errors by taking advantage of the fact that $\bar{r}_{a_{v'}, b_{v_2''}} = \bar{r}_{c_{v'}, d_{v_2''}}$ if a - b = c - d, thereby yielding $R_e^2(\bar{r}_{cd}) = R_e^2(\bar{r}_{ab})$, so that the ratio $p(a_{v'}, b_{v_2''})/p(c_{v'}, d_{v_2''})$ is determined predominantly by the ratio of calculable parameters $q(a_{v'}, b_{v_2''})/q(c_{v'}, d_{v_2''})$. Unfortunately, no work has been performed to determine excitation band strength parameters $p(v', v_1'')$, and one must resort to the usage of the set of excitation Franck-Condon factors $q(v', v_1'')$, thus producing a possible inaccuracy in using Eq. (11).

The intensity of vibrational band pairs is determined by electronically integrating the rotational structure of the vibrational bands; by comparing the experimental band intensity ratio to a plot of calculated band intensity ratio versus vibrational temperature, a vibrational temperature is determined. Plots of the most useful band intensity ratios versus T_v are given in Figs. 15 and 16.

It has been observed in Ref. 11 that the relationship of $N_2^+ [1^-]$ vibrational band relative intensity to nitrogen density (Eq. (3)) is linear up to a density of approximately 7.5×10^{-7} gm/cm^3 which includes the

density range of both Tunnels L and M. However, it can be seen from Eq. (3) that the relative intensity is also a strong function of vibrational temperature. Figures 17 and 18 show the relative intensity of a (0, i) band as a function of nitrogen density in terms of equivalent room temperature pressure (ERTP) and vibrational temperature. The nitrogen density measurements can therefore be made by electronically integrating a vibrational band intensity at the desired tunnel condition and comparing this to the integrated value at a known condition of pressure and temperature and correcting for vibrational temperature effects using the measured value of vibrational temperature.

SECTION V
EXPERIMENTS AND RESULTS

5.1 4 N_2 NOZZLE—TUNNEL L

The 4 N_2 nozzle is a cold flow nozzle operated at either of two fixed conditions, the flow parameters of which are listed below:

$M_\infty \approx 4$

Standard Condition	Off-Standard Condition
p_o = 0.0160 atm	p_o = 0.0184 atm
T_∞ = 67°K (120.6°R)	T_∞ = 66°K (118.8°R)
U_∞ = 678.2 m/sec (2225 ft/sec)	U_∞ = 679.7 m/sec (2230 ft/sec)
$\rho_\infty = 4.8 \times 10^{-7}$ gm/cm^3 (3.0×10^{-5} lbm/ft^3)	$\rho_\infty = 5.6 \times 10^{-7}$ gm/cm^3 (3.5×10^{-5} lbm/ft^3)
p_∞ = 0.075 torr	p_∞ = 0.092 torr
M_∞ = 4.05	M_∞ = 4.10
ERTP = 0.320 torr	ERTP = 0.371 torr

The foregoing conditions, and those presented as predicted or calibrated for other flows, are based on nozzle calibrations made with impact pressure probes, directly measured reservoir pressure, and total temperature derived both from nonequilibrium thermo-chemical-kinetic calculations and from measured total enthalpy of the test section flow. With p_o' and p_o determined, the ratio p_o'/p_o yields a Mach number, M_∞ for a particular gas. Then T_∞, p_∞, and ρ_∞ are calculated on the basis of p_o, T_o, and M_∞ using the same gas thermo-chemical- kinetic

model assumed in deriving M_∞ from p_0'/p_0. This model is a perfect gas for the $M_\infty = 4$ case. Thus, T_∞ and ρ_∞ are not directly measured in the gas-dynamic flow calibration, but their values should be reasonably certain at $M_\infty = 4$ because of the accuracy of p_0', p_0, and T_0 values and the rather strong basis for the assumption of a frozen ($\gamma = 1.400$) expansion. For the nozzle flows to be discussed later, the same could be said, except then it is possible that the flow does not freeze to a constant γ process until it reaches the nozzle throat. The freezing referred to concerns molecular vibration which is believed the only nonequilibrium mode in any case considered (Refs. 1 and 12).

If appreciable error exists, in the higher T_0 flows, the worst cases studied show that the values of T_∞ predicted from the standard nozzle calibrations may be low by as much as 30 or 40 percent, whereas the predicted values of ρ_∞ should be high by no more than 5 or 10 percent. These approximate maximum uncertainty levels are based on comparison of the listed T_∞ and ρ_∞ values with corresponding results which would have been calculated if full thermo-chemical-kinetic equilibrium had been assumed throughout the nozzles (cf., Ref. 1).

Beam measurements were made approximately 1 in. from the nozzle exit at $M_\infty = 4$. The length of the beam observed was approximately 0.25 in. in the radial direction centered on the flow core centerline, and the diameter of the flow core was approximately 1.25 in.

Two sets of six rotational line scans were made for each nozzle condition. A typical spectral scan is shown in Fig. 19, and the temperature results (calculated by Program TROT) are shown in Figs. 20 and 21. The variation of the measured T_R value with rotational quantum number and the discrepancy between the measured value and the predicted value were to be expected on the basis of the results in Refs. 7 and 8 (see Figs. 22 and 23). From Fig. 23 it is seen that a 13 to 20°K correction to the experimental data is needed when ten rotational lines are used in the T_R determination. From Figs. 20 and 21 this would yield T_R values from 60 to 67°K. For the case of 15 rotational lines used to determine T_R a 28 to 32°K correction must be made. From Figs. 20 and 21 this would yield values from 64 to 68°K. Therefore, reasonable agreement between measured and predicted T_R values was obtained from the data by taking into account effects of density and number of rotational lines used.

The nitrogen density measurements were made by electronically integrating the $N_2^+ [1^-] (0, 0)$ band intensity at the tunnel condition and comparing this to the integrated value at a static condition of 0.100 torr

and room temperature. The measured ρ_∞ values were 5.61×10^{-7} gm/cm^3 and 6.56×10^{-7} gm/cm^3 for the standard and off-standard conditions, respectively. The measured values are observed to be approximately 15 percent high, and this discrepancy may be the result of beam spreading effects at the collector cup since a beam of only 20 kv was used. It is felt that a repetition of those measurements using a beam energy from 50 to 100 kev would prevent significant beam spreading and might result in a smaller discrepancy in the density value.

For each nozzle flow a scan of the beam induced radiation was made from 3500 to 6000 Å to detect the presence of contaminative radiation which might affect the measurements. The 4 N_2 nozzle beam radiation scan is shown in Fig. 24, and it is shown that all significant radiation is attributable to excited or ionized nitrogen.

5.2 9 N_2 NOZZLE–TUNNEL L

The 9 N_2 nozzle, designed for arc-heated flow, is operated at either of two fixed conditions. The flow parameters which are listed below are also based on the calibration with aerodynamic probes as described in the previous section.

$M_\infty \approx 9$

Standard Condition	Off-Standard Condition
p_o = 2.04 atm	p_o = 1.70 atm
T_o = 2365°K (4257°R)	T_o = 1662°K (2992°R)
T_∞ = 135°K (243°R)	T_∞ = 93°K (167°R)
U_∞ = 2204 m/sec (7230 ft/sec)	U_∞ = 1844 m/sec (6050 ft/sec)
$\rho_\infty = 2.02 \times 10^{-7}$ gm/cm^3 (126×10^{-5} lbm/ft^3)	$\rho_\infty = 2.32 \times 10^{-7}$ gm/cm^3 (1.45×10^{-5} lbm/ft^3)
p_∞ = 0.0615 torr	p_∞ = 0.049 torr
M_∞ = 9.37	M_∞ = 9.30
ERTP = 0.134 torr	ERTP = 0.155 torr

Again, beam measurements were made approximately 1 in. from the nozzle exit. The diameter of the flow core was approximately 2.0 in. and a 0.25-in. beam length at the core centerline was observed.

Two sets of six rotational scans were made for each nozzle condition. Typical spectral scans are shown in Figs. 25 and 26. The results

(calculated by Program TROT) are shown in Figs. 27 and 28. On the basis of the laboratory data findings shown in Fig. 23 for 78°K data and Figs. 29 and 30 for 192°K data, a correction of 11 to 16°K would be necessary for the case of ten rotational lines used in the standard condition data and Fig. 27. This yields rotational temperatures from 140 to 145°K. For the case where 15 rotational lines are used, Fig. 23 would predict a correction of 19 to 24°K, and from Fig. 27 one obtains values of rotational temperatures from 138 to 143°K. For the off-standard condition data, when ten rotational lines are used, Fig. 23 predicts a correction of about 12°K, which yields from Fig. 28 a temperature of 98°K. When 15 rotational lines are used Fig. 23 predicts a correction of 20 to 25°K, and this gives rotational temperatures from 92 to 97°K. Again, reasonable agreement between measured and predicted T_R values was obtained by taking into account the effects of density and number of rotational lines used.

The (0, 1)/(1, 2) band intensity ratio in the off-standard condition was measured to be 3.94 (average of ten integrations) and after correction for wavelength sensitivity was 3.78. From Fig. 15 this gives a T_V of 1630°K. An average of another ten integrations gave a corrected value of 3.72 for the (0, 1)/(1, 2) band intensity ratio, and this gives a T_V of 1665°K. An average of eight integrations of the (0, 2)/(1, 3) band ratio gave an uncorrected ratio of 2.16 and a corrected value of 2.09, which gives from Fig. 15 a T_V of 1740°K. Therefore, the average value of T_V for the off-standard condition is 1678°K with a standard deviation of ±56°K, which is to be compared with the T_O value of 1662°K at which temperature the specific heat ratio, γ, of nitrogen is 1.31. Assuming one-dimensional isentropic flow, if the vibrational mode remained in equilibrium to the nozzle throat and remained frozen afterwards, one would find the free-stream vibrational temperature to be 1444°K which when compared with the measured value of T_V of 1678 ± 56°K indicates that the vibrational mode remains frozen in energy very close to its reservoir value throughout the flow.

The average intensity of the (0, 0) band during flow at the off-standard condition relative to the intensity at 0.100 torr at room temperature was measured to be 1.54, which, when used with the average T_V = 1678°K in Fig. 18, gives $\rho_\infty = 2.64 \times 10^{-7} \pm 0.06 \times 10^{-7}$ gm/cm^3. This density value is within 15 percent of the predicted value of 2.32×10^{-7} gm/cm^3; however, for this condition it is difficult to blame beam spreading for the discrepancy.

In the standard flow condition an average of eight integrations gave a (0, 1)/(1, 2) band intensity ratio of 2.91 and a corrected value of 2.79, which yields a T_V of 2125°K from Fig. 15. An average of eight

integrations gave a (0, 2)/(1, 3) ratio of 1.50 and a corrected value of 1.45, which yields a T_V of 2600°K. Therefore, the average value of T_V for the standard condition is 2363 ± 237°K, which is to be compared with the reservoir temperature, T_O = 2365°K, for which γ of nitrogen is 1.296. For one-dimensional, isentropic equilibrium flow, T_V at the throat of the nozzle would be 2060°K which would be the free-stream value of T_V if the vibrational mode froze at the nozzle throat. As in the previous case, the T_V data indicate vibrational freezing throughout the flow which is not unexpected in view of the low reservoir pressure. Time was not available for density determination in the standard condition.

A spectral scan of the beam induced radiation in the off-standard condition from 3500 to 6000 Å is shown in Fig. 31.

5.3 10 N_2 NOZZLE–TUNNEL L

The 10 N_2 nozzle is a contoured nozzle designed for arc-heated flow, the parameters of which are given below:

$M_\infty \approx 10$

Standard Condition

p_O = 1.22 atm

T_O = 3100°K (5580°R)

T_∞ = 145°K (261°R)

U_∞ = 2444 m/sec (8020 ft/sec)

ρ_∞ = 6.16 x 10^{-8} gm/cm^3

(3.85 x 10^{-6} lbm/ft^3)

p_∞ = 0.0205 torr

M_∞ = 10.15

ERTP = 0.041 torr

The nozzle may also be operated in a cold-flow mode to achieve a condition of an extremely low rotational temperature.

The diameter of the flow core was approximately 2.0 in., and beam measurements were made on the centerline 1 in. from the nozzle exit. Normally a 0.25-in. beam length was observed by the spectrometer.

It was expected on the basis of laboratory temperature measurements at 192°K (Ref. 7), the experiments of Robbin and Talbot (Ref. 13) (Fig. 32), and the predicted low free-stream density for this nozzle that no more than a 10°K correction would be necessary to eliminate both the density and kinetic temperature dependencies of the electron beam determined rotational temperature. Therefore, of all the flow fields available for study in Tunnels L and M, it was felt that the 10 N_2 condition of Tunnel L was the most ideal.

The results of three sets of six rotational line scans are shown in Fig. 33, and a typical spectral scan is shown in Fig. 34. The variation of T_R with the number of rotational lines used was not inordinately large when compared with previous data and, in fact, is similar to the 192°K laboratory data shown in Fig. 29. However, the allowable 10°K correction to the data yields a temperature from 175 to 180°K, when from 6 to 15 rotational lines are used, which is 30 to 35°K above the predicted value. Approximately 36 more rotational scans yielded results similar to those shown in Fig. 33.

The average value of the (0, 1)/(1, 2) band intensity ratio was 2.19 corrected to 2.10, which gives a T_V of 3280°K. The average (0, 2)/(1, 3) band intensity ratio was 1.215 corrected to 1.175, which gives a T_V of 3490°K. The average value of the (0, 3)/(1, 4) band intensity ratio was 0.8095 corrected to 0.830, which gives a T_V of 3440°K. The average value of the (1, 3)/(2, 4) band intensity ratio was 1.764 corrected to 1.706, which gives a T_V of 3620°K. Therefore, the average value of T_V is 3458 ± 141°K which is 358°K higher than the reservoir temperature, T_O, of 3100°K.

The average intensity of the (0, 0) band during flow relative to the intensity at 0.100 torr at room temperature was measured to be 0.314, which, when used with the average T_V = 3458°K in Fig. 17, gives $\rho_\infty = 6.49 \times 10^{-8} \pm 0.6 \times 10^{-8}$ gm/cm^3. This is in good agreement with the predicted value of 6.15×10^{-8} gm/cm^3.

A scan of the beam induced radiation in the standard condition from 3500 to 6000 Å is shown in Fig. 35 which shows that all significant radiation is attributable to excited or ionized nitrogen.

The 10 N_2 nozzle was also operated in a cold-flow condition. The results of two sets of six rotational line scans are shown in Fig. 36, with a typical spectral scan shown in Fig. 37. The variation of T_R with K′ is considerable above K′ = 6. Predicted values of the flow parameters at this condition are not known at this time, and definition of the isentropic core by impact pressure surveys has not been obtained.

5.4 18 N_2 NOZZLE-TUNNEL M

The 18 N_2 nozzle is contoured and designed for arc-heated flow, the parameters of which are given below:

$$\underline{M_\infty \approx 18}$$

p_o = 18.9 to 19.2 atm

T_o = 2800 to 3200°K (5040 to 5760°R)

T_∞ = 44 to 52°K (79.2 to 93.6°R)

U_∞ = 2438 to 2621 m/sec (8000 to 8600 ft/sec)

ρ_∞ = 5.45 x 10^{-8} to 6.25 x 10^{-8} gm/cm^3
(3.4 x 10^{-6} to 3.9 x 10^{-6} lbm/ft^3)

p_∞ = 0.060 to 0.068 torr

M_∞ = 17.9 to 18.3

ERTP = 0.036 to 0.041 torr

Beam measurements were made at two axial positions: 15.24 cm (6 in.) and 31.12 cm (12.25 in.) downstream of the nozzle exit. The diameter of the flow core was approximately 25.4 to 30.5 cm (10 to 12 in.), and a 2.0-cm beam length was observed.

Normally, four rotational spectra scans were used in each rotational temperature determination. Figures 38 and 39 show typical rotational temperature results on the centerline at the 12.25-in. and 6.0-in. position, respectively, and Fig. 40 shows a typical rotational spectral scan.

Unlike Tunnel L, Tunnel M has the capability of on-line computer calculation of tunnel flow parameters using the measurement of impact pressure p_o'; therefore, for each rotational spectral scan, a tunnel parameter datum point was taken. Tunnel M was also operated at two slightly different mass flow rates, but the calculated flow parameters were always within the range given in the preceding list. The different flow rates will be referred to as $\dot{m}_{low}$ and $\dot{m}_{high}$.

Figure 41 shows the results of a rotational temperature radial profile measurement at the x' = 12.25-in. position with $\dot{m}_{low}$. The temperature profile is seen to be flat within ±5°K out to 12 cm. The rotational temperatures for this profile, as for all T_R profiles, were determined using ten rotational lines. The average rotational temperature over the radial distance of 0 to 12 cm was 68.4°K, which can

be corrected to 59.4°K from Fig. 23 using a calculated average ρ_∞ of 6.4×10^{-8} gm/cm^3. However, since the predicted free-stream temperature was 51.2°K, the rotational temperature determined is approximately 16 percent higher than the calculated free-stream temperature.

Figure 42 shows the results of a T_R radial profile measurement at the $x' = 6.0$-in. position with $\dot{m}_{low}$. The temperature profile is observed to be flat within ±5°K in the radial direction out to 14 cm. The average T_R over the 14 cm radial distance was 62.3°K, which can be corrected to 53.3°K using Fig. 23, which agrees to within 9 percent with the average aerodynamic free-stream temperature value of 49.1°K.

Figure 43 shows the results of a T_R radial profile at the $x' = 6.0$-in. position with $\dot{m}_{high}$. The temperature profile is again observed to be flat out to 14 cm within ±7°K and the average T_R over this distance was 60.6°K, which can be corrected to 51.6°K. This is in good agreement with the average aerodynamic T_∞ of 49.6°K.

An average value of T_V was obtained at $x' = 12.25$ in. on the centerline using the four band intensity ratios (0, 1)/(1, 2), (0, 2)/(1, 3), (0, 3)/(1, 4), and (1, 3)/(2, 4) yielding $T_V = 3216 \pm 58$°K (Table V). The average T_o for which the T_V data were obtained was 2825 ± 50°K; therefore, a difference of nearly 400°K exists between the measured value of T_V and the calculated value of T_o.

The Tunnel M test cabin could not be evacuated below 0.75 torr with no flow, so a density calibration at room temperature could not be made. However, the radial variation of free-stream density relative to the centerline density was measured. Figure 44 shows the radial variation of density measured with the electron beam and also pitot probe at $x' = 12.25$ in., $\dot{m}_{low}$. It is shown that the electron beam data predicts a smaller flat density core than the pitot probe data, but the observed difference may be attributable to the electron beam data having been obtained at a different test cabin pressure p_T, as is discussed in Section 6.1.2. Figure 45 shows the radial density profile at the $x' = 6.0$-in. position, $\dot{m}_{low}$, and the radial density gradient is observed to be much less as one moves closer to the nozzle exit for the $\dot{m}_{low}$ condition. Figure 46 shows the radial density profile for the $x' = 6.0$-in., $\dot{m}_{high}$ condition. The profile is observed to be very similar to the $x' = 12.25$-in., $\dot{m}_{low}$ condition with, however, a somewhat smaller flat core.

SECTION VI
CONCLUSIONS AND RECOMMENDATIONS FOR FUTURE WORK

6.1 SUMMARY AND CONCLUSIONS

A summary of the Tunnels L and M electron beam data is shown in comparison with the calculated free-stream parameters in Table VI.

6.1.1 Vibrational Temperature

From Table VI it can be seen that all values of T_V except one measured by the electron beam technique are higher than the calorimetrically inferred reservoir temperatures, T_o, and all values are significantly higher than the predicted temperature at the nozzle throat, which T_V of N_2 should approach if significant vibrational energy transfer occurs in the expansion from the reservoir to the throat, and that the difference in the experimental values of T_V and T_o increase as T_o increases. There are three obvious possible sources of this discrepancy which will be discussed.

6.1.1.1 Inaccurate Calorimetric Determination of T_o

If one assumes equilibrium reservoir conditions, i. e., T_V (experimental) = T_R = T_o, it can be seen that the error in T_o and reservoir enthalpy for all flow conditions except the off-standard 9 N_2 nozzle flow amounts to at least 10 percent, which is more than 5 percent larger than the experimental uncertainty associated with the calorimetric determination of T_o, as described in Ref. 12. For this reason this source of discrepancy is considered no further.

6.1.1.2 Inaccurate Excitation Band Strength

It has been stated that calculable excitation Franck-Condon factors $q(v', v_1'')$ have been used in Eq. (11) rather than the presently unknown excitation band strengths $p(v', v_1'')$, and their usage is justified on the basis that during the short-duration ($\approx 10^{-15}$ sec) high energy collision of a primary electron with a nitrogen molecule, the molecule has little time to move either by rotation or vibration and the Franck-Condon principle is applicable. However, if sufficient low energy secondary electrons exist in the flow, a significant fraction of excitations could occur for which the ratio of interaction time and period of vibration is considerably increased; this situation would violate the criterion of applicability of the Franck-Condon principle and would necessitate usage

of the excitation band strengths $p(v', v_1'')$, for which the first-order approximation can be written as

$$p(v', v_1'') = q(v', v_1'')[1 + b\bar{r}_{v', v_1''}] \quad (14)$$

where b is an unknown excitation band strength parameter. If Eq. (11) is now calculated with b as a parameter, the b = 0 curve represents the Franck-Condon approximation, and if the source of the T_V discrepancy can be attributed to the usage of the b = 0 curve given by Eq. (11), one can attempt to effectively scale the experimental values of T_V to an estimated free-stream T_V by the judicious selection of a unique value of b.

For the low p_o expansions, i. e., $p_o \leq 2$ atm, it is reasonable to expect T_V to freeze near the reservoir value T_o, and one can determine the value of b required to reduce T_V (experimental) to $T_V = T_o$. Doing this with the (0, 2)/(1, 3) band ratios for the 9 N_2 off-standard condition one finds b = 0.75 and for the 9 N_2 standard condition one finds b = 1.3, whereas the 10 N_2 data give b = 1.5. For the 18 N_2 nozzle of Tunnel M, b is found to be approximately 2.0. However, if one assumes that $T_V \approx T$ at the throat of the 18 N_2 nozzle because of the high reservoir pressures in Tunnel M, then one gets $b \geq 3$. Therefore, the values of b thusly obtained vary from 0.75 to 3, yielding no unique value of b to enable a scaling of the electron beam results of T_V. This result does not imply that b = 0, or that Franck-Condon excitation is appropriate, but rather that a breakdown of Franck-Condon excitation rules is not the sole source of the discrepancy. For all flow fields investigated b is always greater than or equal to 0.75, so that it is entirely possible that an increase of b from 0 to 0.75 is indicated and that an additional source (or sources) of discrepancy exists. In the event b = 0.75, the experimental T_V from the (0, 2)/(1, 3) bands is changed from 1740 to 1662°K for the off-standard 9 N_2 nozzle where T_o = 1662°K. For the standard 9 N_2 condition, if b = 0.75, T_V is decreased from 2600 to 2500°K, and the corresponding T_o = 2365°K; the 10 N_2 result for T_V in the test section is changed from 3490 to 3325°K, whereas T_o = 3100°K and the 18 N_2 result for T_V is decreased from 3280 to 3100°K, while T_o = 2825°K. Therefore, it can be seen that for three of the four cases, the decrease in T_V effected by adjusting b from 0 to 0.75 is insufficient to account for the finding of T_V greater than T_o. However, it should be noted that each of these three discrepancies then becomes less than 10 percent.

6.1.1.3 Electron Heating of the Vibrational Mode of N_2

As a final cause of the (presumed) T_V anomaly one may question the assumption of the attainment of thermal equilibrium in the stilling chamber, or reservoir, thereby enabling T_V to have a higher starting value for expansion than T_O. The mechanism whereby the nonequilibrium steady-state condition $T_V \neq T_O$ in the reservoir is maintained could well be the low energy electrons produced in the arc heater, carried into the reservoir gas and, by means of, say, negative ion formation and subsequent ionization, producing an excessively high vibrational mode energy; the collision can be represented as

$$N_2(v=0) + e^- \rightarrow (N_2)^- \rightarrow N_2(v = 1, 2, 3, \ldots.) + e^-$$

For the case of the Tunnel M 18 N_2 flow one would expect thermalization to occur in the reservoir since the residence time, t_r, of an N_2 molecule in the reservoir is over 1000 times the magnitude of the vibrational relaxation time, τ_V, of N_2 at 3000°K; one would reasonably expect this excessive vibrational energy to be transferred by collisions into the rotational and translational modes before emergence into the nozzle. The only way this cannot be the case is for electrons to persist within the reservoir without being thermalized, thereby maintaining a nonequilibrium situation such that $T_V \neq T_O$ in the settling chamber.

The next question to answer, assuming this supposition to be true, is whether calorimetric determinations of T_O are sufficiently sensitive to detect the nonequilibrium environment. If T_V in the reservoir were 4000°K, maintained by electron heating, and both the translational and rotational modes had temperatures of 3000°K, the enthalpy difference associated with this assumed value of T_V and the case where $T_V = T_O = 3000$°K is approximately 65.5 cal/gm, as compared with the 932 cal/gm total enthalpy of the reservoir; this difference of approximately 7 percent, which is marginal with regard to detection by the calorimeter, is sufficiently large to explain the anomalies in the T_V measurements.

Therefore, of the three sources of discrepancy discussed, it is concluded that, although no unique adjustment of b resolves the T_V anomaly, an increase of b from 0 to 0.75 coupled with the assumption on a nonequilibrium reservoir condition, $T_V \neq T_O$, can as easily account for the discrepancy as can the assumption that b = 0 and that the inequality of T_V and T_O is the sole source of the result. Neither approach invalidates accuracy statements of Ref. 12 regarding the calorimetric evaluation of reservoir enthalpy.

6.1.2 Density Measurements

Free-stream density measurements in the Tunnel L flows were always higher than the predicted values. However, for all cases the measured values were within 15 percent of the predicted values, and it is believed that a large portion of this error can be attributed to inaccurate measurement of beam current caused by beam spreading effects. It is to be noted that such a systematic discrepancy in ρ might be attributed to the T_V dependence of the density measurement, as shown by Figs. 17 and 18, particularly since the experimental values of T_V were consistently higher than expected. Figure 47 shows the ERTP as a function of T_V for a constant band intensity value, approximately equal to the measured value, for the Tunnel L 10 N_2 nozzle. To lower the experimental ERTP by approximately 5 percent to the predicted ERTP requires a decrease in the measured T_V ($\approx$ 3500°K) of approximately 300°K which is not unreasonable. However, for the Tunnel L 9 N_2 nozzle, off-standard condition, Fig. 48 shows that the required decrease in ρ of approximately 15 percent requires that the free-stream T_V be less than 1200°K rather than the measured value of 1678°K, and a change in T_V of this magnitude is felt to be unwarranted. Consequently, spreading effects of the electron beam remain as the primary suspected cause of the discrepancy in density values.

The radial density profiles measured for Tunnel M consistently showed a smaller uniform density core diameter than that shown by impact pressure measurements. Furthermore, the much steeper profile at x′= 6.0 in. for $\dot{m}_{high}$ than for $\dot{m}_{low}$ is quite interesting, for this slight difference in $\dot{m}$ values should have had no effect on the profile. However these differences cannot be viewed seriously because it is possible that the ratio of tank pressure to free-stream pressure may not have been constant in all cases; during the density data acquisition for the x′= 6.0 in., $\dot{m}_{high}$ condition, a malfunction occurred in the data system that caused the loss of tunnel flow parameter data.

6.1.3 Rotational Temperature

Rotational temperature measurements for all conditions except the 10 N_2 nozzle and 18 N_2 nozzle at x′= 12.25 in. were within 10 percent of the predicted free-stream temperature values. For the 18 N_2 nozzle at x′= 12.25 in. the measured value of T_R was 16 percent higher than the predicted value. However, if the proper density-temperature correction factor for 50°K rotational temperature measurement were used instead of the 78°K correction factor, as given in Fig. 23, this 16 percent error will quite likely be reduced as will the small discrepancy detected at the 6-in. position. Unfortunately, for the 35 to 40°K

discrepancy between measured and predicted rotational temperature for the 10 N_2 nozzle, there would appear to be little further correction possible unless rotational relaxation effects are surprisingly large. The discrepancy is glaring and should be of concern to electron beam experimenters and gas dynamicists.

In an effort to examine the effects that the electron beam measured values would have on the calculated flow parameters for the 10 N_2 nozzle, D. E. Boylan, ARO, Inc., AEDC, has calculated four different cases for 10 N_2 flow conditions. The standard flow parameters were calculated using either standard (aerodynamic) tunnel measurements, electron beam measurements, or combinations of the two as known values in gas dynamic equations. Case I (Table VII) conditions were calculated using the standard tunnel measurements of mass flow rate, impact pressure, reservoir pressure, total enthalpy, and product of $\rho_\infty U_\infty$ obtained by a probe. Case II conditions were calculated assuming the flow parameters to be defined by the most plausible measured value of rotational temperature, the impact pressure, the reservoir pressure, and the nozzle mass flow rate. To produce such a flow would require a 500°K higher value of T_0 and, moreover, an effective throat diameter of 0.154 in. — significantly larger than the measured value of 0.148 in. Case III conditions were calculated assuming the flow parameters to be defined by the electron beam measured values of rotational temperature and density and the standard measurement of mass flow rate and reservoir pressure. For Case III a value of impact pressure approximately 20 percent higher than that normally measured would be required, and it is the belief of the gas dynamicists that this much error in impact pressure measurement is impossible. For Case IV conditions the electron beam measured value of density and the standard measurements of impact pressure, reservoir pressure, and mass flow rate were assumed to define the flow parameters. Although this approach does not eliminate the gap between measured rotational temperature and predicted free-stream temperature, the other quantities tabulated do not differ by impossible amounts when the Case I and Case IV results are compared. Note also that in Case II a result is obtained for T_0 which differs markedly from the value derived by directly measuring H_0, and in Case III a serious discrepancy arises when the computed p_0' is compared to the directly measured value. Thus, it may be said that Cases II and III are not nearly as well supported by impact pressure and reservoir enthalpy data as is Case IV, but for Case IV the calculated value of T_∞ differs significantly from the measured value of rotational temperature.

Using a different rotational line intensity data reduction technique called the least-squares quadratic fitting technique, all the rotational

spectral data were reanalyzed. Results from this method of data reduction are also shown in Table VI. Good agreement is obtained with the experimental values obtained from the least-squares linear fitting technique. The quadratic fitting technique is discussed in detail in Appendix III.

6.2 RECOMMENDATIONS FOR FUTURE WORK

For the 10 N_2 nozzle the discrepancy in measured and predicted temperature should be resolved. Two experiments should be performed: (1) various stilling chamber lengths should be used to see if the T_R discrepancy is a result of nonequilibrium processes in the stilling chamber, and (2) the 10 N_2 free-stream conditions should be duplicated with a conical nozzle operating at a much lower stagnation temperature. This latter experiment was brought to mind since the departure of T_R from the predicted value has been observed to increase with T_o as shown in Figs. 49 and 50. This variation has also been observed by Sebacher (Ref. 14) and MacDermott and Marshall (Ref. 15). However, MacDermott and Marshall were able to obtain agreement between rotational temperature measurements and static temperature predicted using finite-rate theory with magnified vibrational rates based on their vibrational temperature measurements. Such an approach is, of course, impossible for the 10 N_2 nozzle data since measured vibrational temperatures were always greater than or equal to the predicted T_o.

Future flow diagnostic efforts in Tunnels L and M should also be concentrated on direct measurements of T_o and T_v of the reservoir using:

1. Spectral line reversal apparatus
2. Emission spectroscopic observations of the N_2^+ $[1^-]$ system for T_v
3. Consideration of seeding N_2 with trace amounts of H_2 or He to look for Stark broadening of emission lines attributable to high values of the electron density in the reservoir.
4. Seeding the flow with trace amounts of CO or CN to determine the reservoir values of T_R (or T_o) using molecular band emission attributable to arc heater excitation.
5. Investigation of the feasibility of making spatially resolved measurements of density and temperature in the reservoir by means of laser Raman scattering.

A repeat of all the ρ_∞ measurements using the electron beam at a higher energy would also be desirable in order to investigate the effect on the measurements reported herein.

REFERENCES

1. Potter, J. L., Kinslow, M., Arney, G. D., and Bailey, A. B. "Description and Preliminary Calibration of a Low-Density, Hypervelocity Wind Tunnel." AEDC-TN-61-83 (AD262466), August 1961.
2. Potter, J. L. and Boylan, David E. "Experience with an Over-expanded Nozzle in a Low-Density, Hypervelocity Wind Tunnel." AEDC-TDR-62-85 (AD274383), April 1962.
3. Muntz, E. P. "Measurement of Rotational Temperature, Vibrational Temperature, and Molecule Concentration in Non-Radiating Flows of Low Density Nitrogen." University of Toronto Institute of Aerophysics Report 71, Toronto, Canada, April 1961.
4. Muntz, E. P. and Abel, S. J. "The Direct Measurement of Static Temperatures in Shock Tunnel Flow." G. E. TIS R645D25, Valley Forge, Pennsylvania, 1964.
5. Muntz, E. P. and Marsden, D. J. Rarefied Gas Dynamics II. Edited by J. A. Laurmann. Academic Press, New York, 1963.
6. Muntz, E. P., Abel, S. J. and Maguire, B. L. "The Electron Beam Fluorescence Probe in Experimental Gas Dynamics." Supplement to IEEE Transactions on Aerospace, Vol. AS-3, No. 2, June 1965, pp. 210-222.
7. Williams, William D. "Laboratory Verification Studies of Rotational and Vibrational Temperature Measurements by the Electron Beam Technique." AEDC-TR-68-265 (AD683001), February 1969.
8. Ashkenas, H. "On Rotational Temperature Measurements in Electron-Beam Excited Nitrogen." Physics of Fluids, Vol. 10, December 1967, p. 2509.
9. Beers, Y. Introduction to the Theory of Error. Addison-Wesley Publishing Company, Inc., Reading, Massachusetts, 1953.

10. Lewis, J. W. L. and Williams, W. D. "Vibrational Temperature Measurements Using the Electron Beam." AIAA Journal, Technical Note, June 1969.

11. Bogdan, L. and McCaa, D. J. "Experimental Study of Electron-Excited Emission in Air and in Nitrogen up to 8 Torr." CAL AG-2679-Y-1, May 1970.

12. Arney, G. D. and Boylan, D. E. "A Calorimetric Investigation of Some Problems Associated with a Low-Density Hypervelocity Wind Tunnel." AEDC-TR-63-19 (AD295759), February 1963.

13. Robben, F. and Talbot, L. "Some Measurements of Rotational Temperatures in a Low-Density Wind Tunnel Using Electron Beam Fluorescence." University of California Rept. No. AS-65-5, Berkeley, California, May 1965.

14. Sebacher, D. I. "An Electron Beam Study of Vibrational and Rotational Relaxing Flows of Nitrogen and Air." Proc. Heat Transfer Fluid Mech. Inst., Vol. 18, 1966, p. 315.

15. MacDermott, W. N. and Marshall, J. C. "Nonequilibrium Nozzle Expansions of Partially Dissociated Air: A Comparison of Theory and Electron Beam Measurements." AEDC-TR-69-66 (AD690493), July 1969.

APPENDIXES

I. ILLUSTRATIONS
II. TABLES
III. ROTATIONAL TEMPERATURE CALCULATIONS USING A LEAST-SQUARES QUADRATIC FITTING PROCEDURE

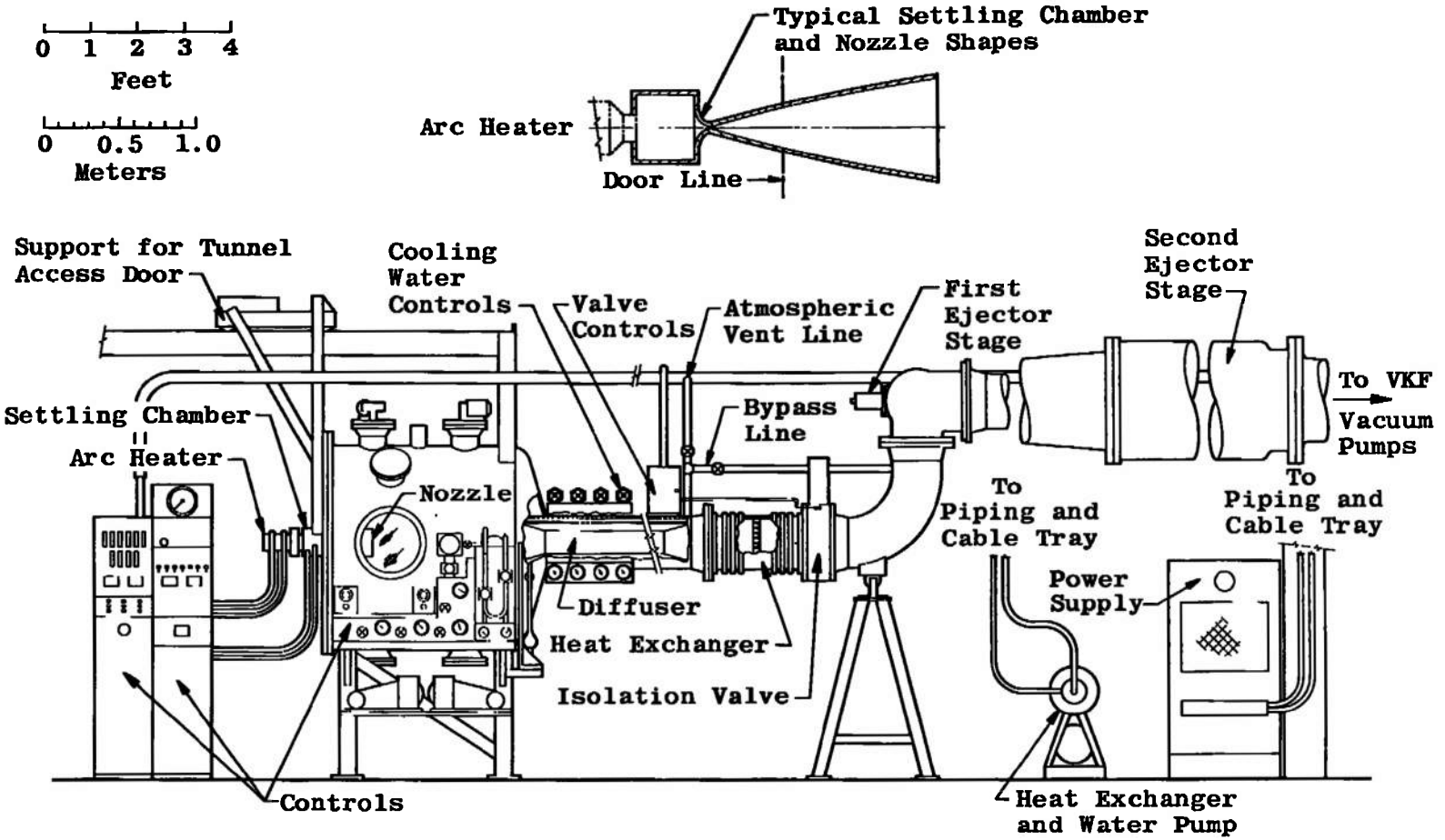

Fig. 1 Elevation View of Tunnel L

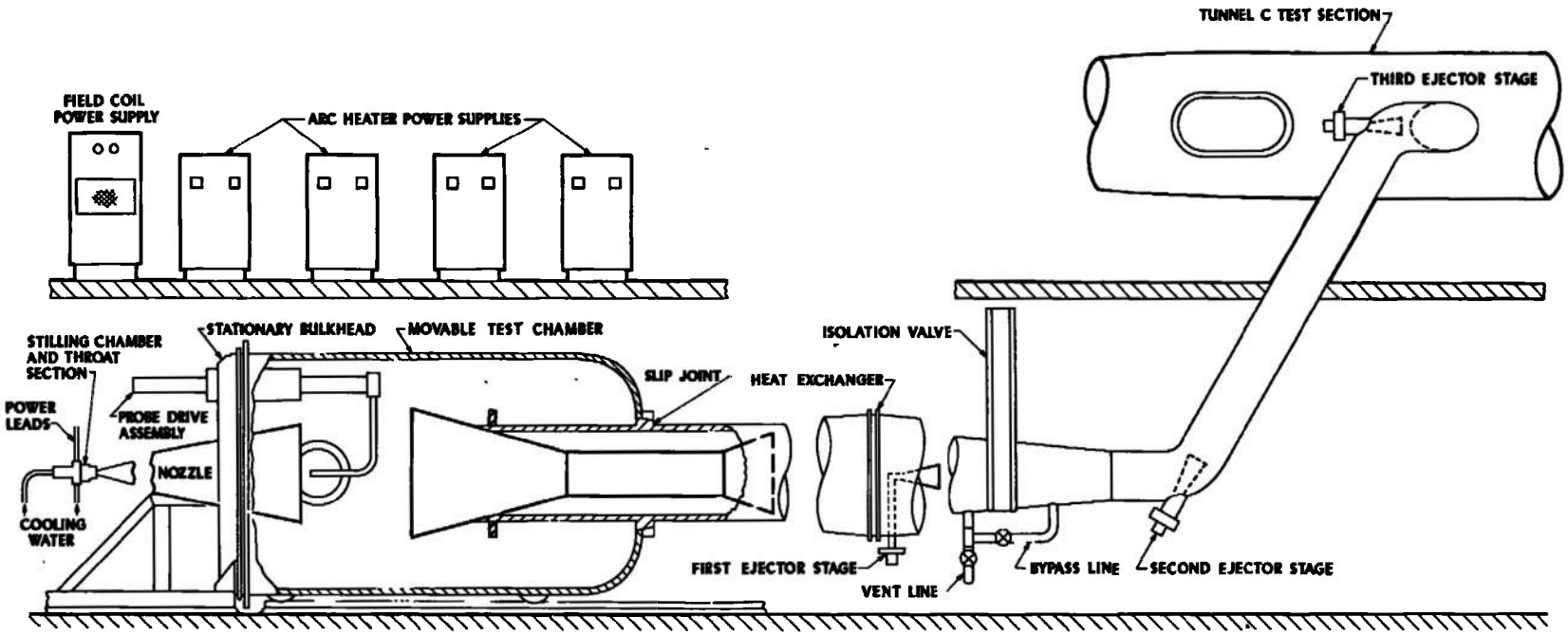

Fig. 2 Elevation View of Tunnel M

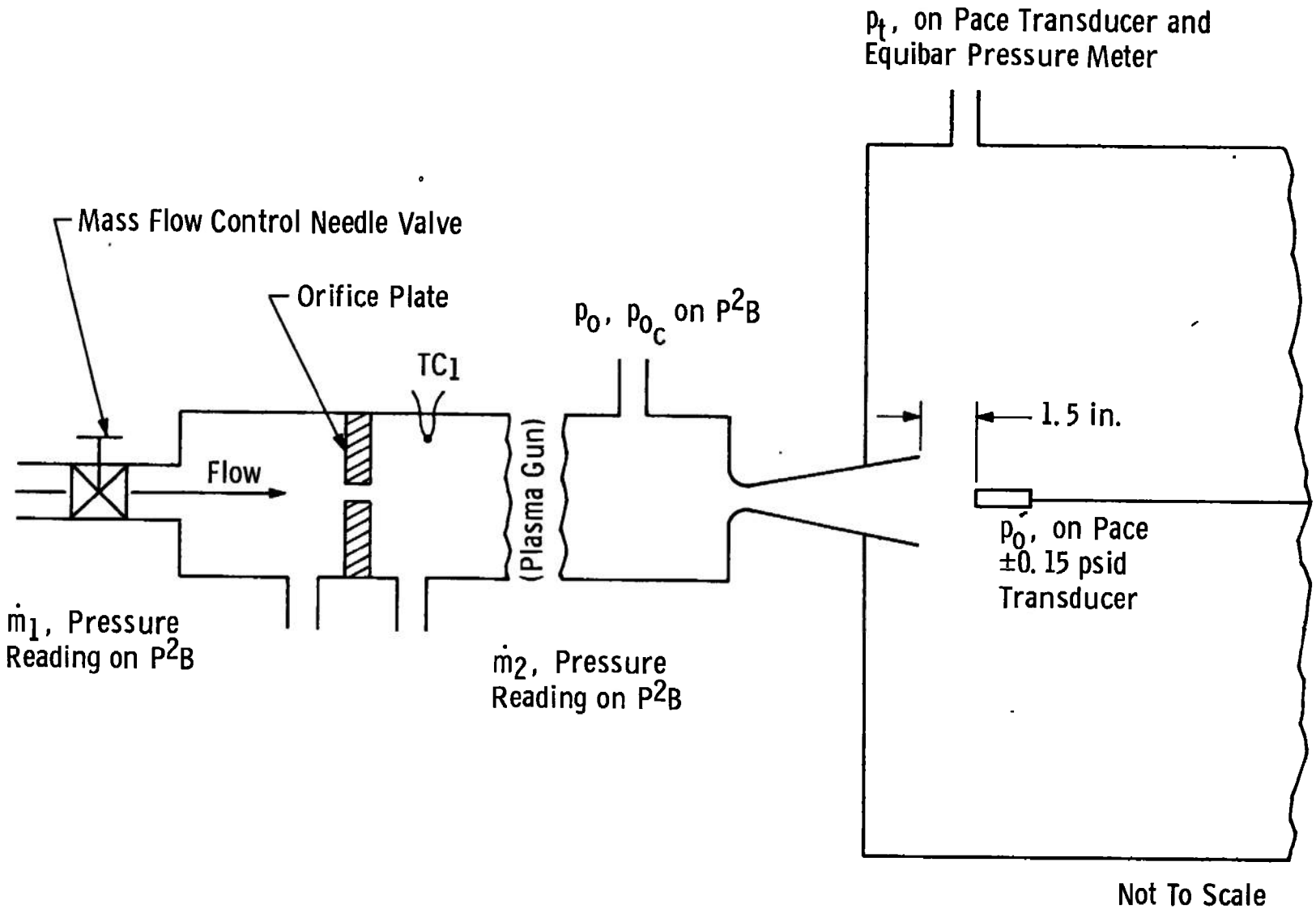

Fig. 3 Tunnel Instrumentation Measurements

AEDC-TR-71-61

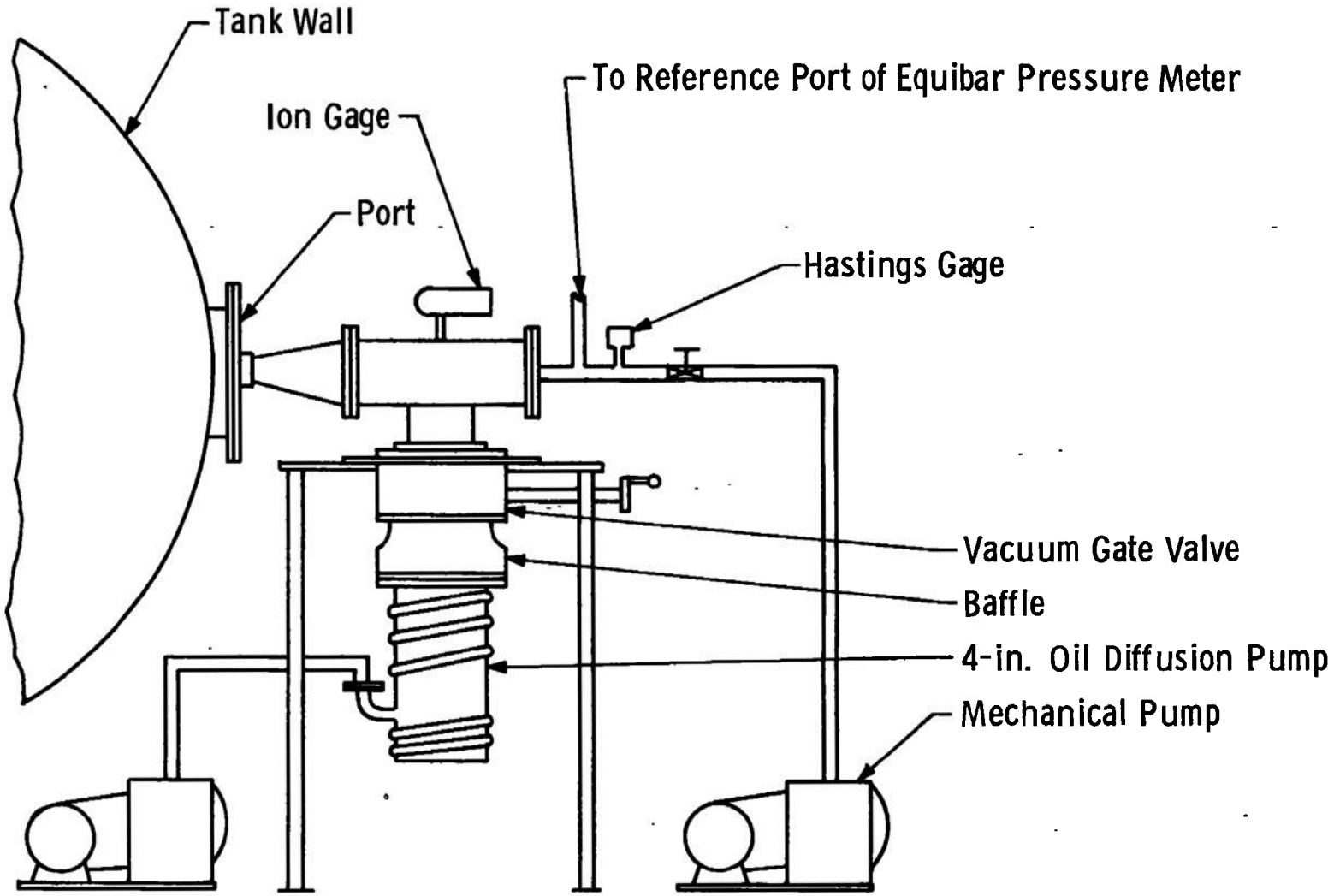

Fig. 4 Schematic Drawing of Electron Beam Vacuum System

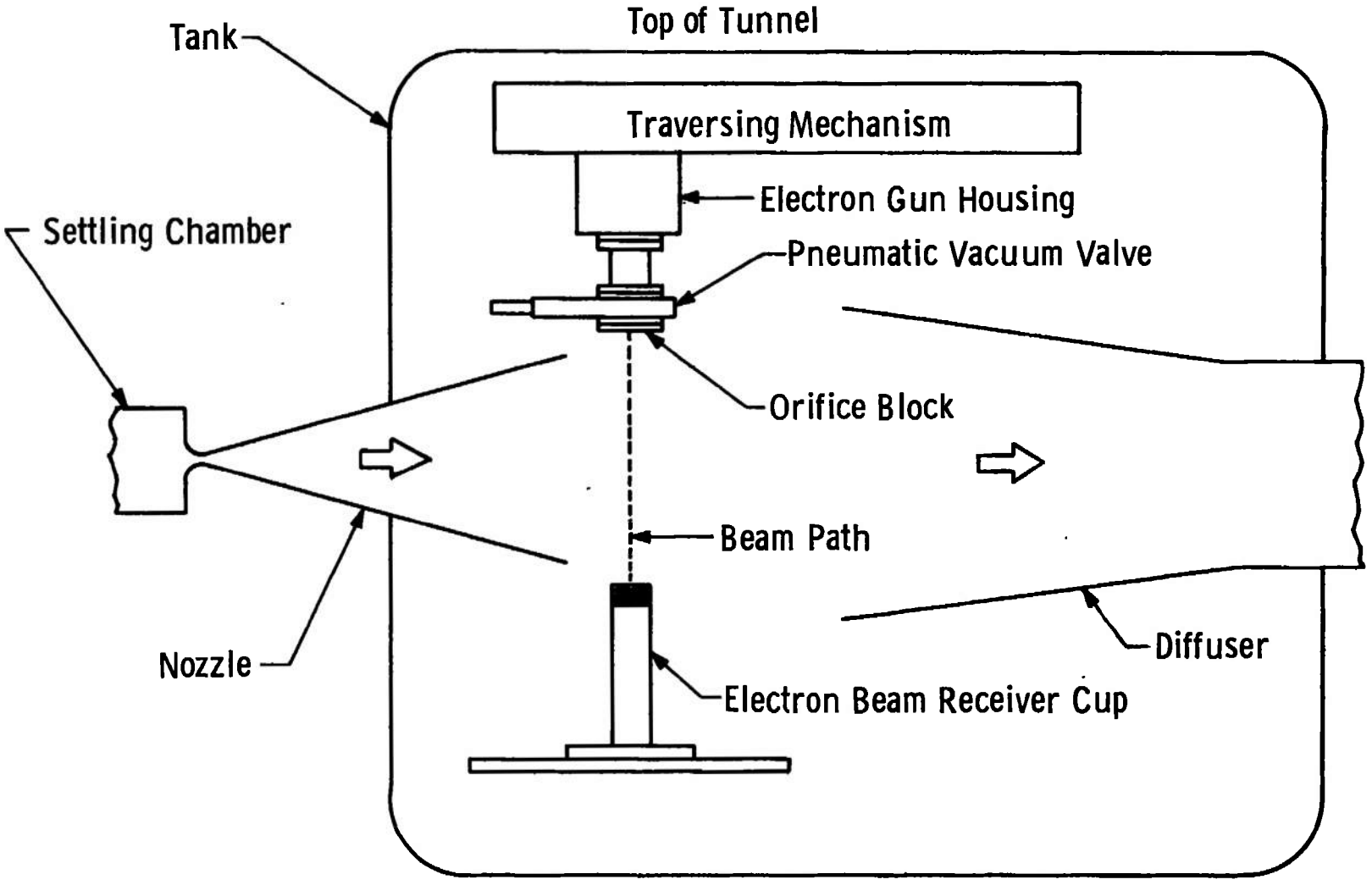

Fig. 5 Schematic Drawing of Tunnel L Electron Beam Installation

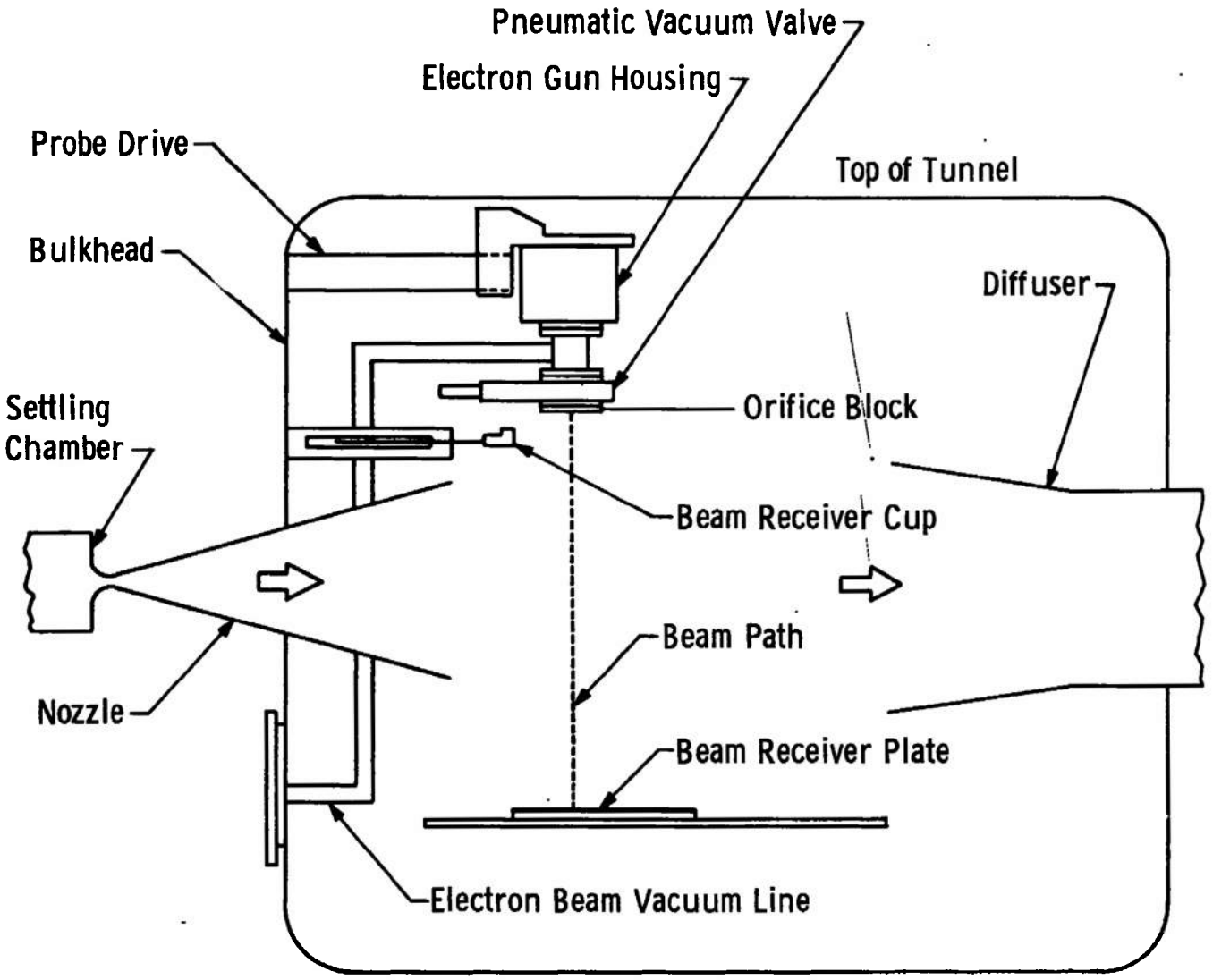

Fig. 6 Schematic Drawing of Tunnel M Electron Beam Installation

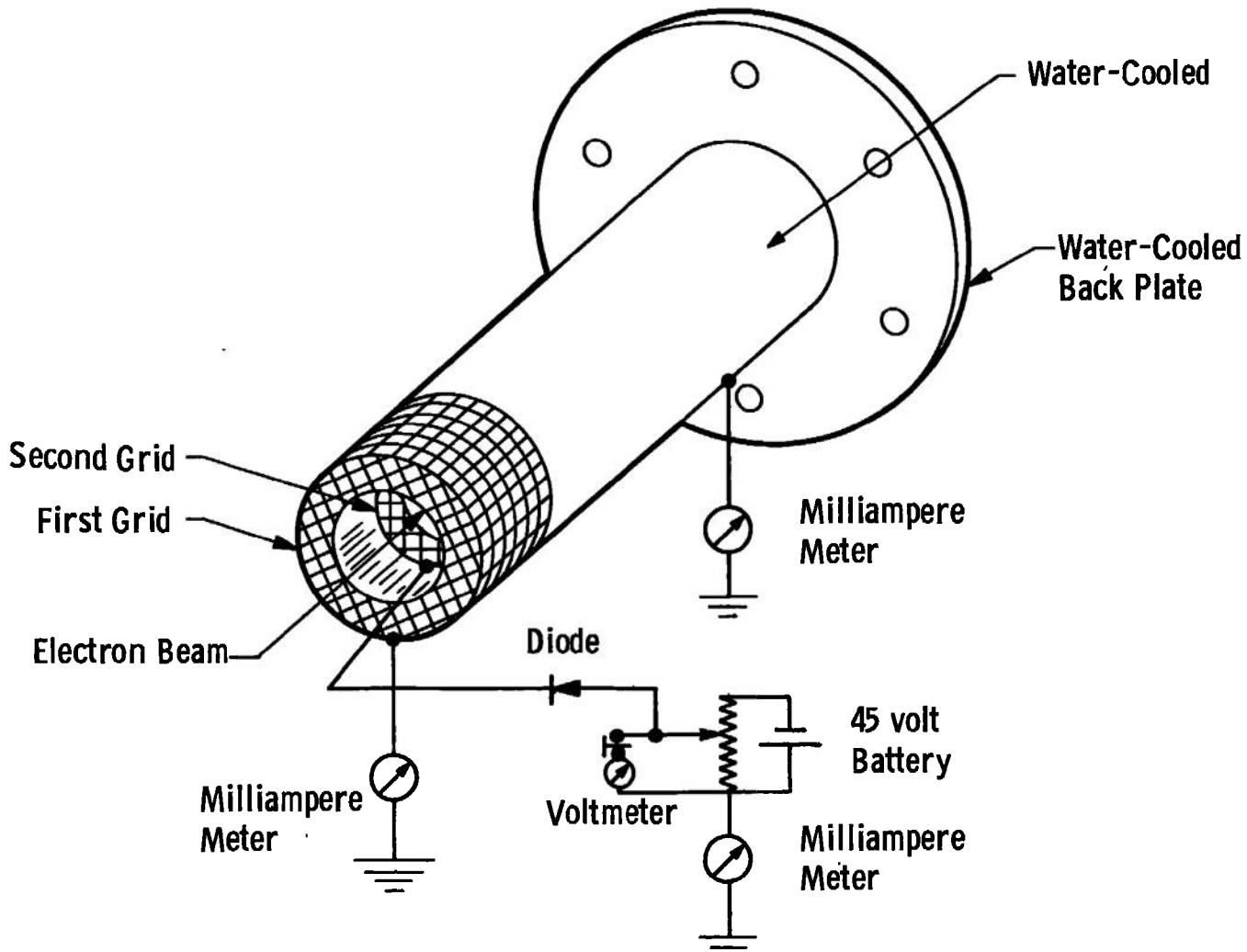

Fig. 7 Diagram of Beam Receiver Cup and Electrical Connections

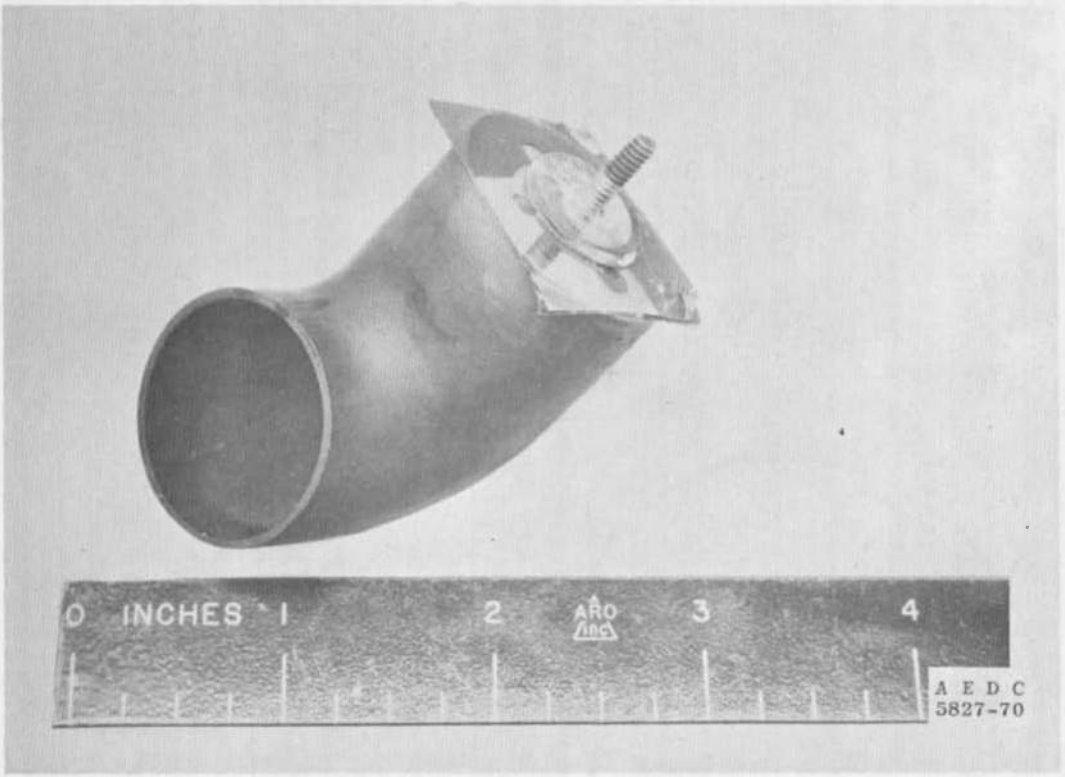

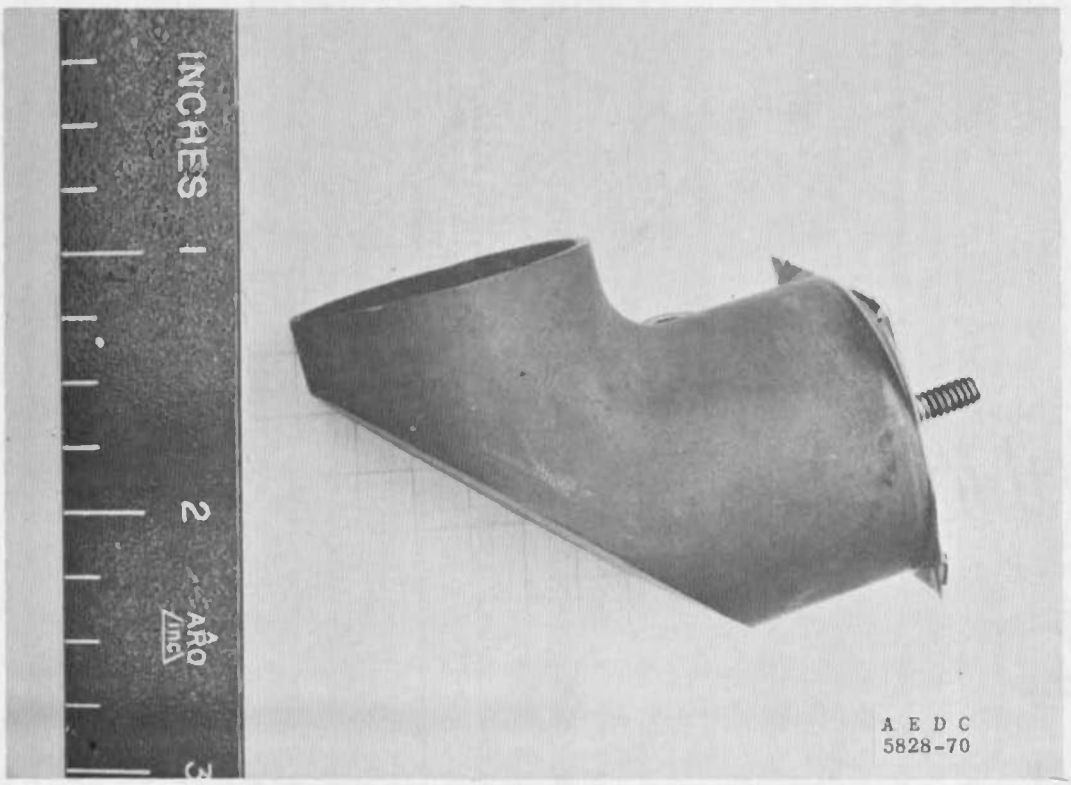

Fig. 8 Tunnel M Auxiliary Beam Receiver Cup

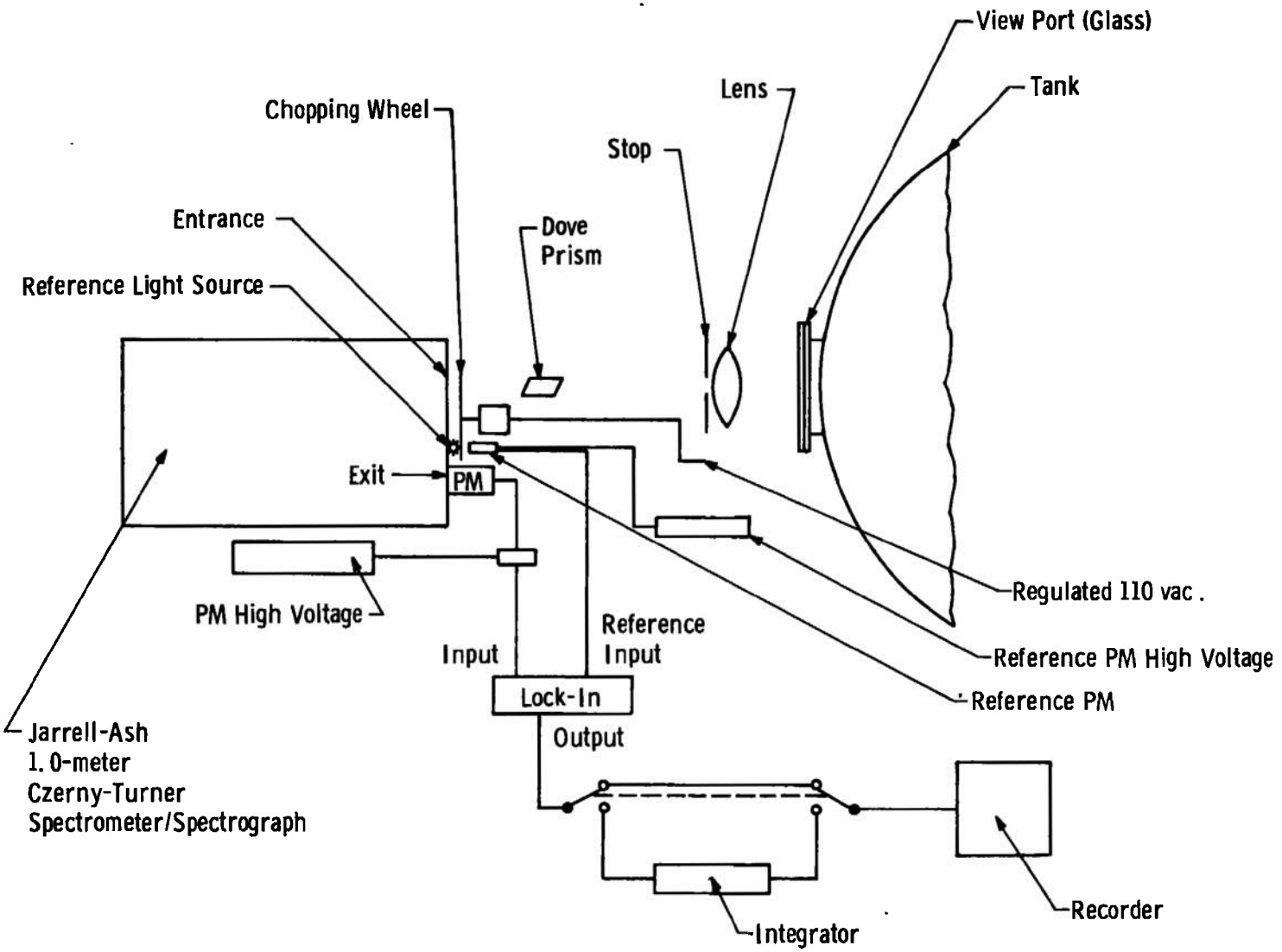

Fig. 9 Schematic Drawing of Tunnel L 1-Meter Spectrometer Setup

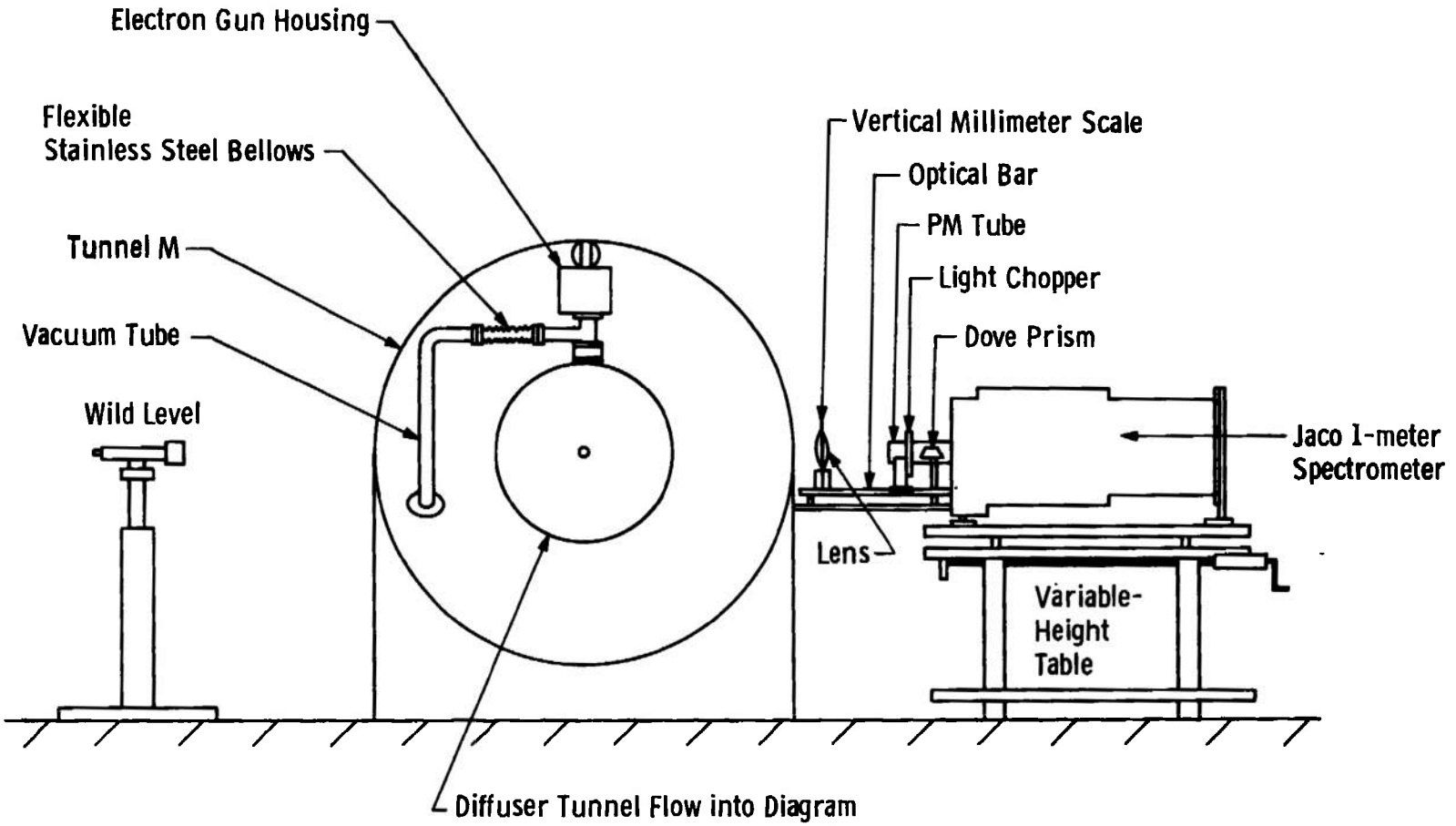

Fig. 10 Schematic Drawing of Tunnel M 1-Meter Spectrometer Setup

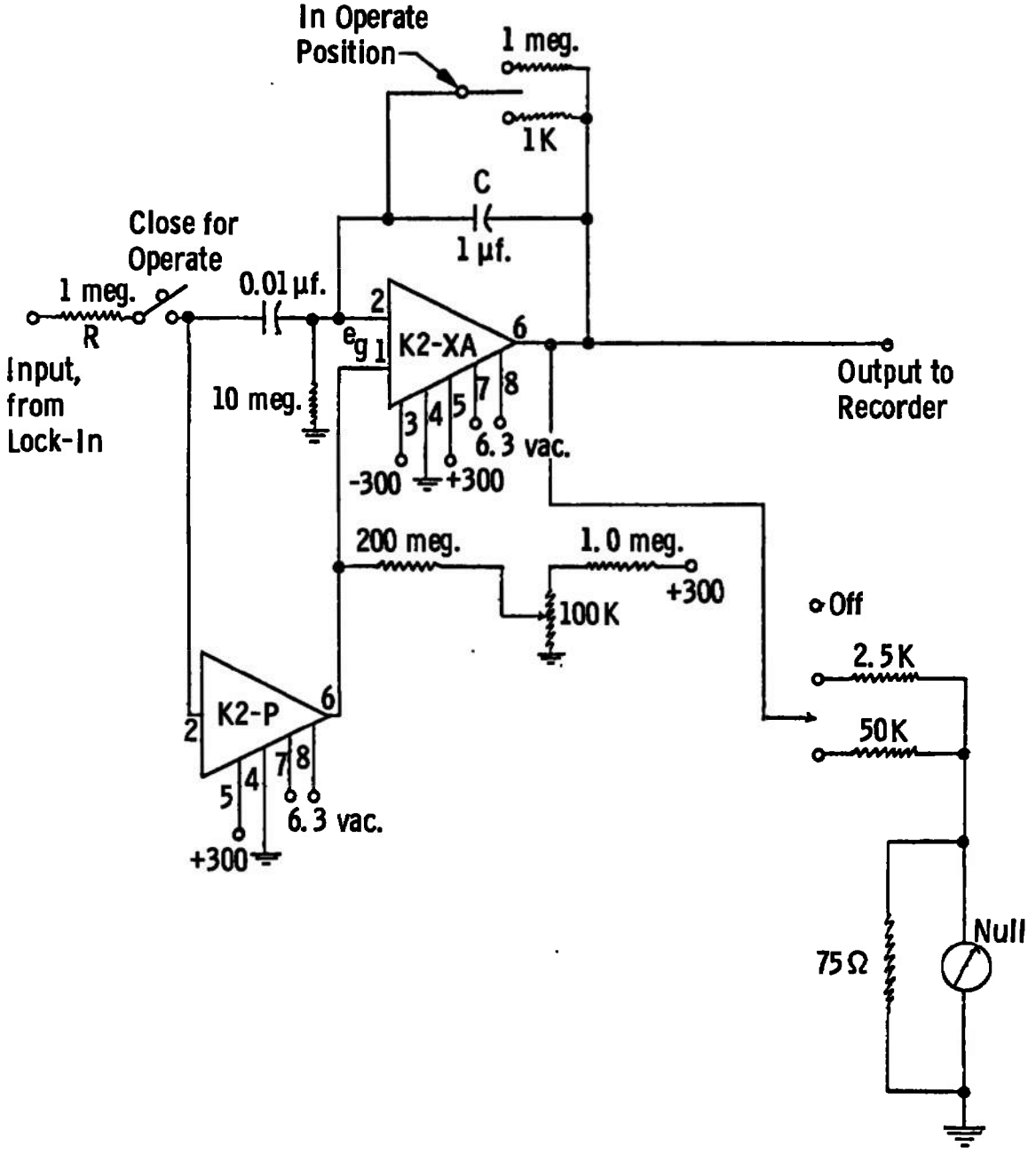

Fig. 11 Tunnel L Electronic Integrator

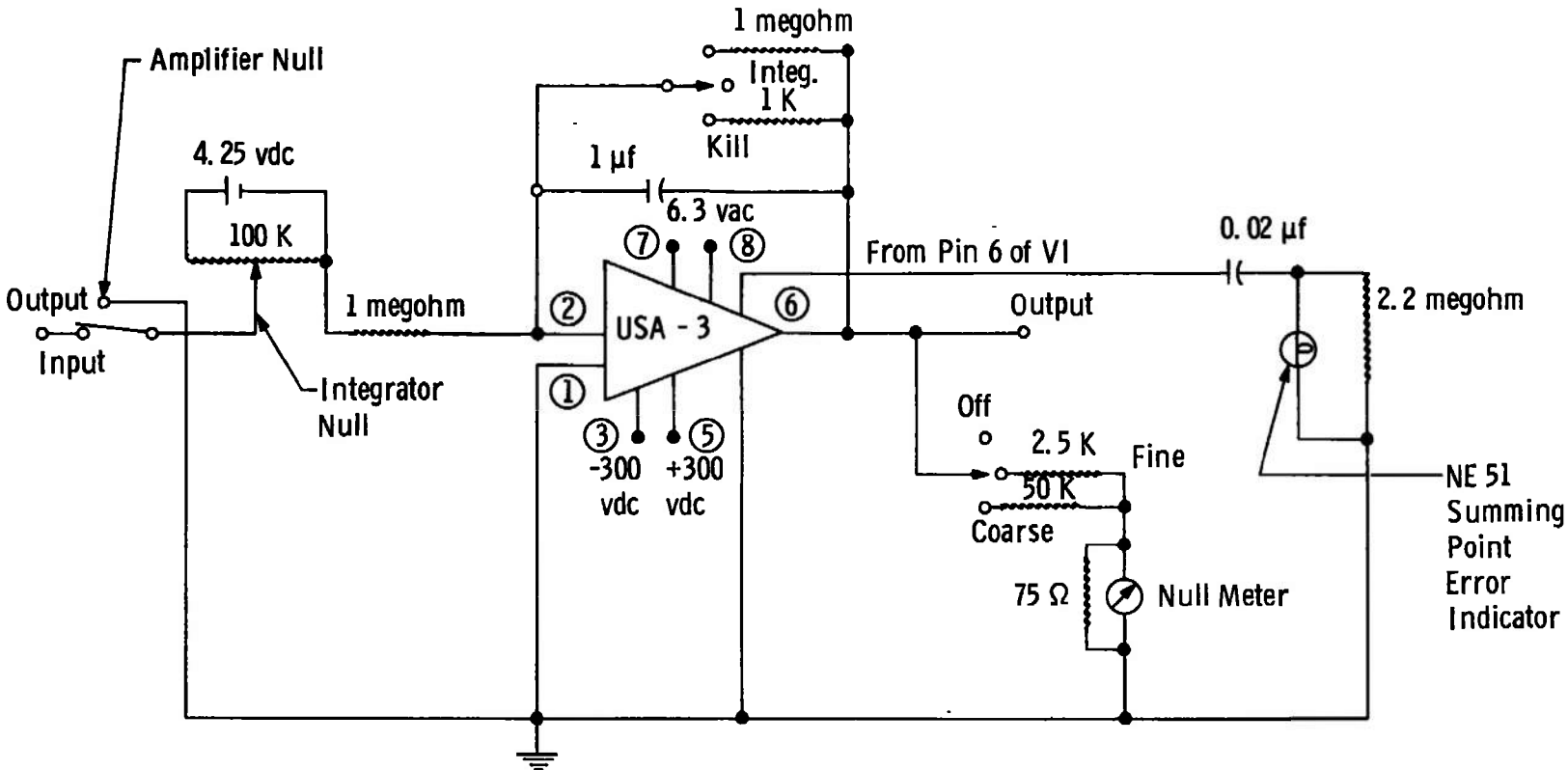

Fig. 12 Tunnel M Electronic Integrator

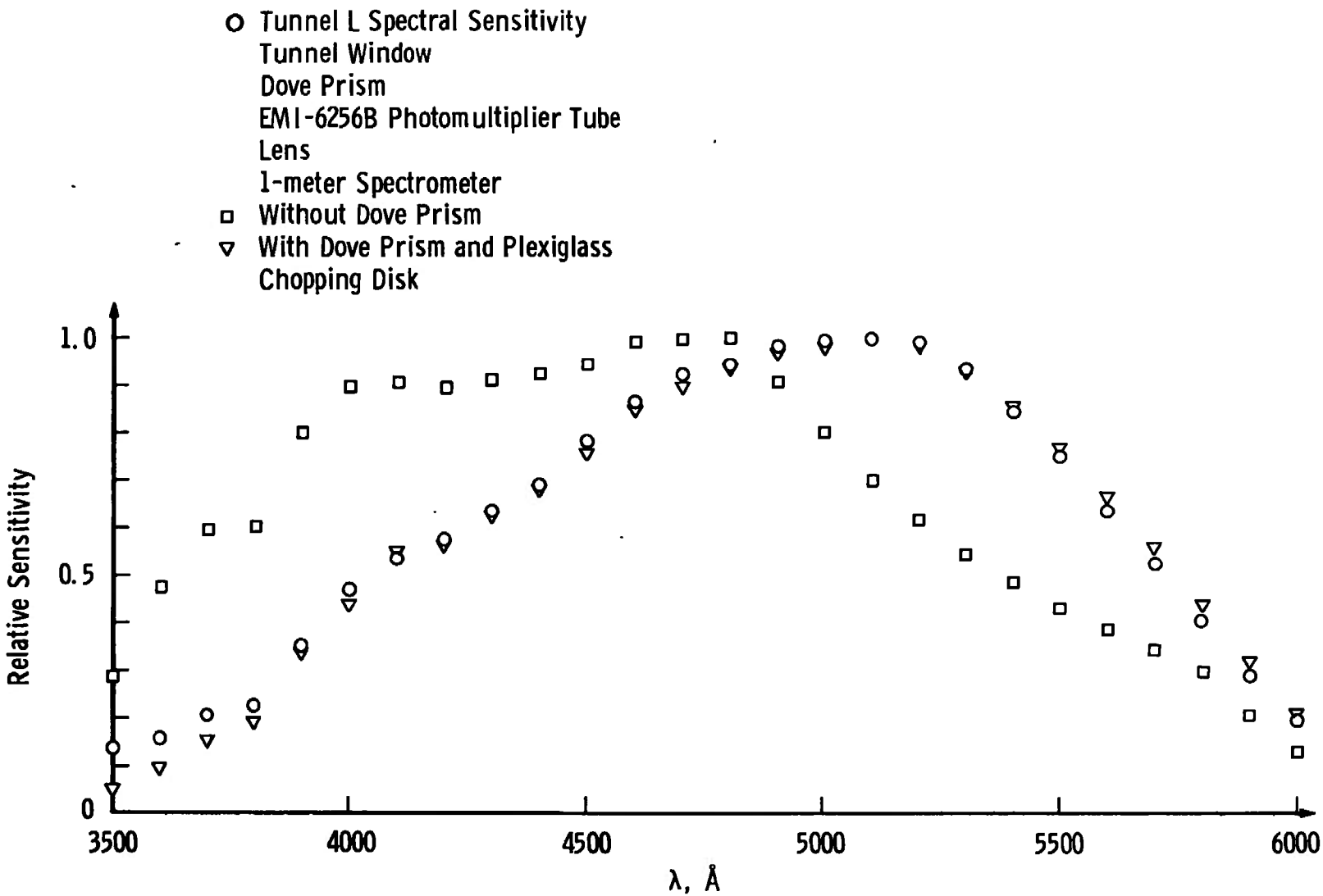

Fig. 13 Spectral Sensitivity of Spectrometer Optical System for Tunnel L

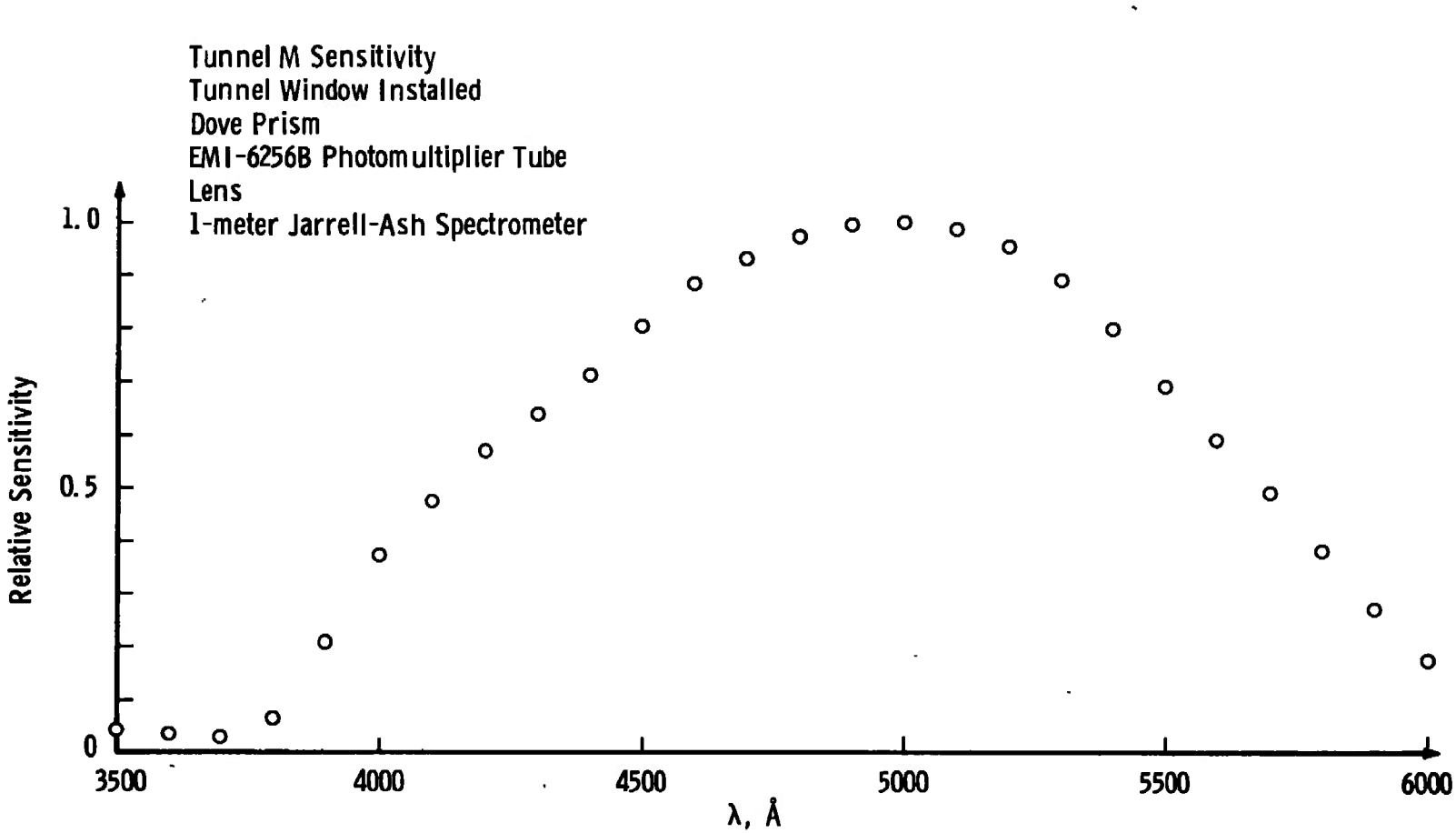

Fig. 14 Spectral Sensitivity of Spectrometer Optical System for Tunnel M

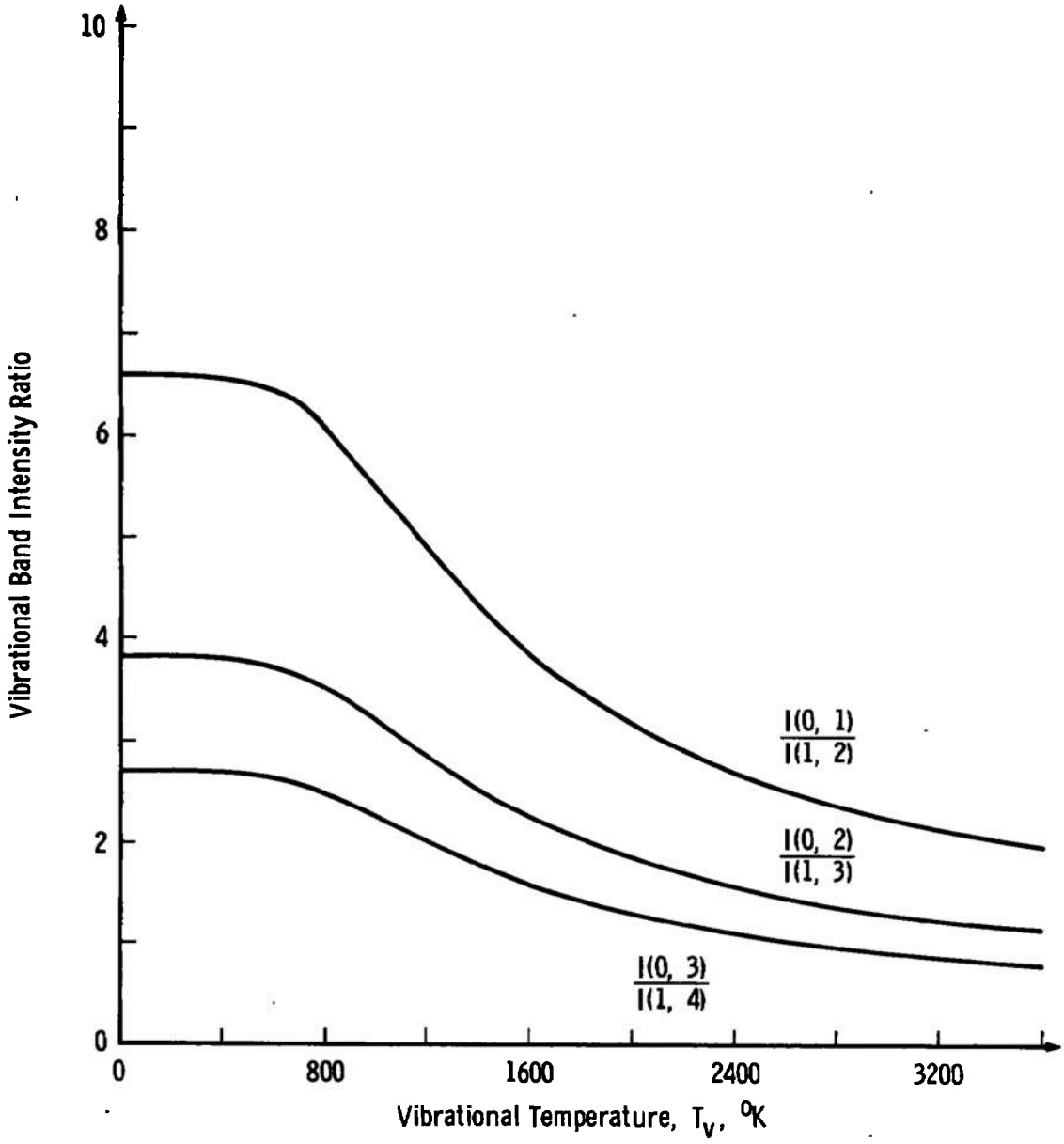

Fig. 15 Theoretical Vibrational Band Intensity Ratios versus Vibrational Temperature

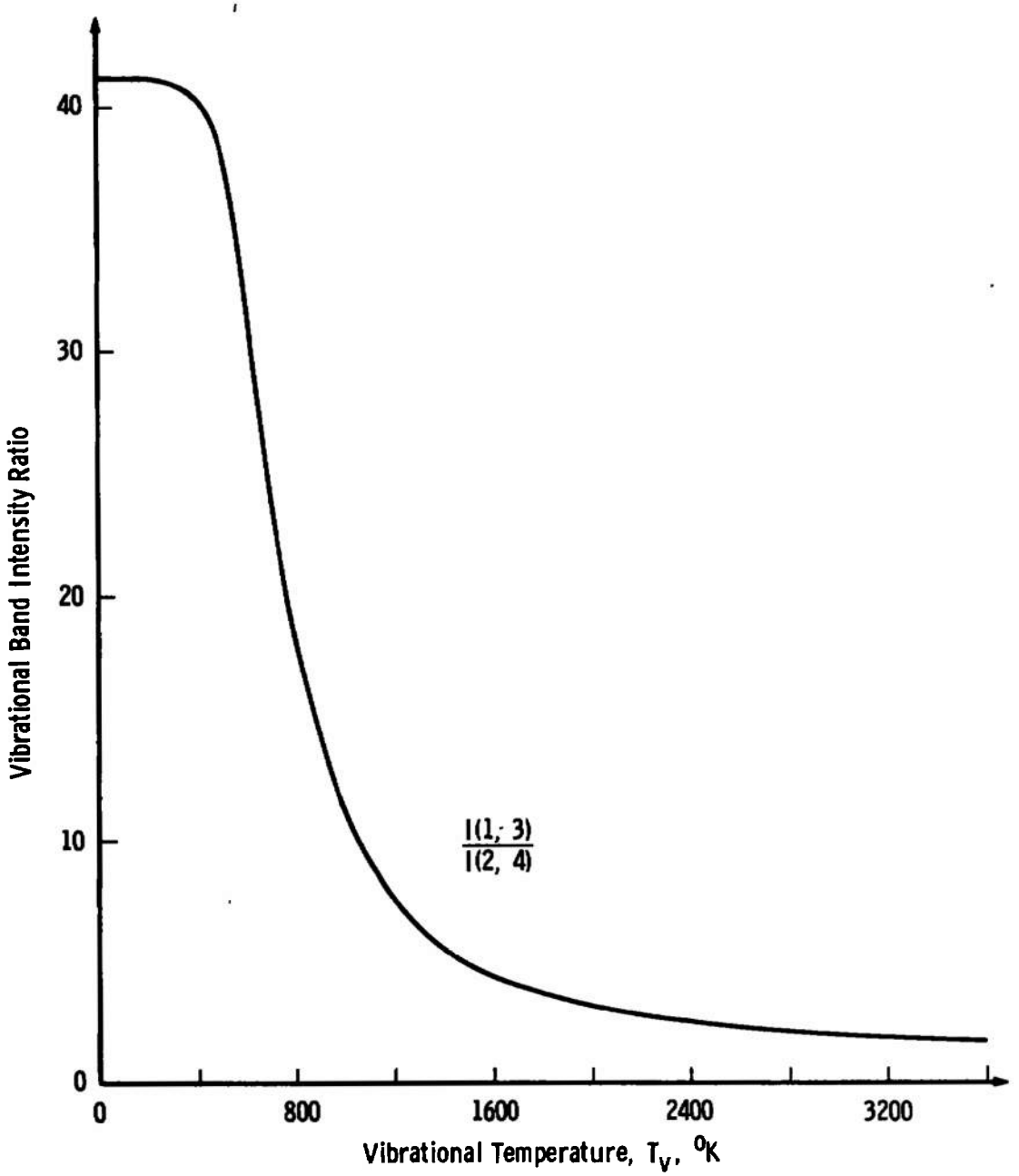

Fig. 16 Theoretical Vibrational Band Intensity Ratio versus Vibrational Temperature

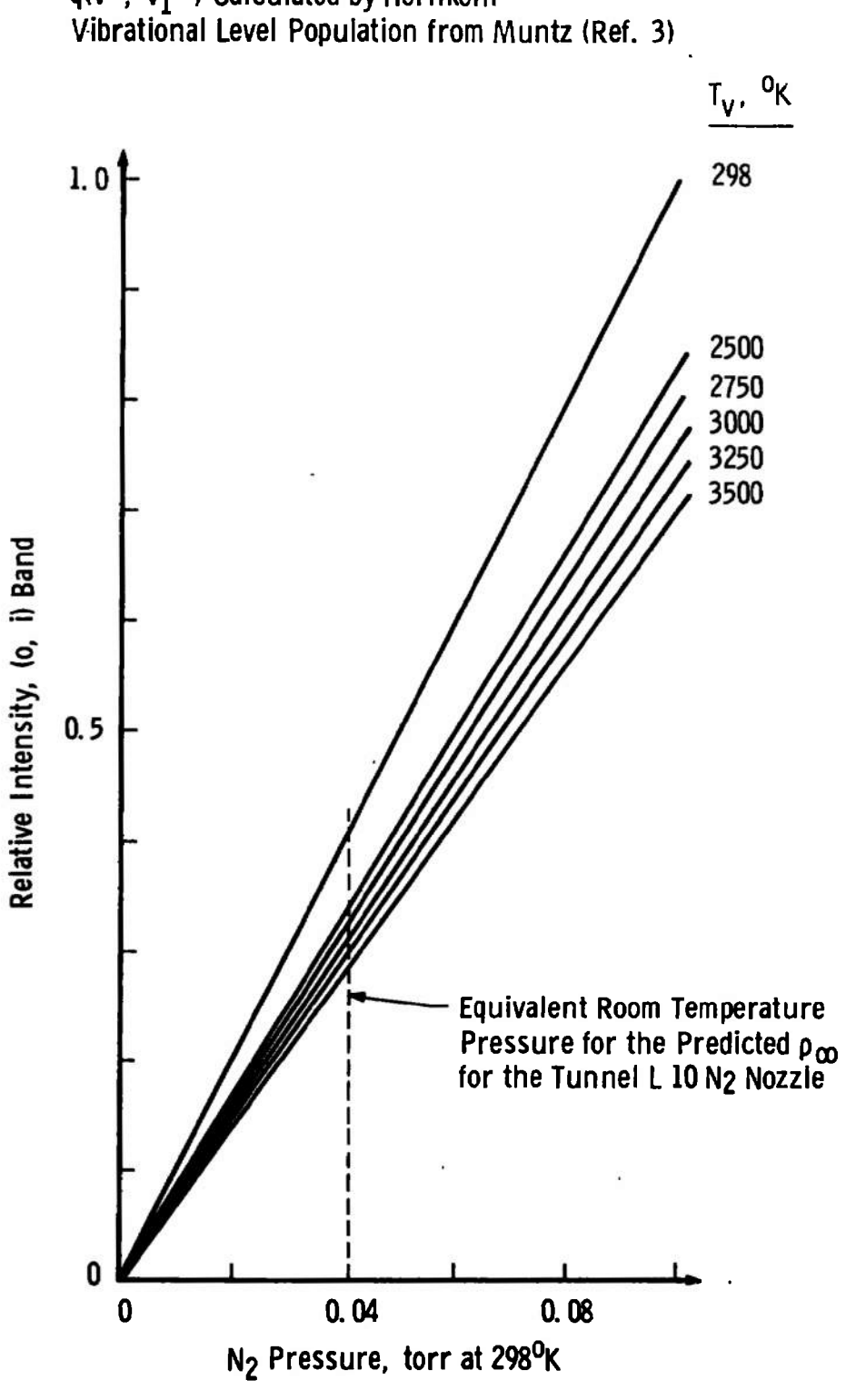

Fig. 17 (0, i) Band Relative Intensity as a Function of Density (ERTP) and T_v

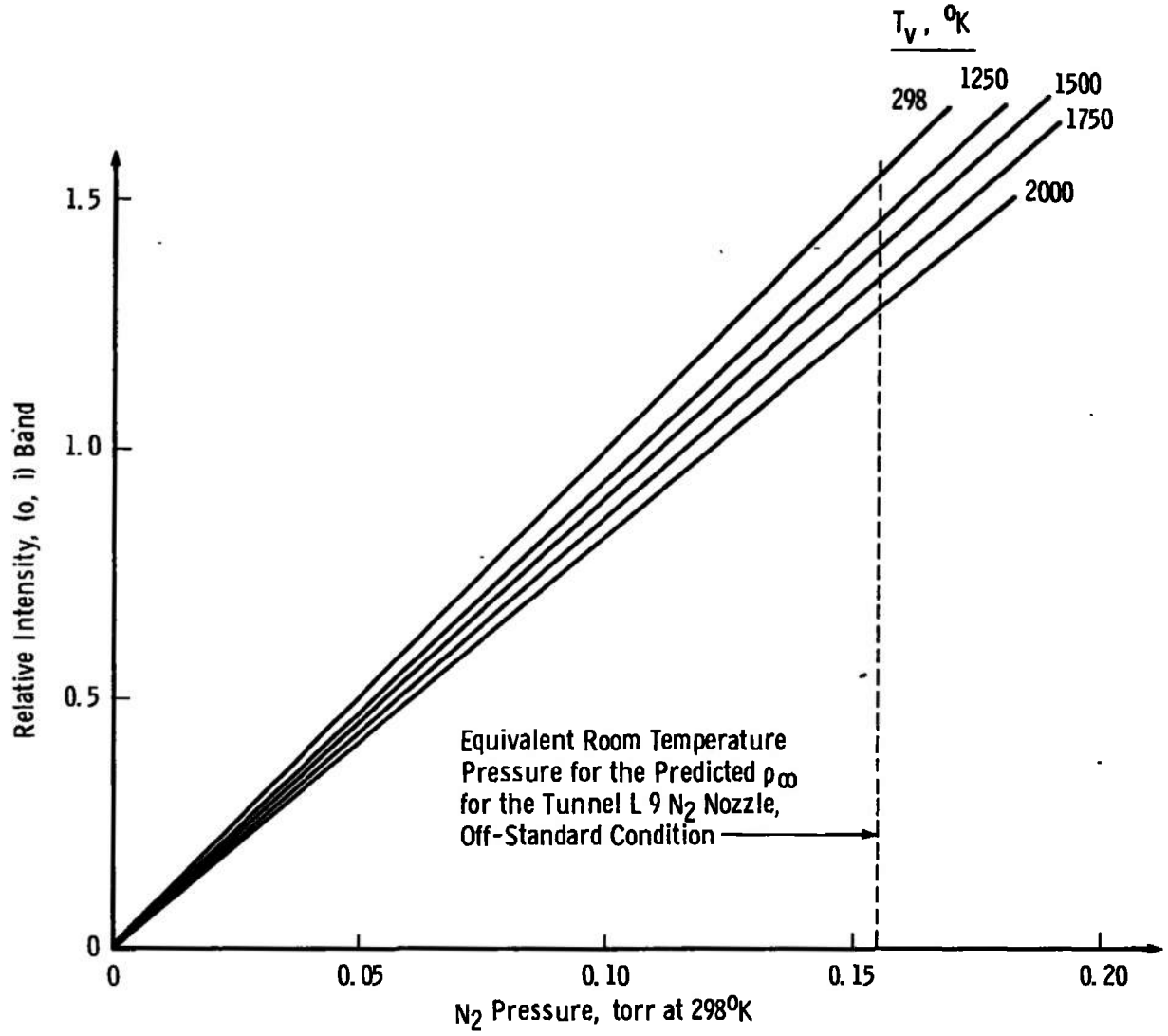

Fig. 18 (0, i) Band Relative Intensity as a Function of Density (ERTP) and T_v

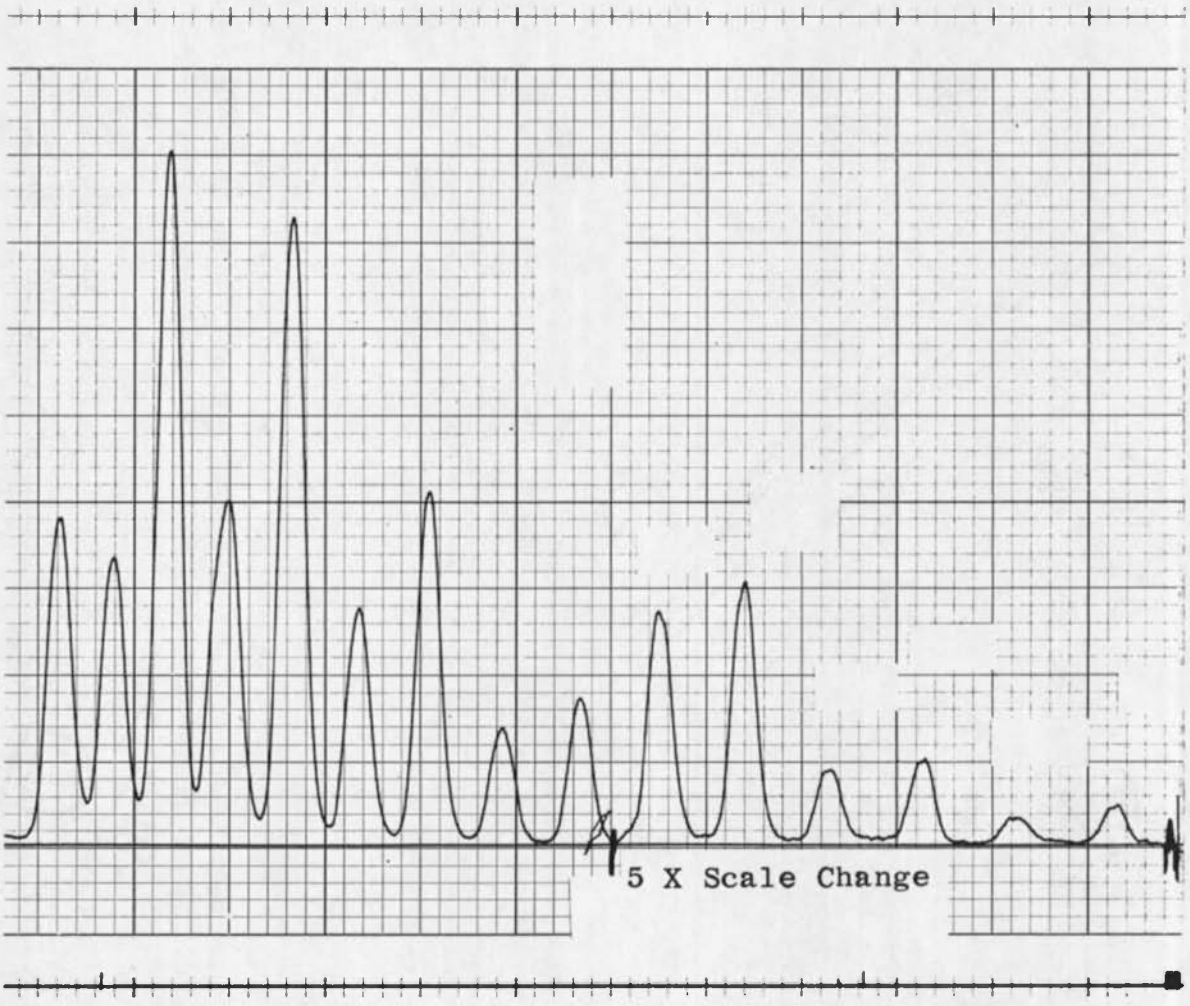

Fig. 19 Typical (0, 0) Band R-Branch Rotational Line Spectral Scan, 4 N_2 Nozzle, Standard Condition

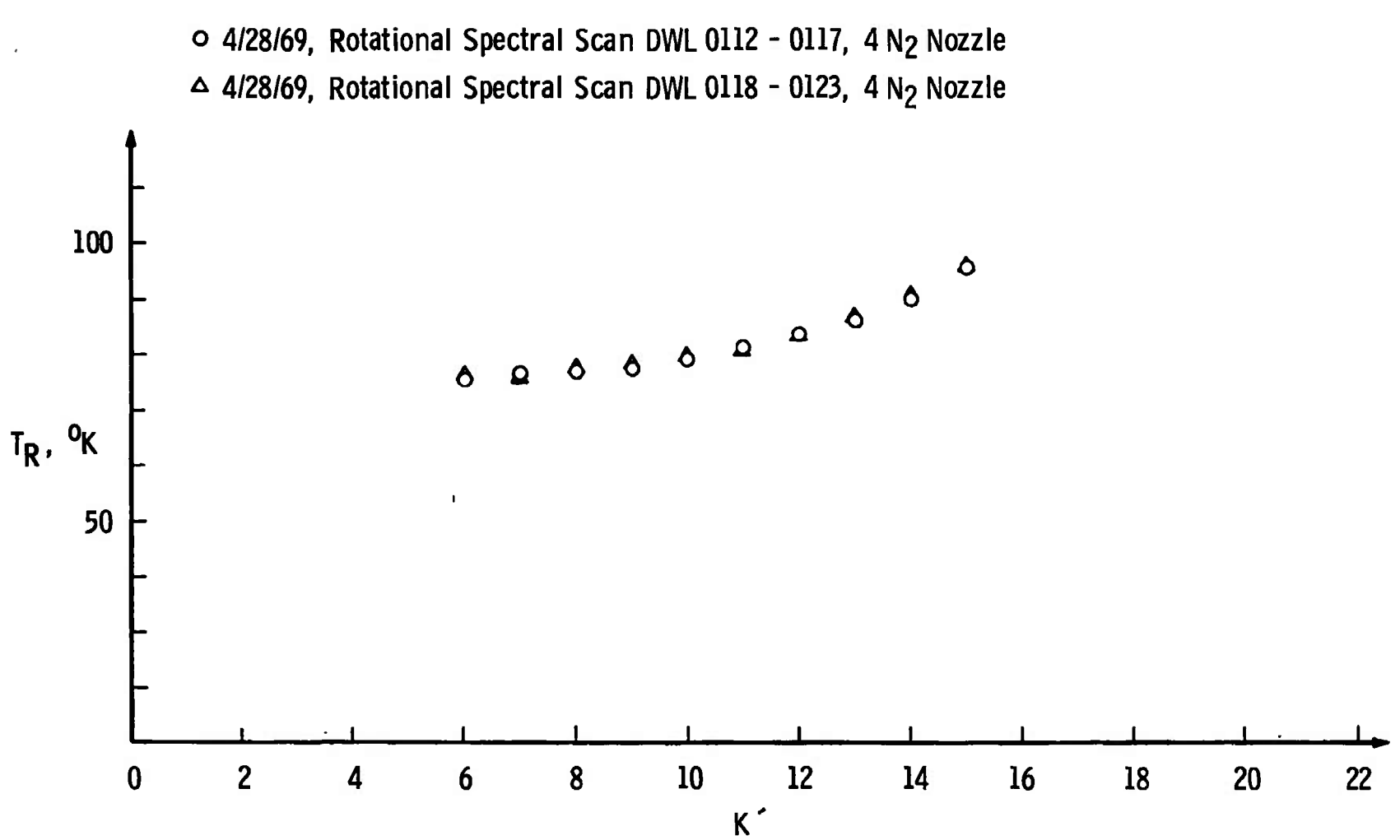

Fig. 20 Rotational Temperature versus Number of Rotational Lines Used in the Temperature Determination, 4 N_2 Nozzle, Standard Condition

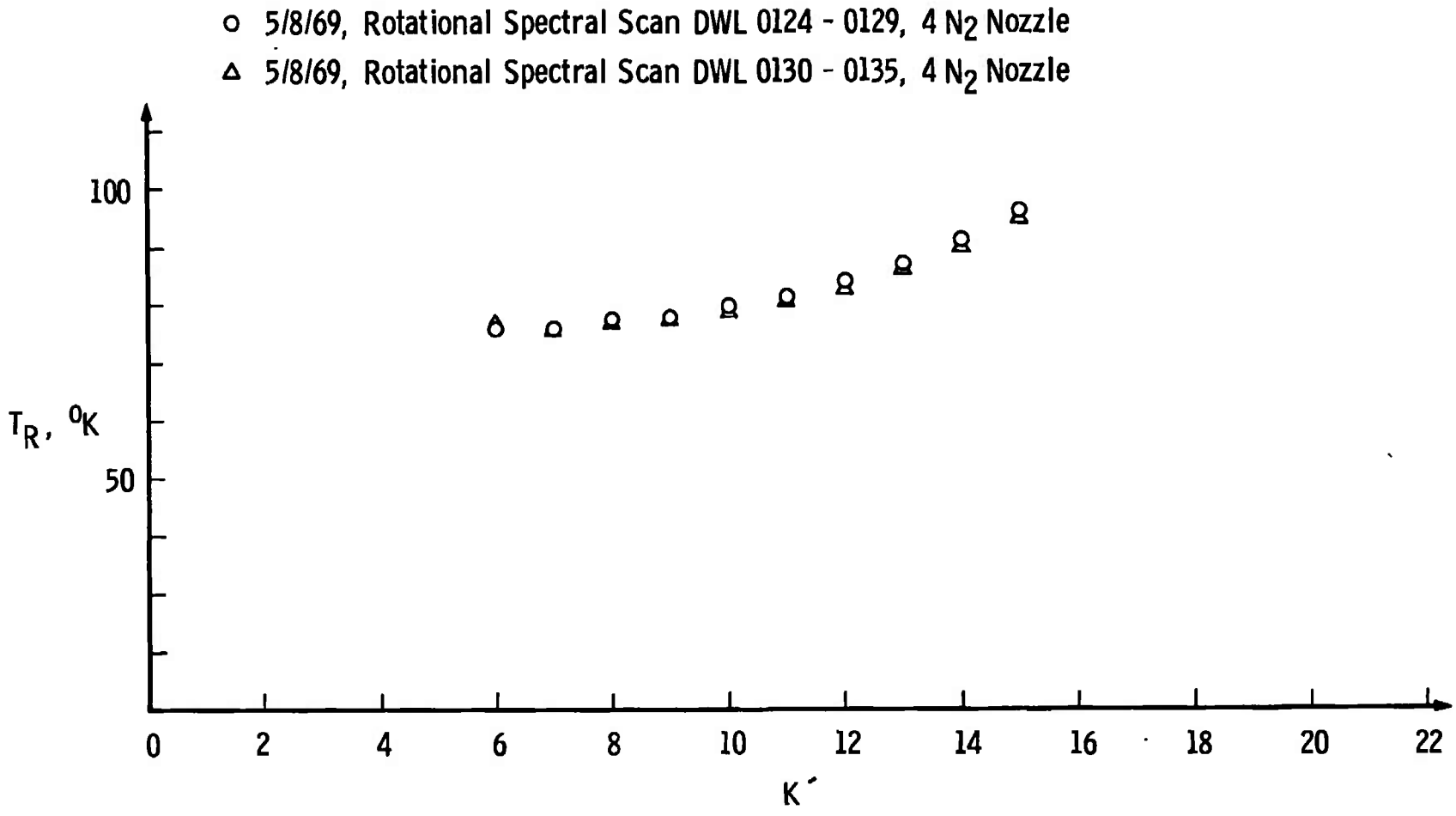

Fig. 21 Rotational Temperature versus Number of Rotational Lines Used in the Temperature Determination, 4 N_2 Nozzle, Off-Standard Condition

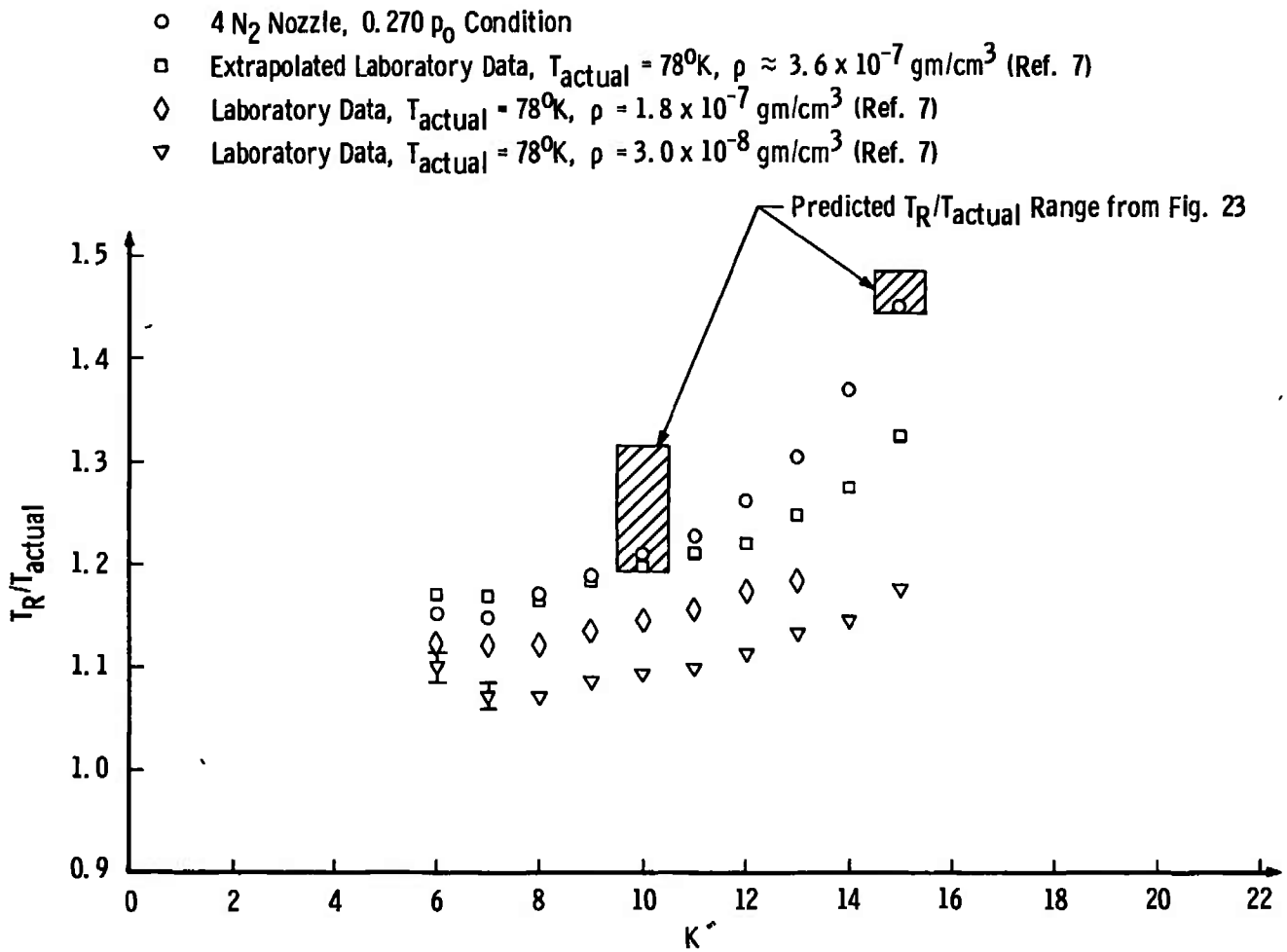

Fig. 22 Ratio of Measured Rotational Temperature to Actual or Predicted Temperature versus Number of Rotational Lines Used in the Temperature Determination, 4 N_2 Nozzle Data and 78° K Laboratory Data

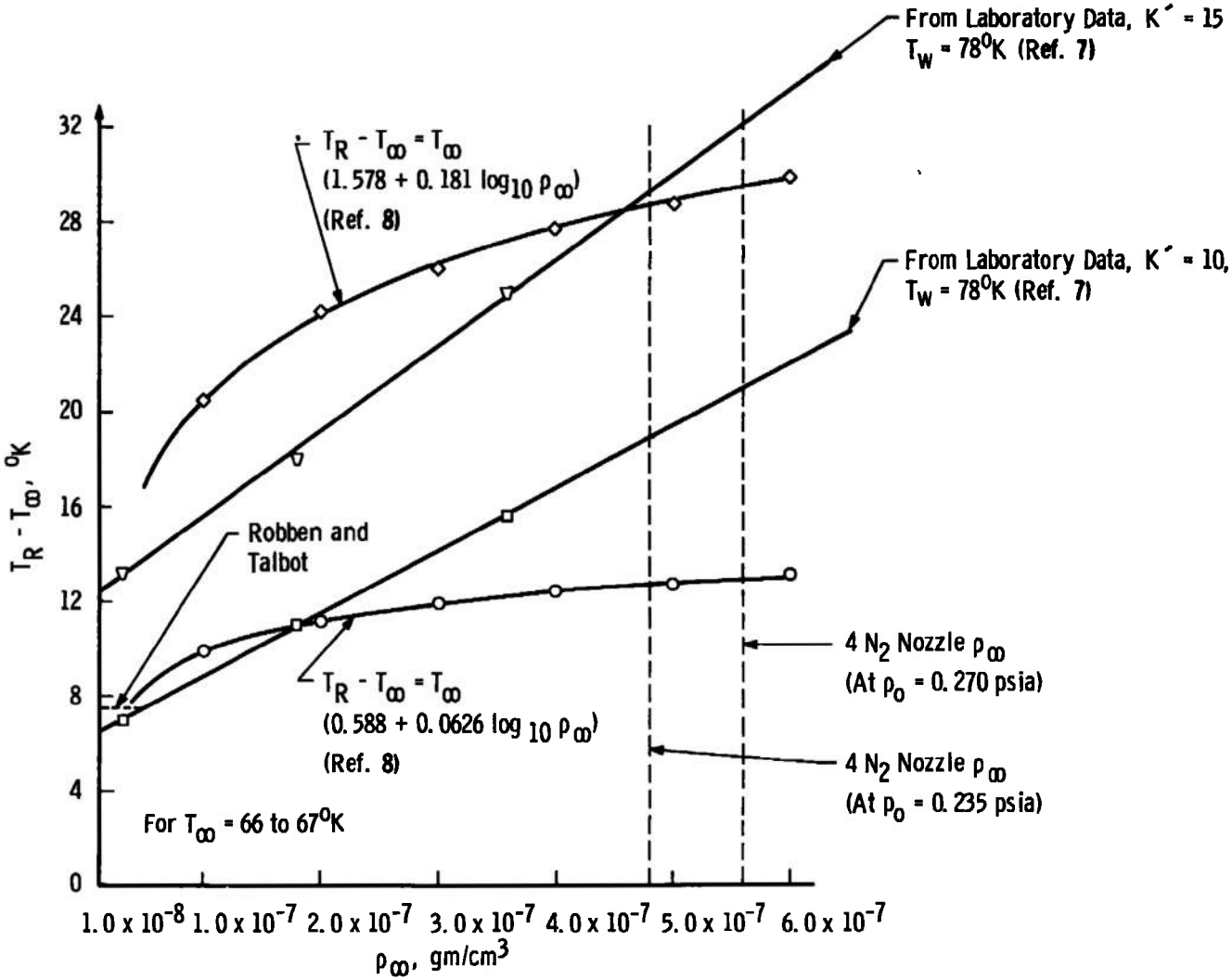

Fig. 23 Empirical Prediction of Rotational Temperature Measurement as a Function of Nitrogen Density and Number of Rotational Lines Used for Temperatures Near 78°K

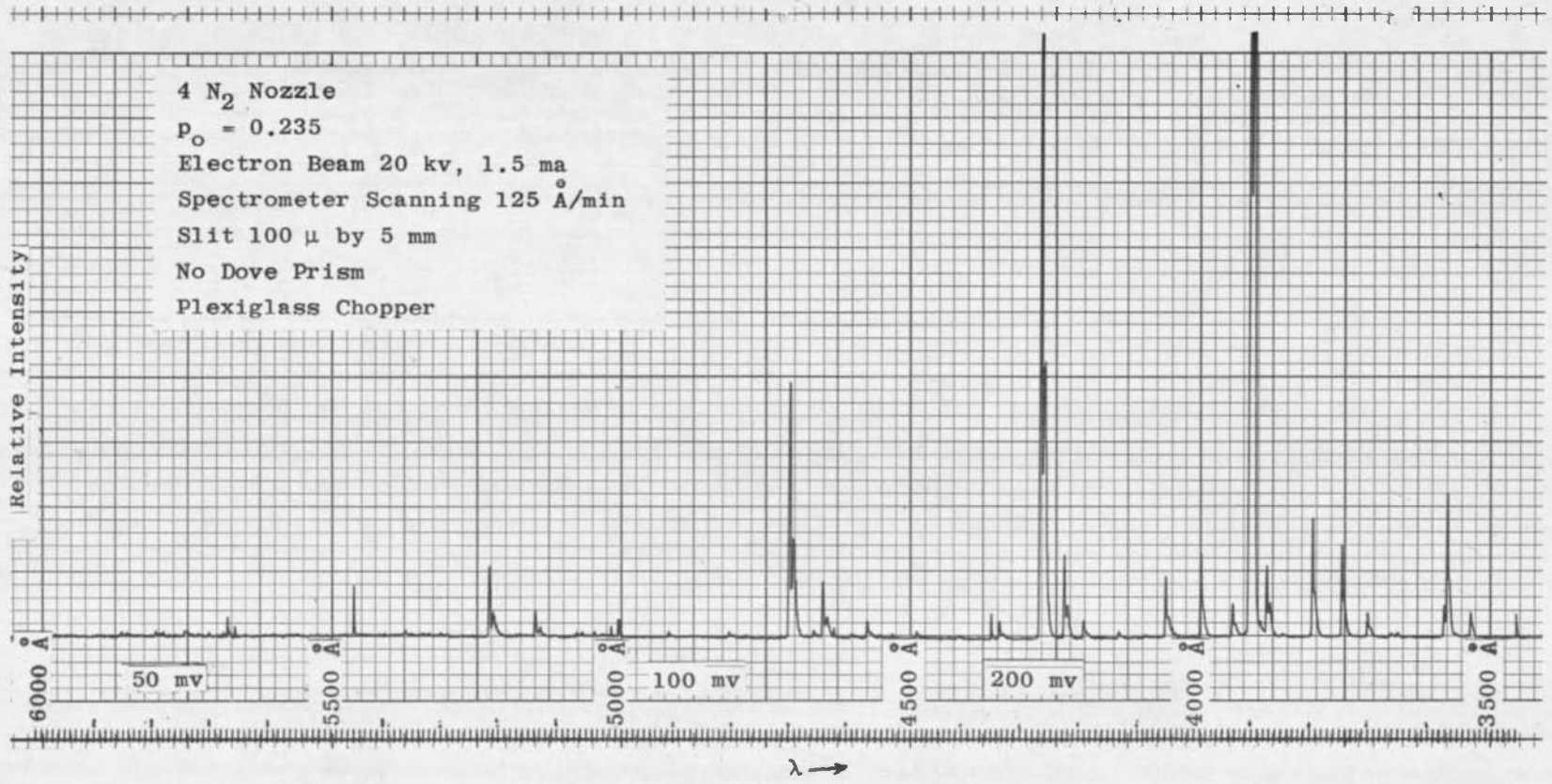

Fig. 24 Electron Beam Induced Radiation, 4 N_2 Nozzle, Standard Condition

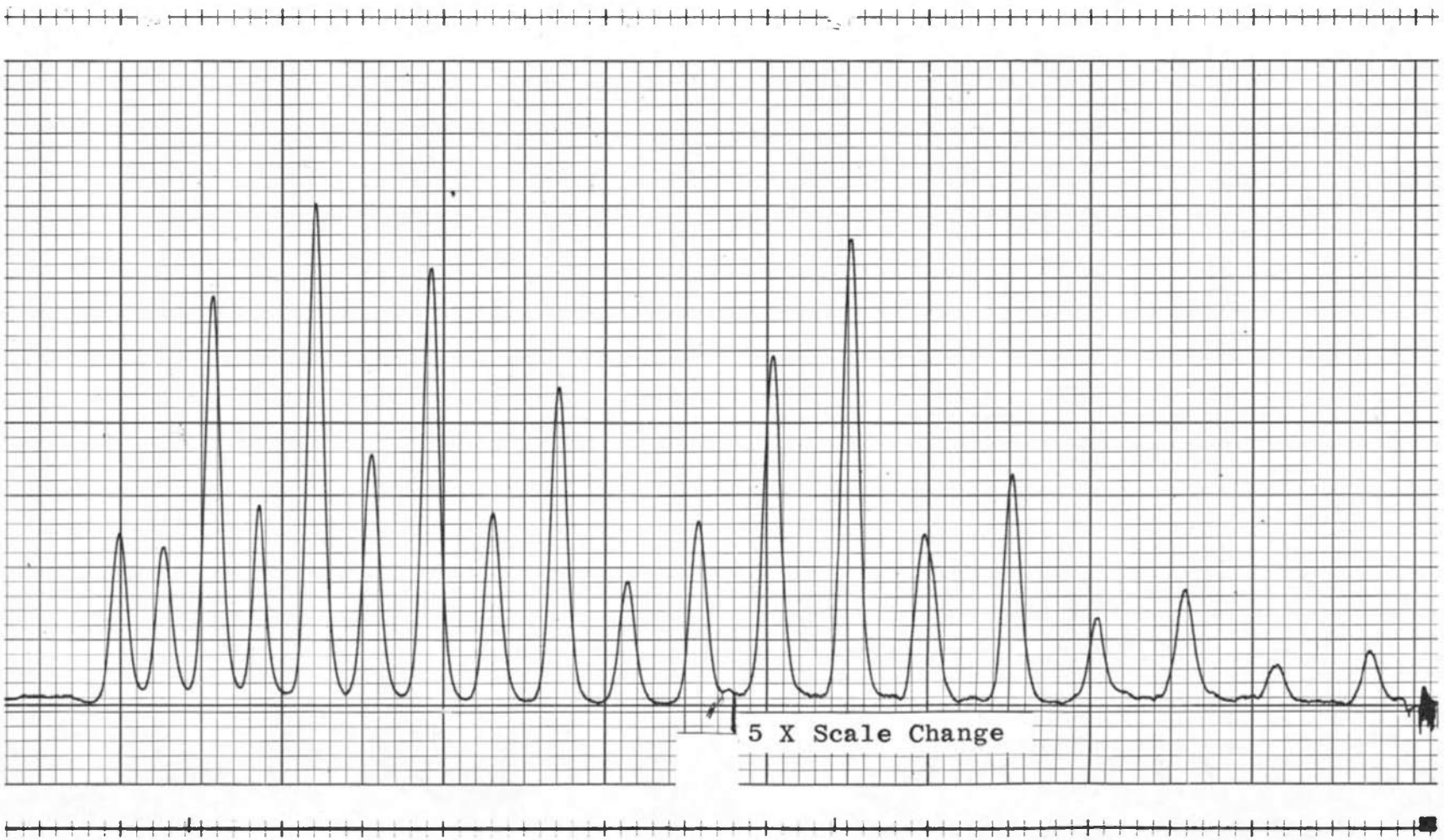

Fig. 25 Typical (0, 0) Band R-Branch Rotational Line Spectral Scan, 9 N_2 Nozzle, Standard Condition

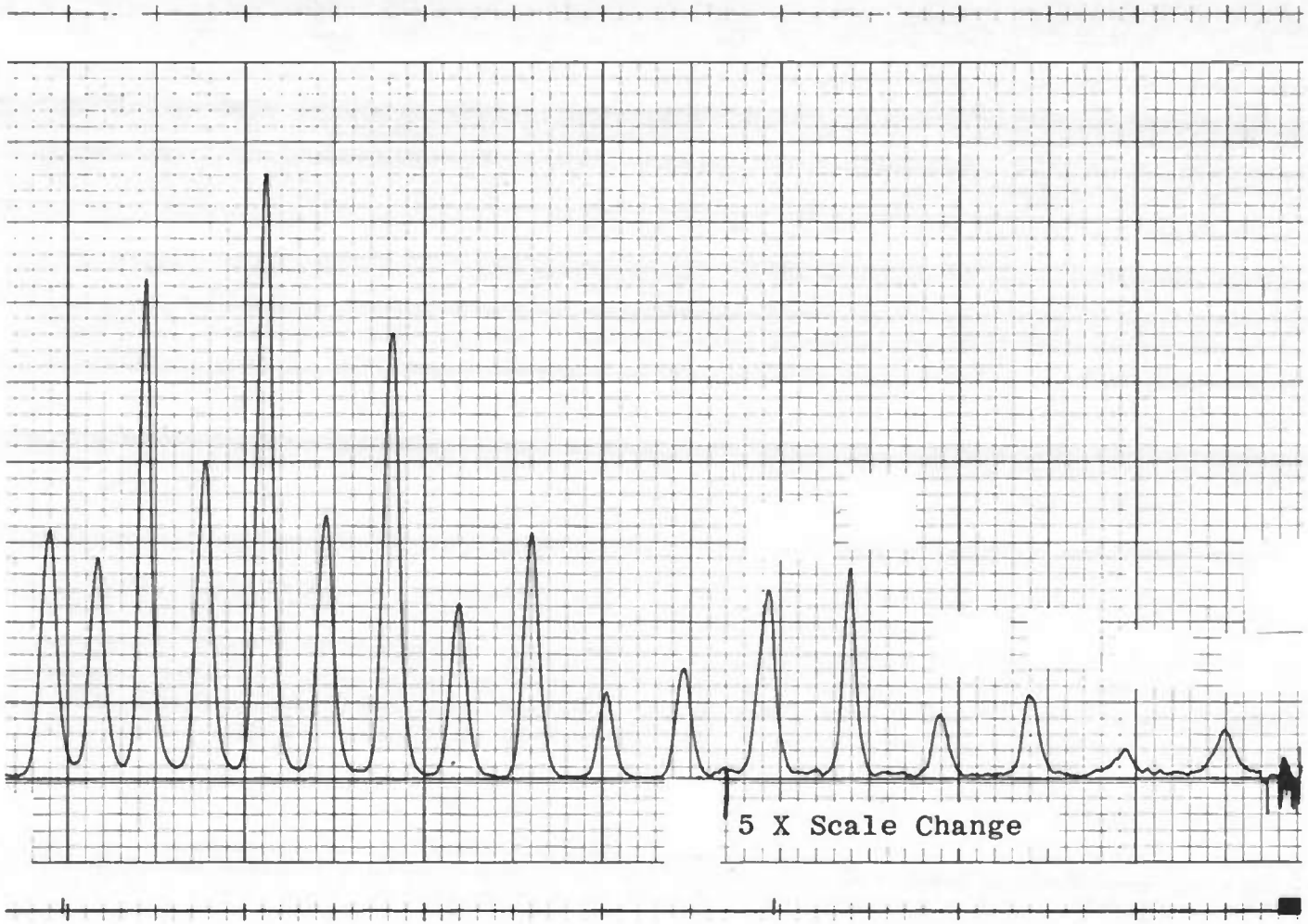

Fig. 26 Typical (0, 0) Band R-Branch Rotational Line Spectral Scan, 9 N_2 Nozzle, Off-Standard Condition

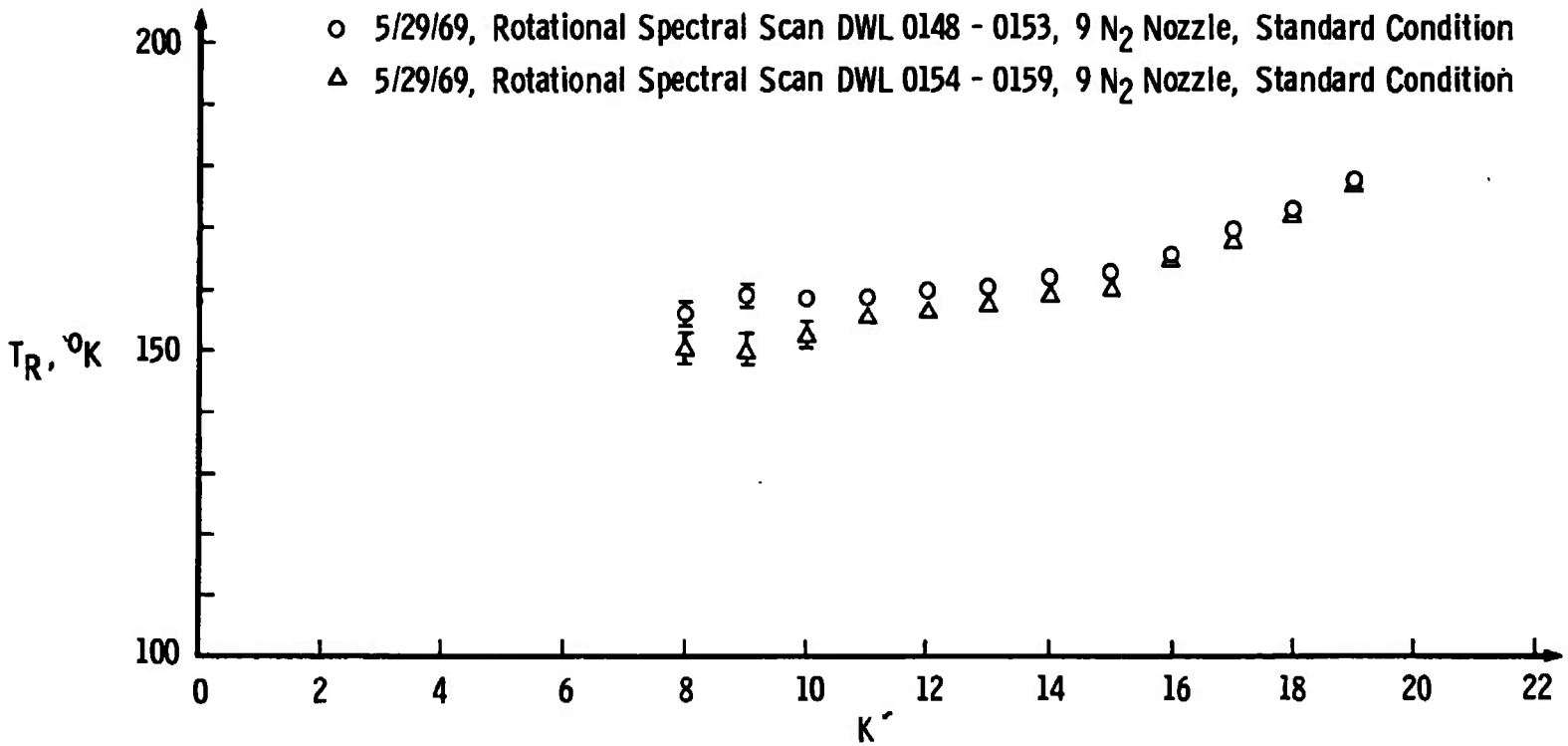

Fig. 27 Rotational Temperature versus Number of Rotational Lines Used in the Temperature Determination, 9 N_2 Nozzle, Standard Condition

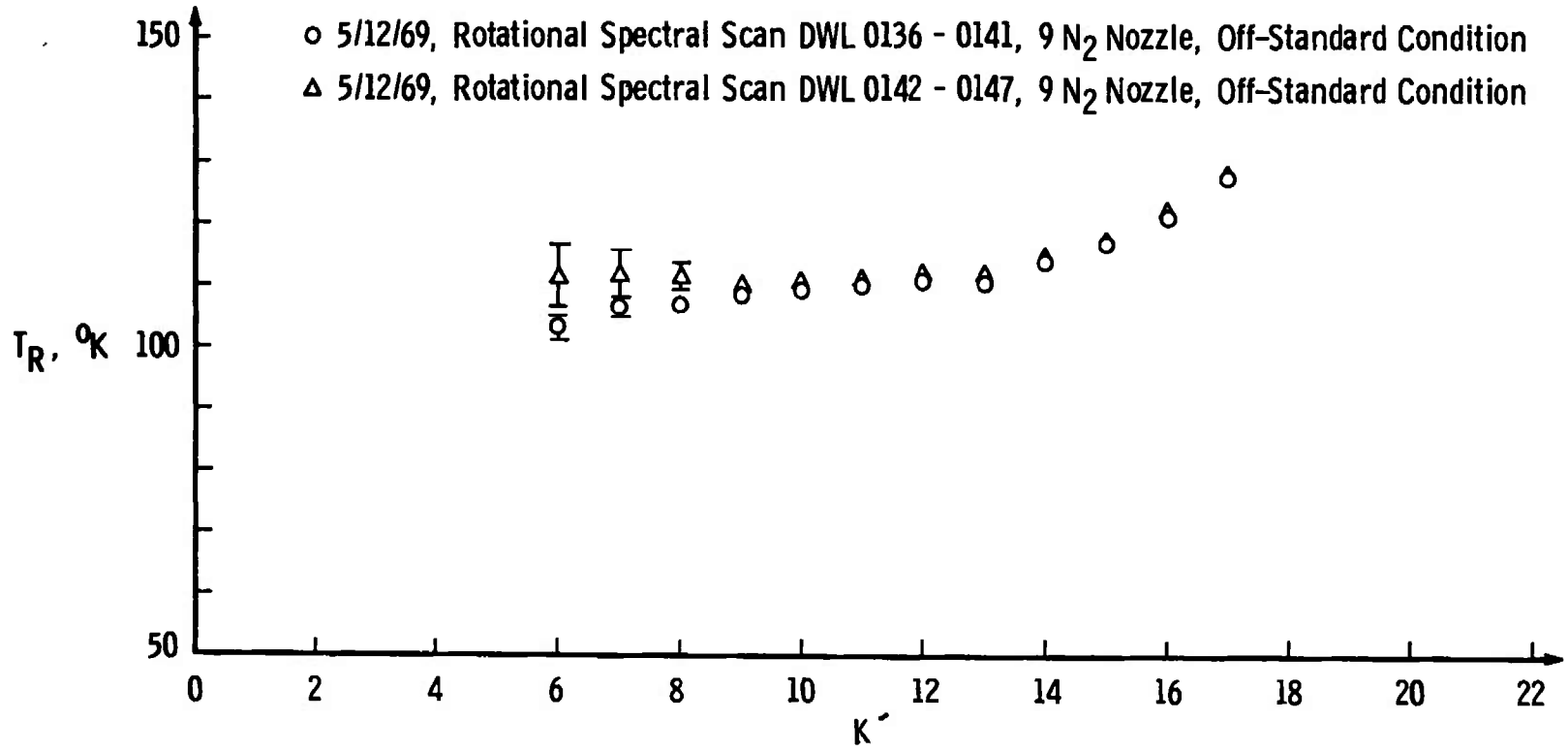

Fig. 28 Rotational Temperature versus Number of Rotational Lines Used in the Temperature Determination, 9 N_2 Nozzle, Off-Standard Condition

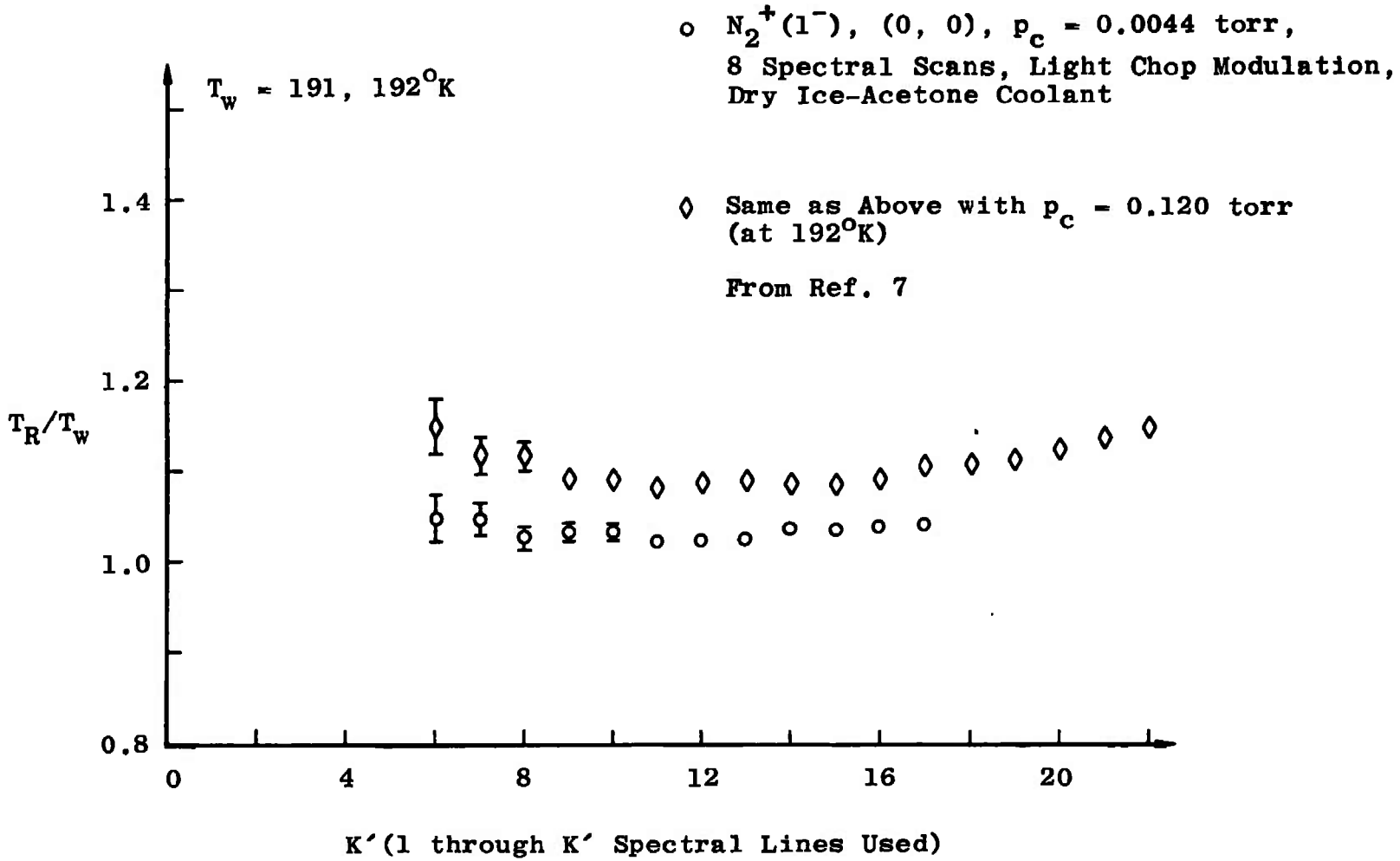

Fig. 29 Ratio of Measured Rotational Temperature to Chamber Wall Temperature versus Number of Spectral Lines Used for the Temperature Determination with Chamber Pressure as a Parameter

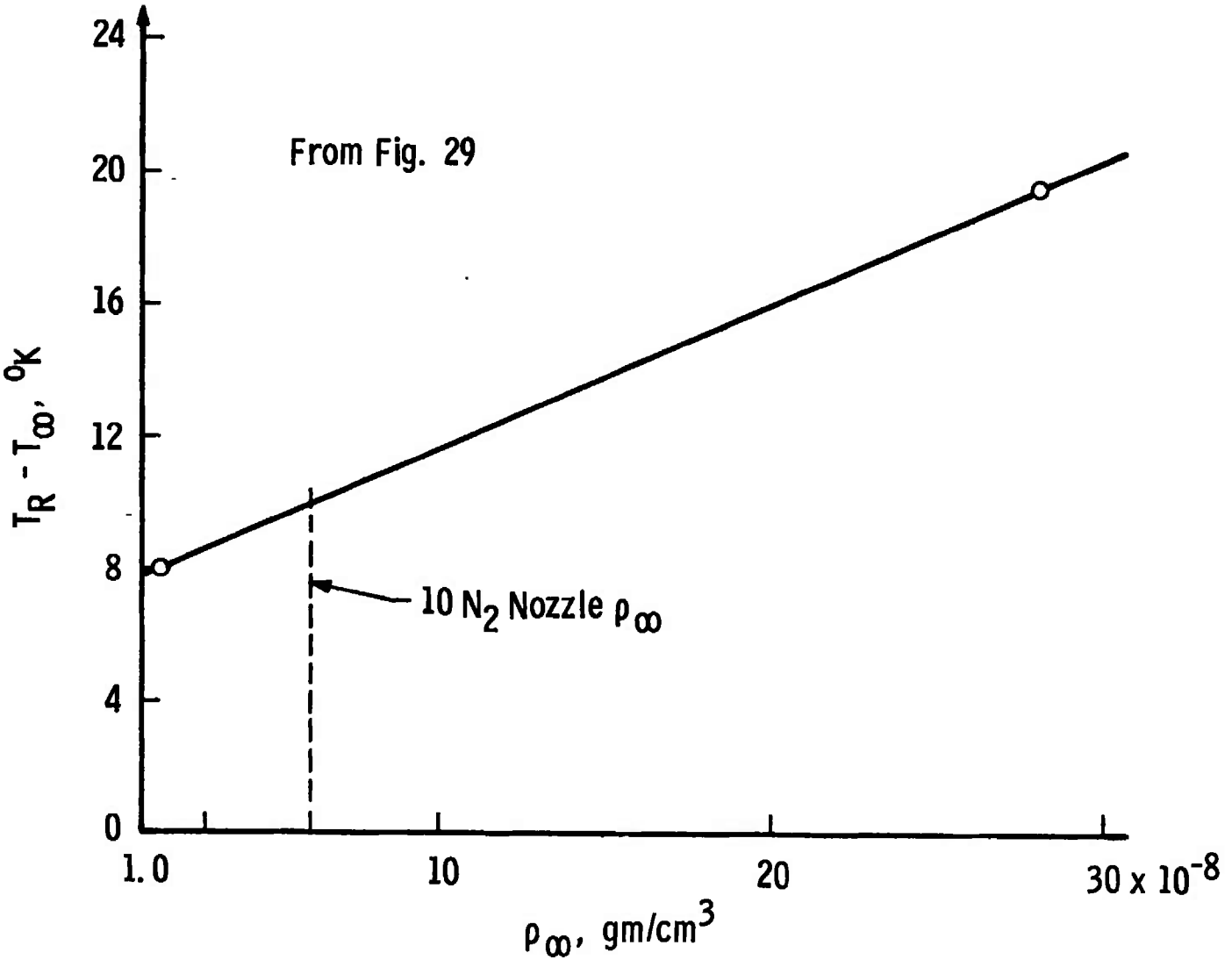

Fig. 30 Empirical Prediction of Rotational Temperature Measurement as a Function of Nitrogen Density for Temperatures Near 192°K

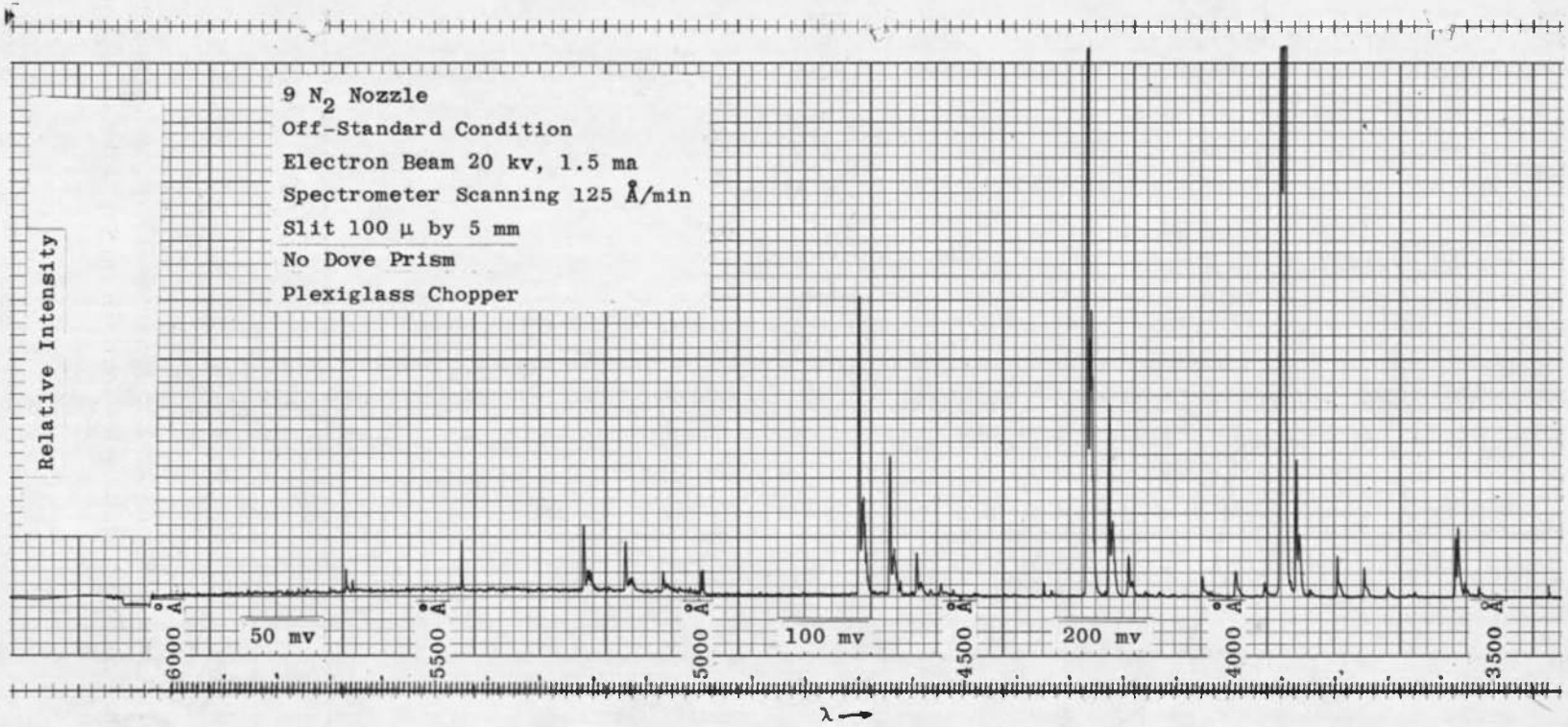

Fig. 31 Electron Beam Induced Radiation, 9 N_2 Nozzle, Off-Standard Condition

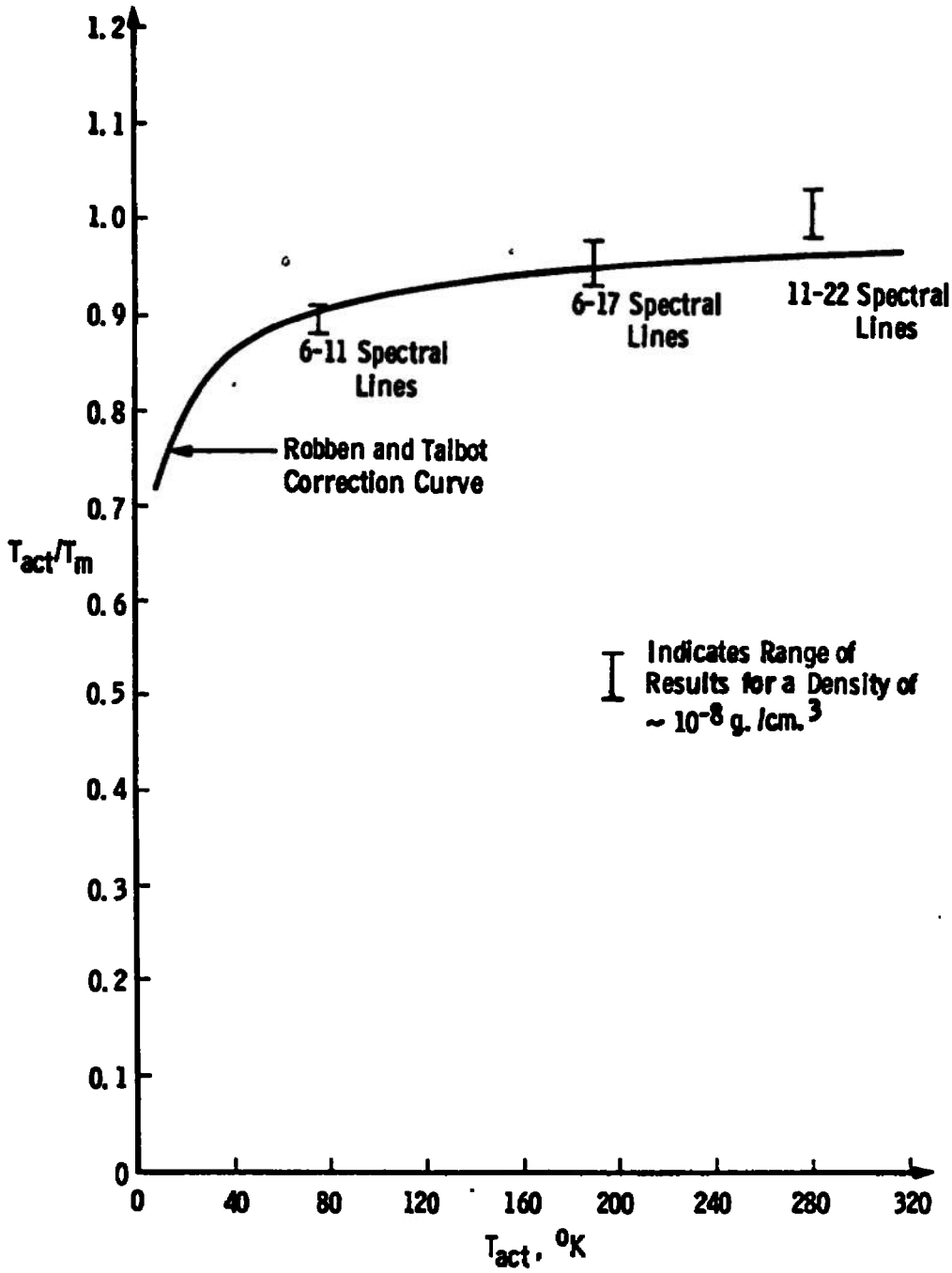

Fig. 32 Ratio of Actual Temperature to Measured Rotational Temperature versus Actual Temperature for Densities on the Order of 10^{-8} gm/cm^3

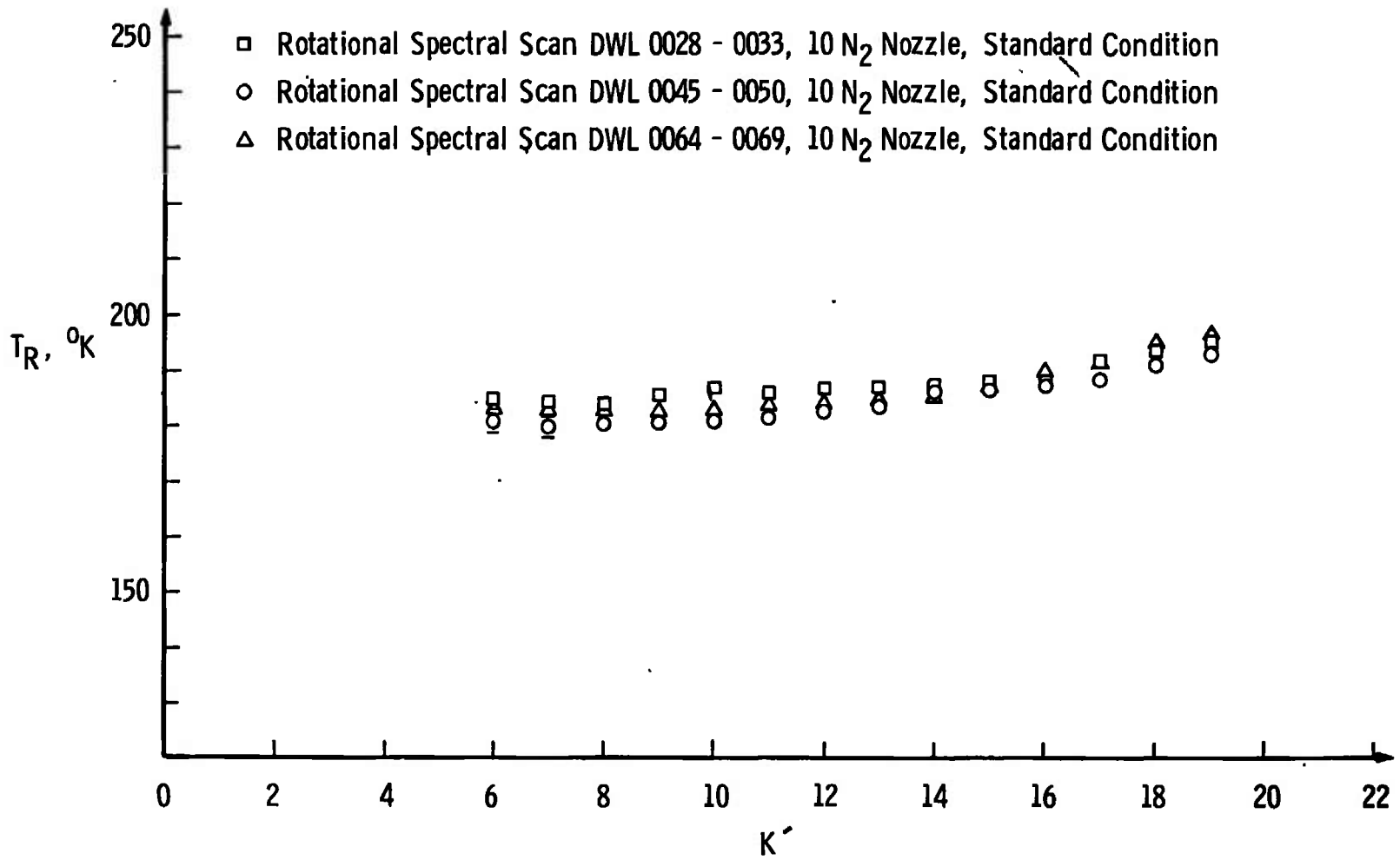

Fig. 33 Rotational Temperature versus Number of Rotational Lines Used in the Temperature Determination, 10 N_2 Nozzle, Standard Condition

Fig. 34 Typical (0, 0) Band R-Branch Rotational Line Spectral Scan, 10 N_2 Nozzle, Standard Condition

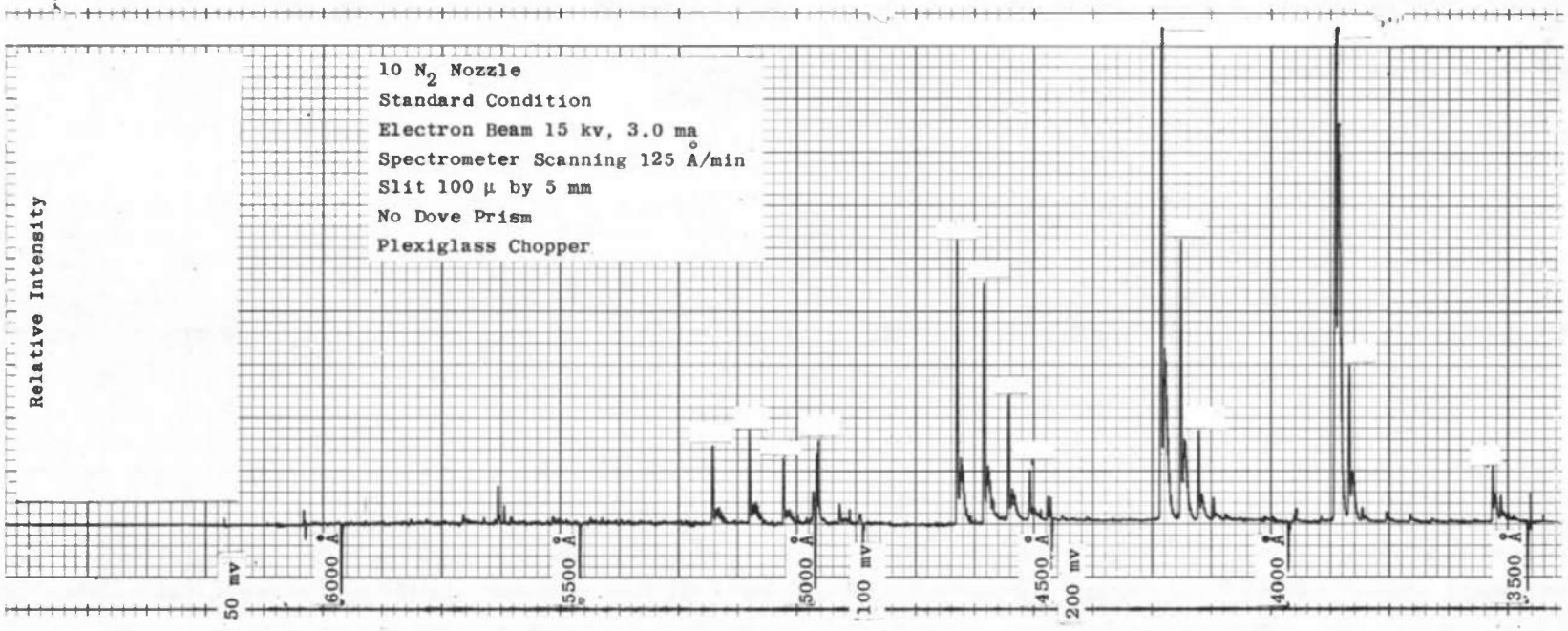

Fig. 35 Electron Beam Induced Radiation, 10 N_2 Nozzle, Standard Condition

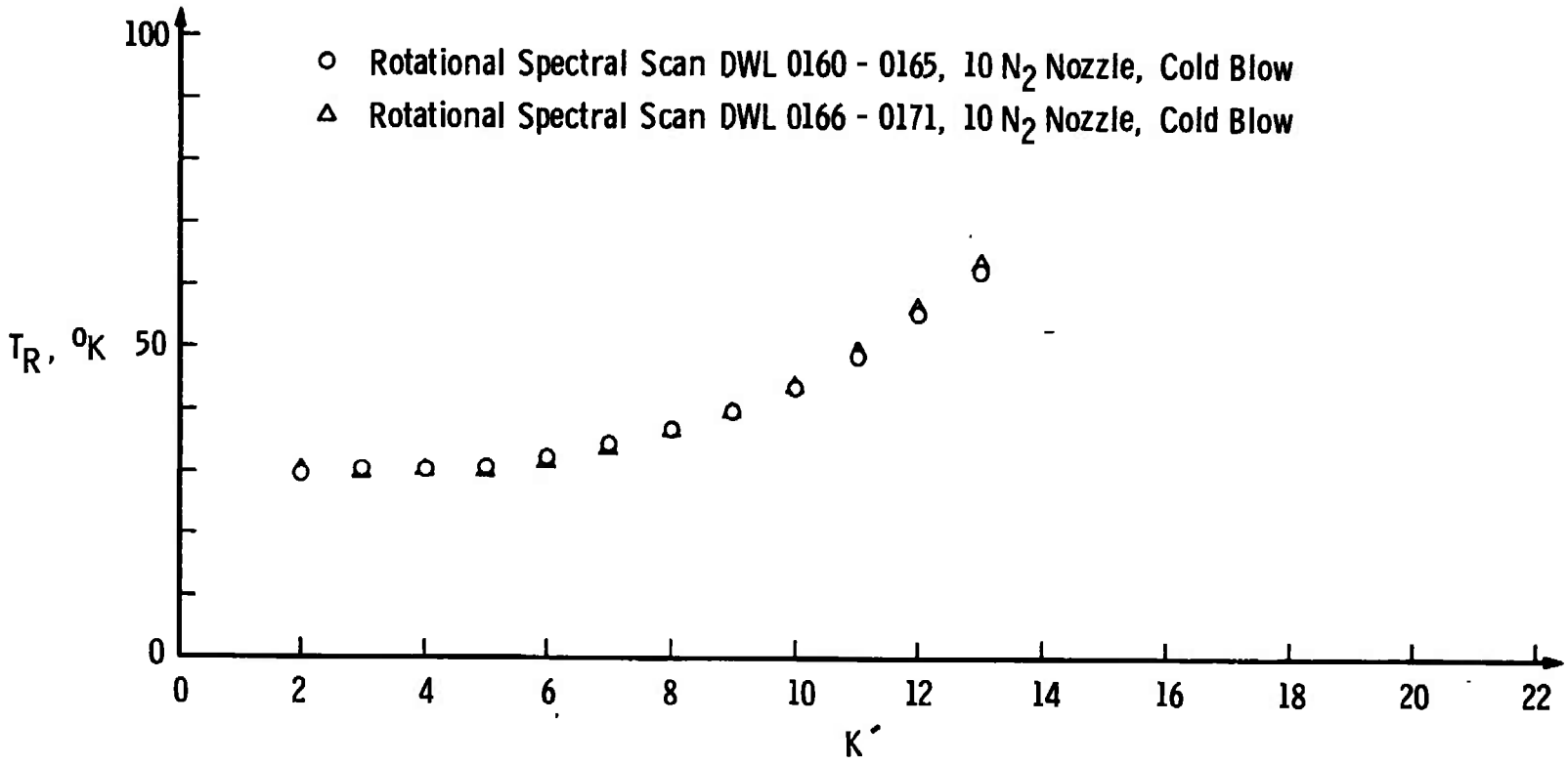

Fig. 36 Rotational Temperature versus Number of Rotational Lines Used in the Temperature Determination, 10 N_2 Nozzle, Cold-Blow Condition

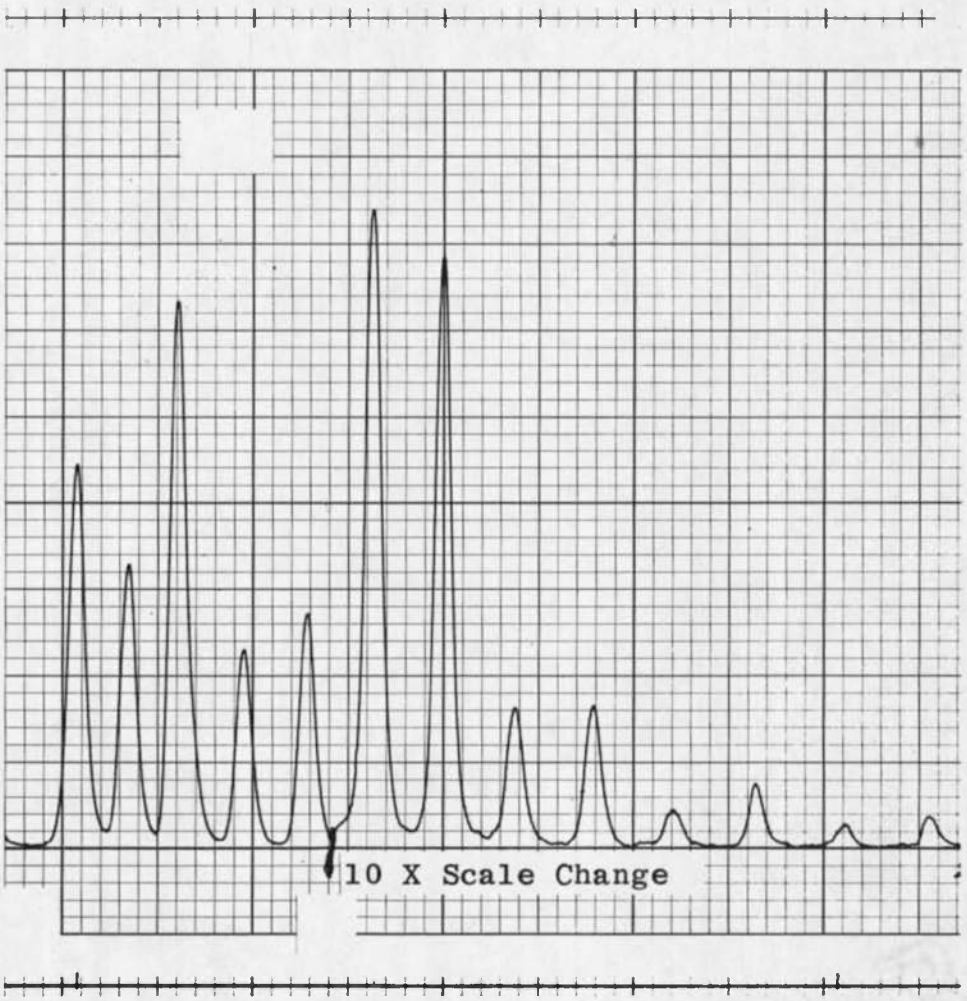

Fig. 37 Typical (0, 0) Band R-Branch Rotational Line Spectral Scan, 10 N_2 Nozzle, Cold-Blow Condition

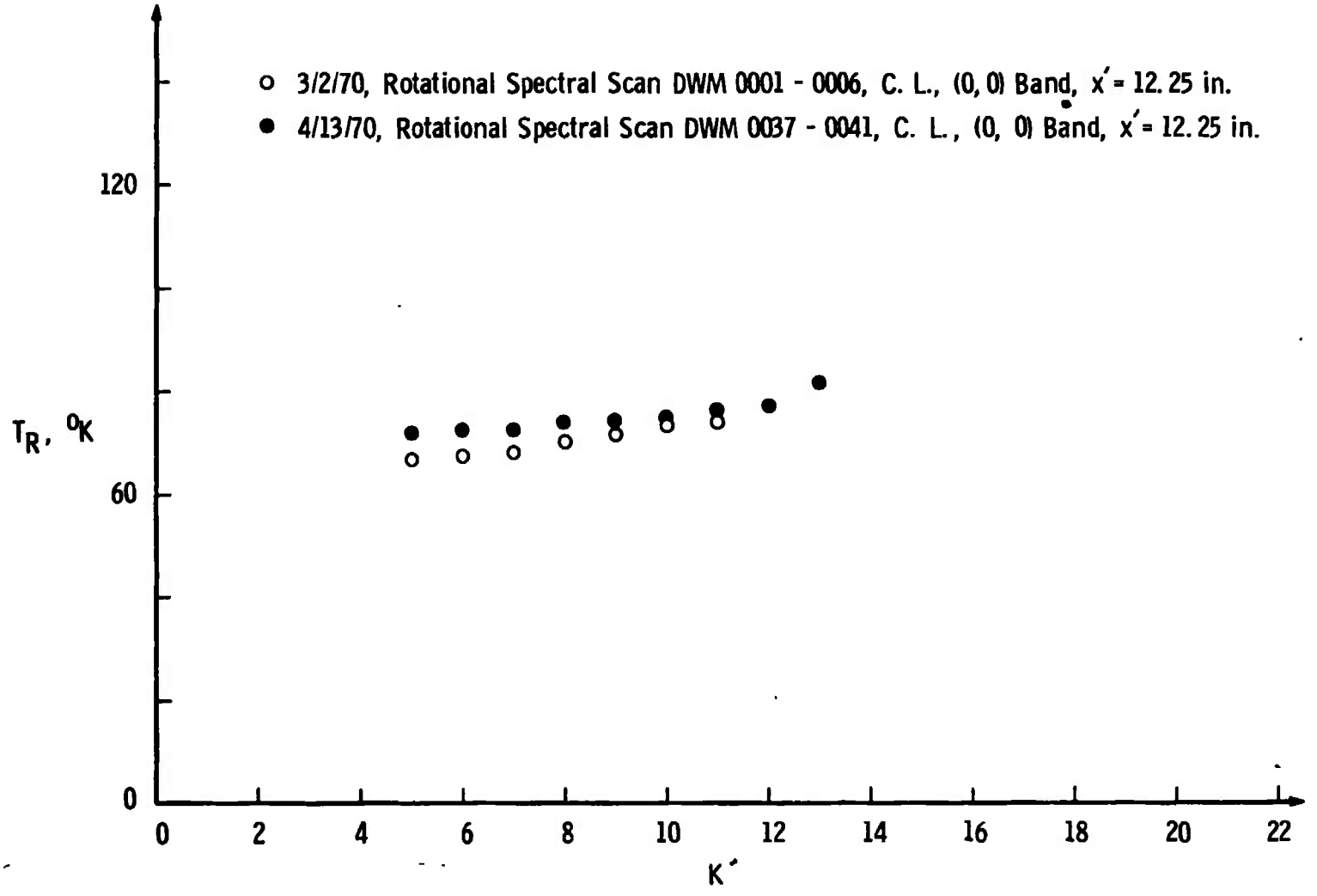

Fig. 38 Typical Rotational Temperature Plots versus Number of Rotational Lines Used in the Temperature Determination, 18 N_2 Nozzle, x′ = 12.25 Inches

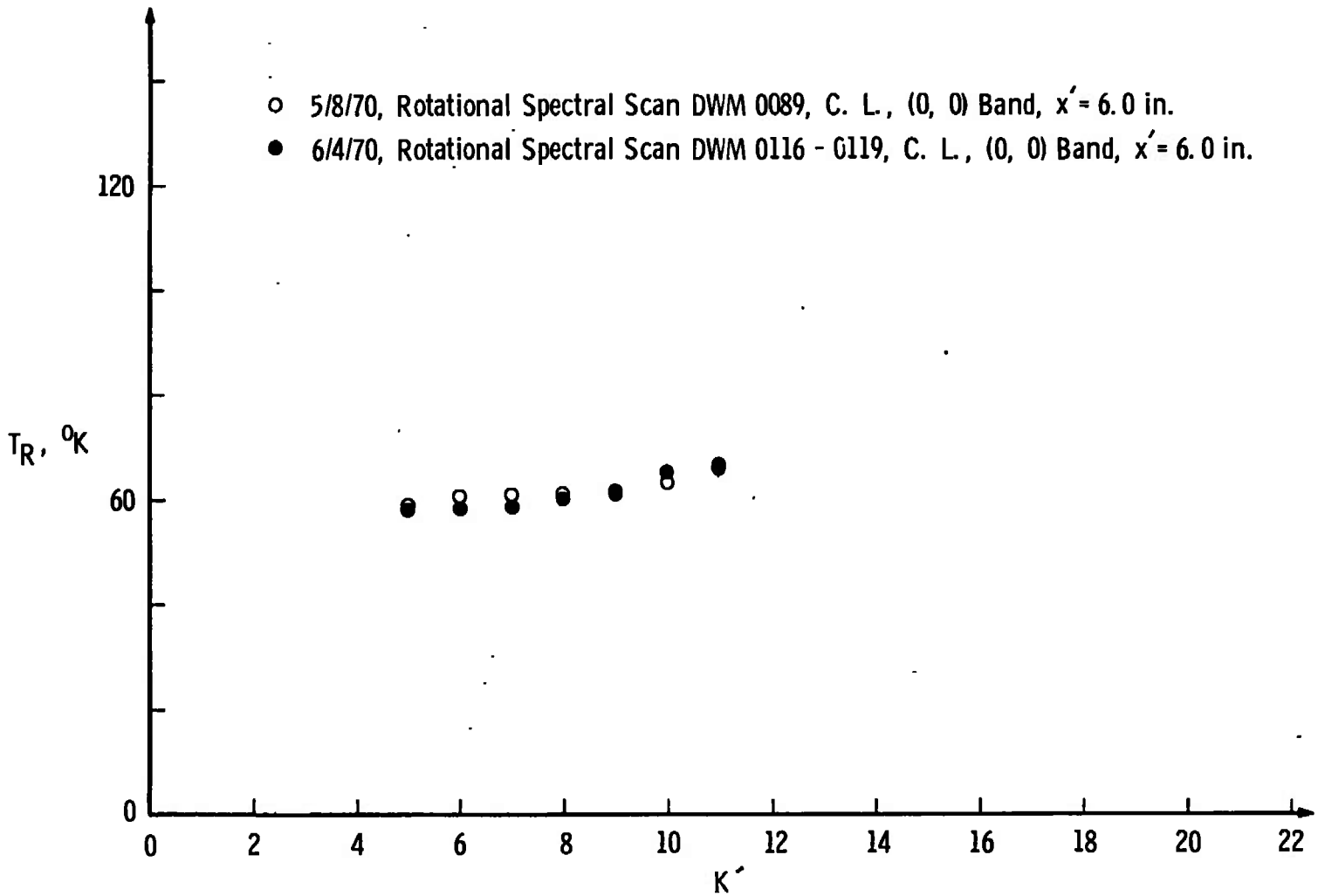

Fig. 39 Typical Rotational Temperature Plots versus Number of Rotational Lines Used in the Temperature Determination, 18 N_2 Nozzle, x' = 6.0 Inches

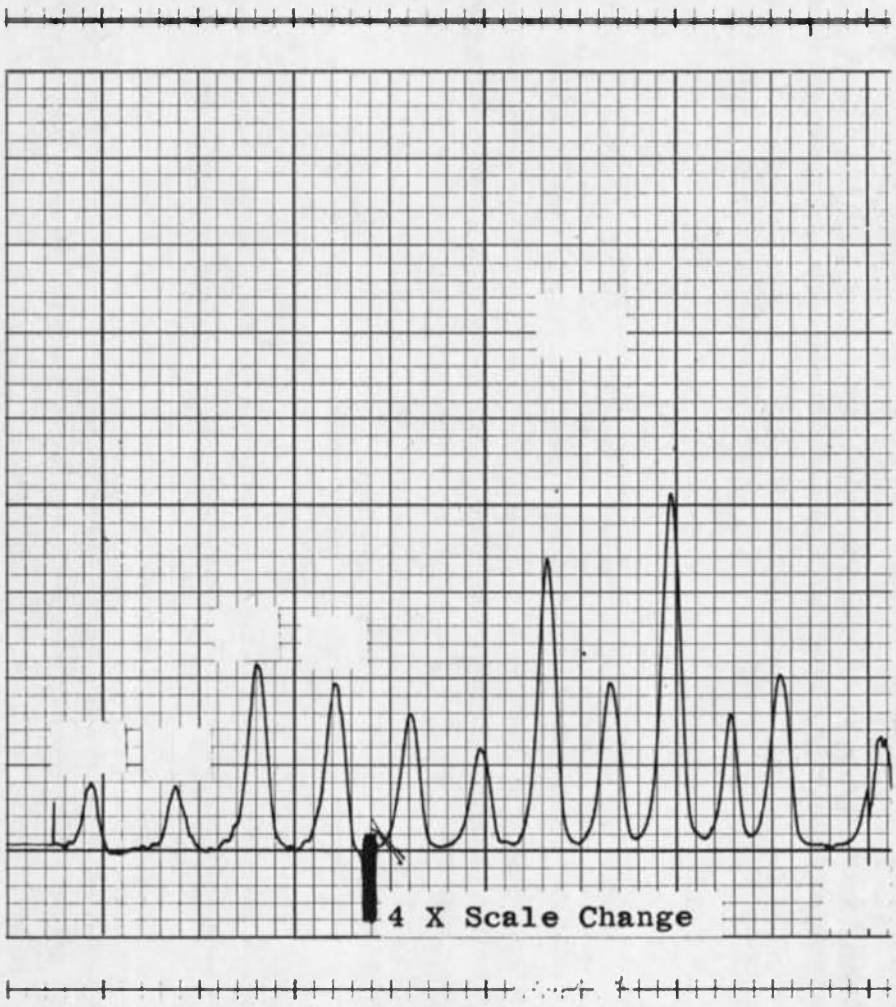

Fig. 40 Typical (0, 0) Band R-Branch Rotational Line Spectral Scan, 18 N_2 NOzzle

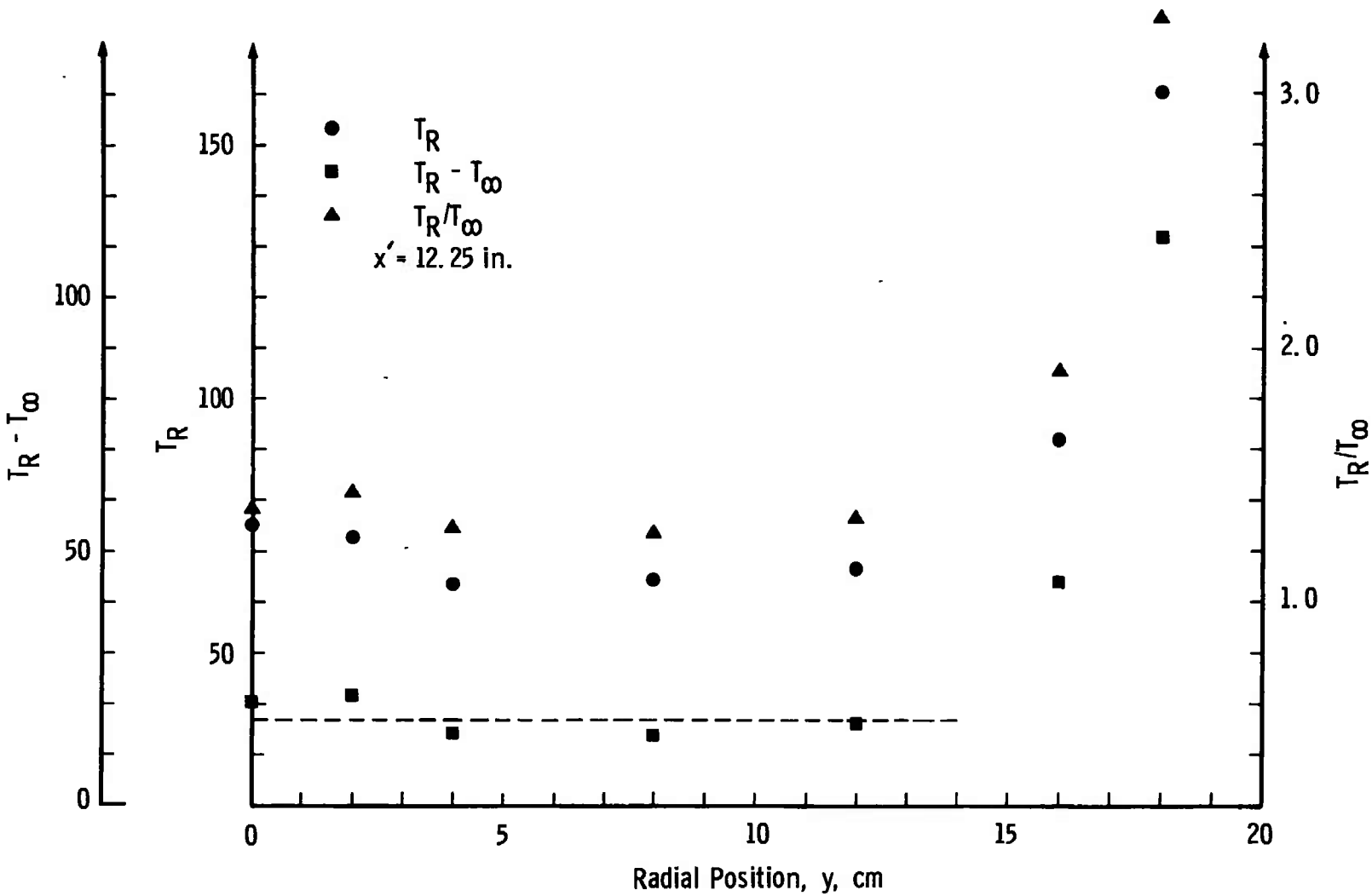

Fig. 41 Rotational Temperature Radial Profile, 18 N_2 Nozzle, x′ = 12.25 Inches

AEDC-TR-71-61

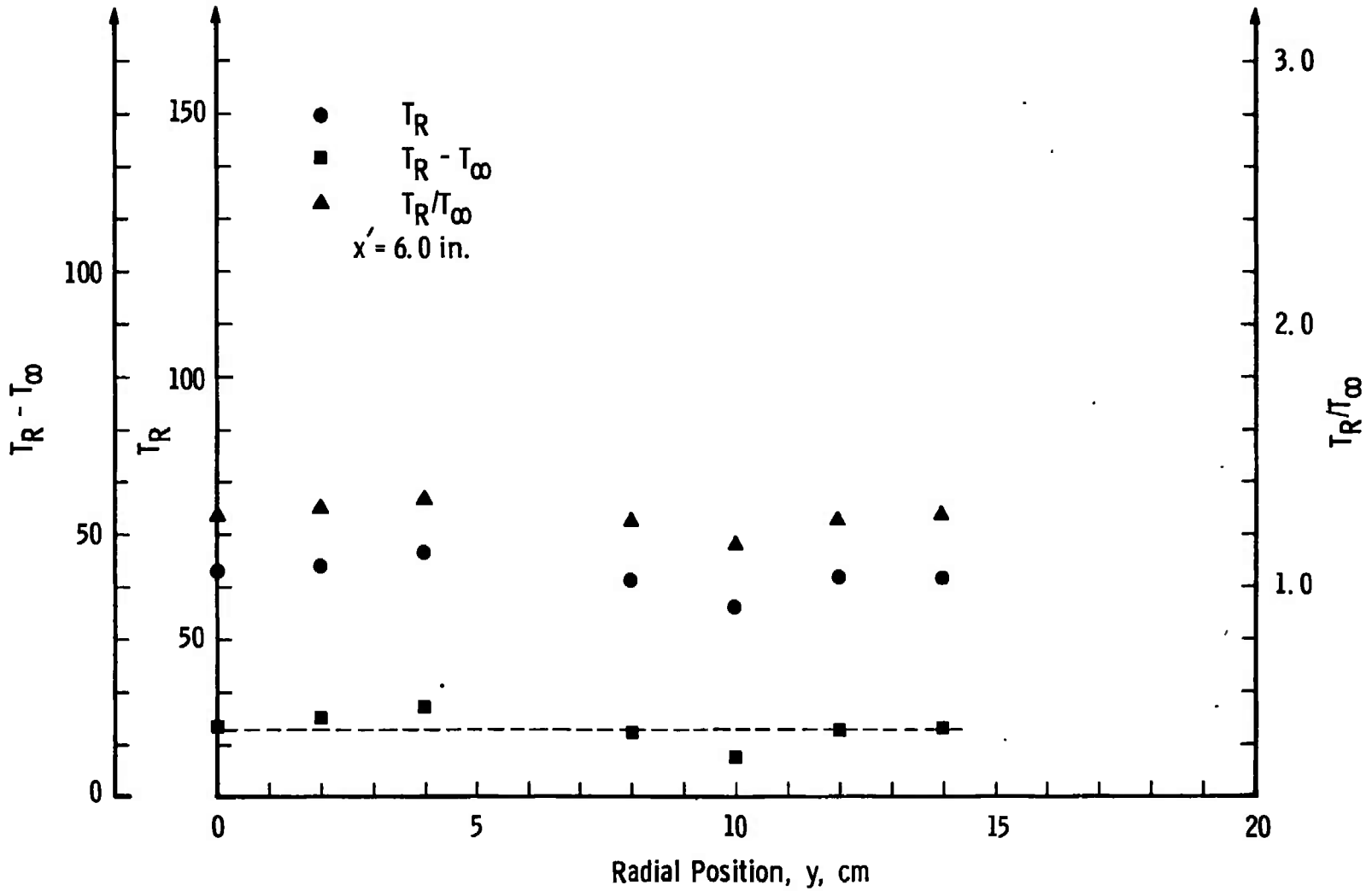

Fig. 42 Rotational Temperature Radial Profile, 18 N_2 Nozzle, x′ = 6.0 Inches

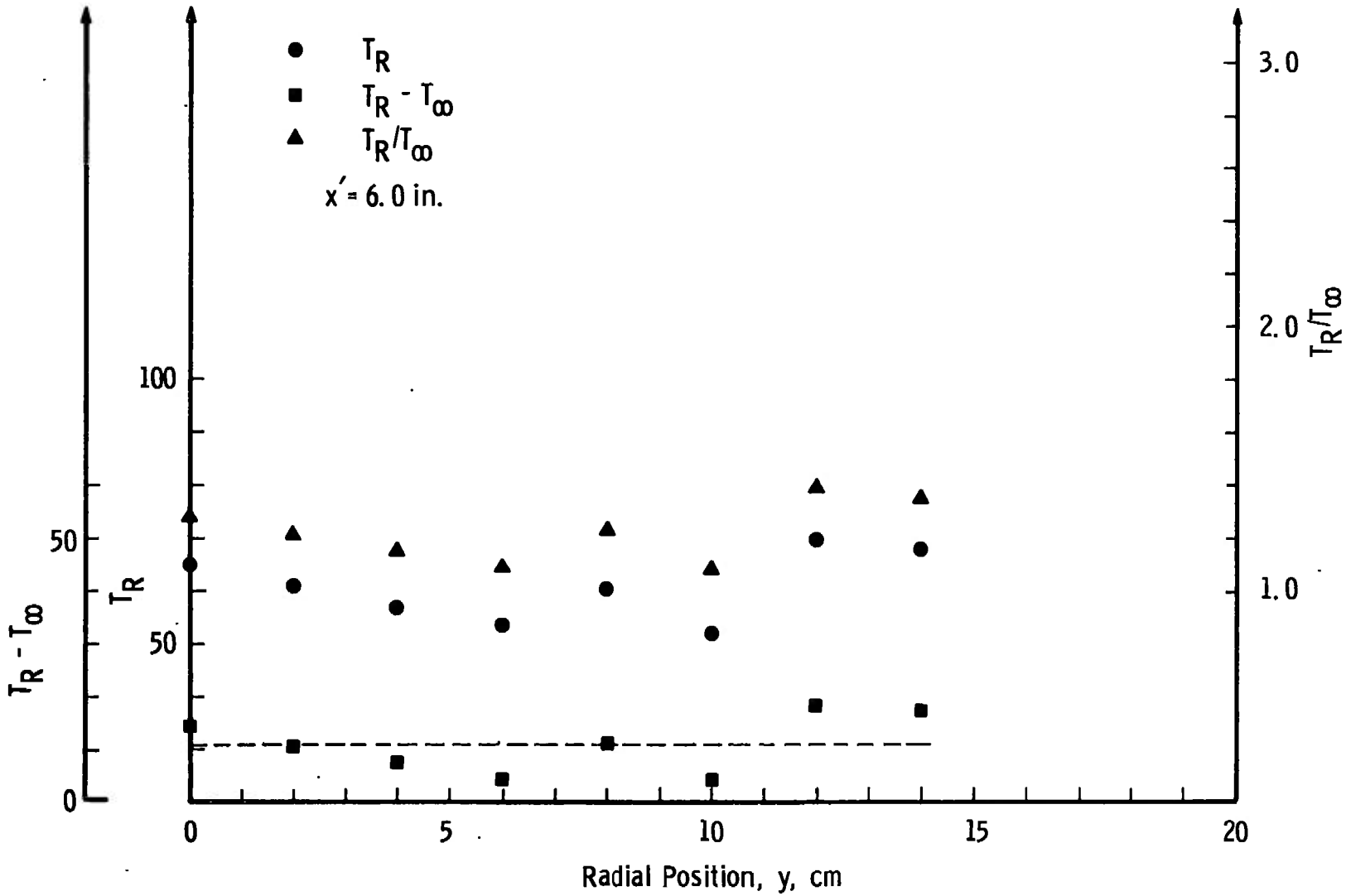

Fig. 43 Rotational Temperature Radial Profile, 18 N_2 Nozzle, x′ = 6.0 Inches

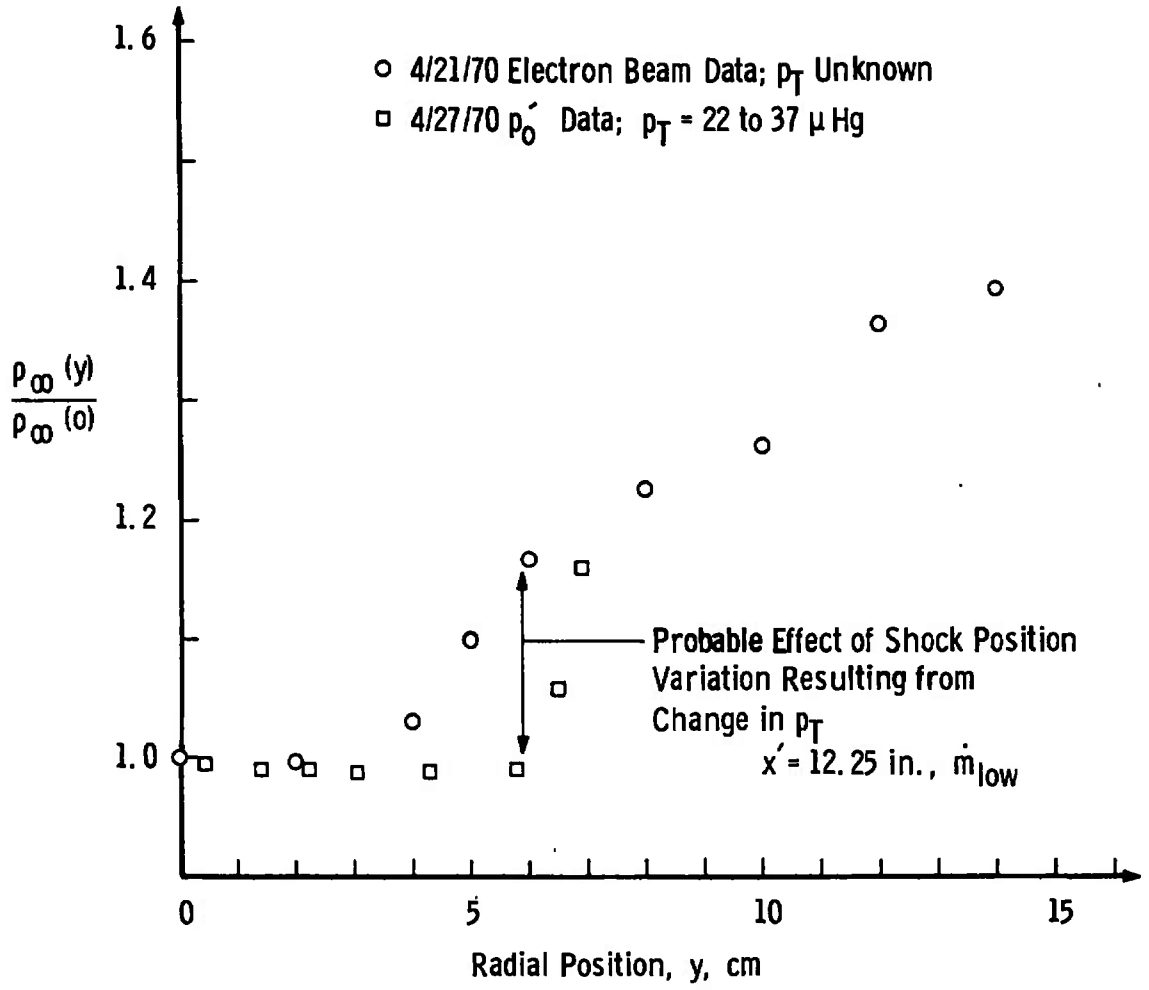

Fig. 44 Relative Nitrogen Density Radial Profile, 18 N_2 Nozzle, x' = 12.25 Inches, $\dot{m}_{low}$

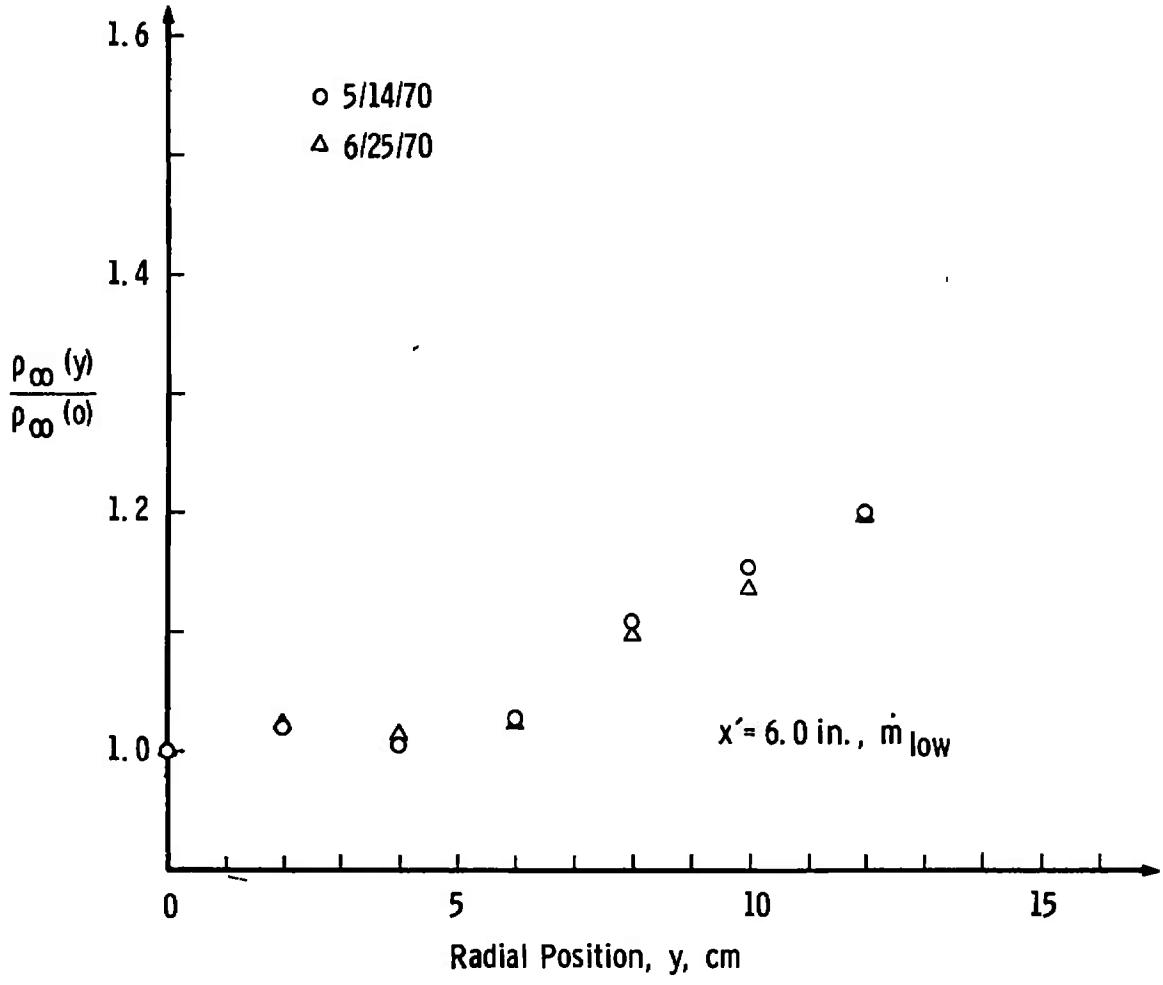

Fig. 45 Relative Nitrogen Density Radial Profile, 18 N_2 Nozzle, x' = 6.0 Inches, $\dot{m}_{low}$

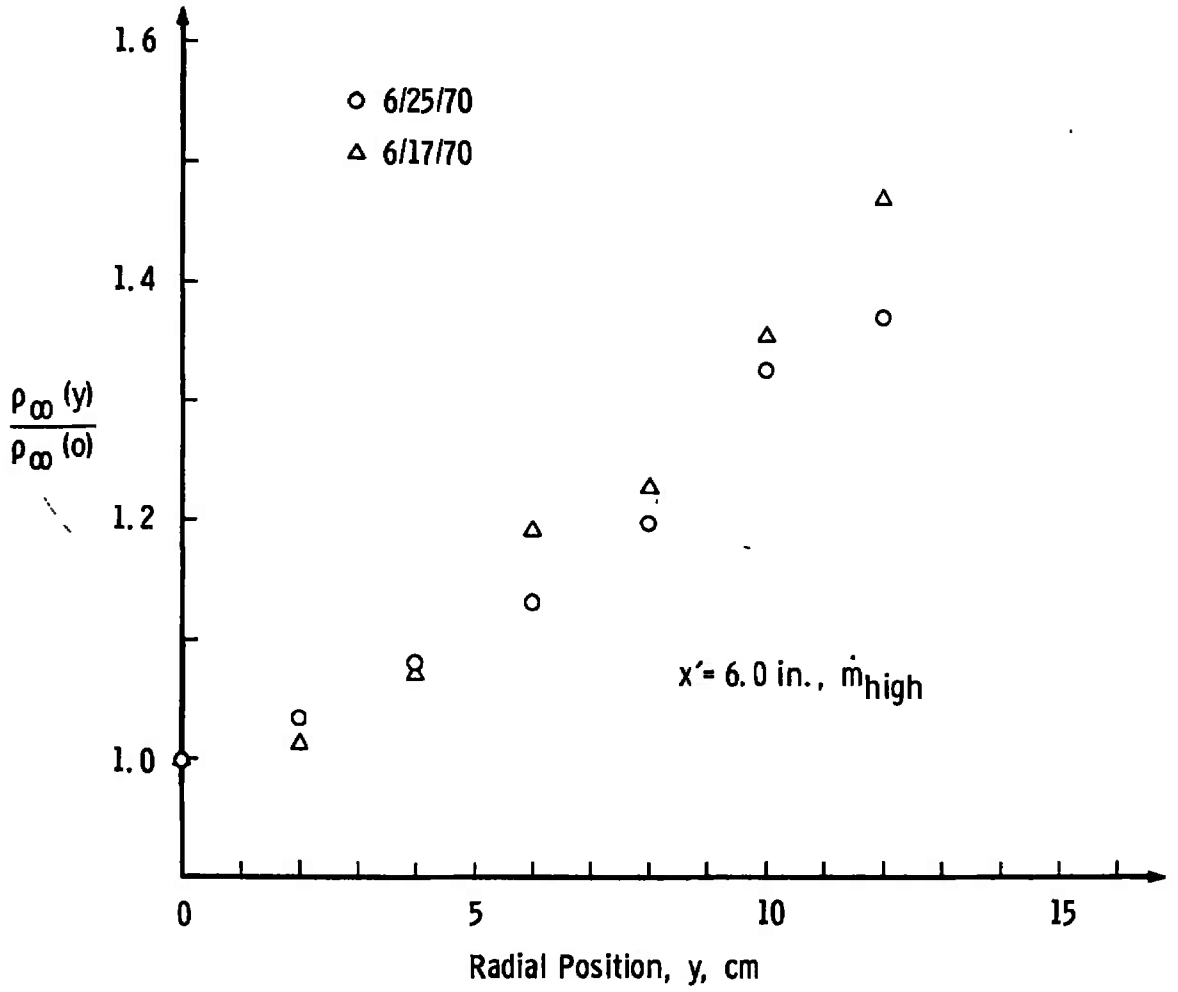

Fig. 46 Relative Nitrogen Density Radial Profile, 18 N_2 Nozzle, x' = 6.0 Inches, $\dot{m}_{high}$

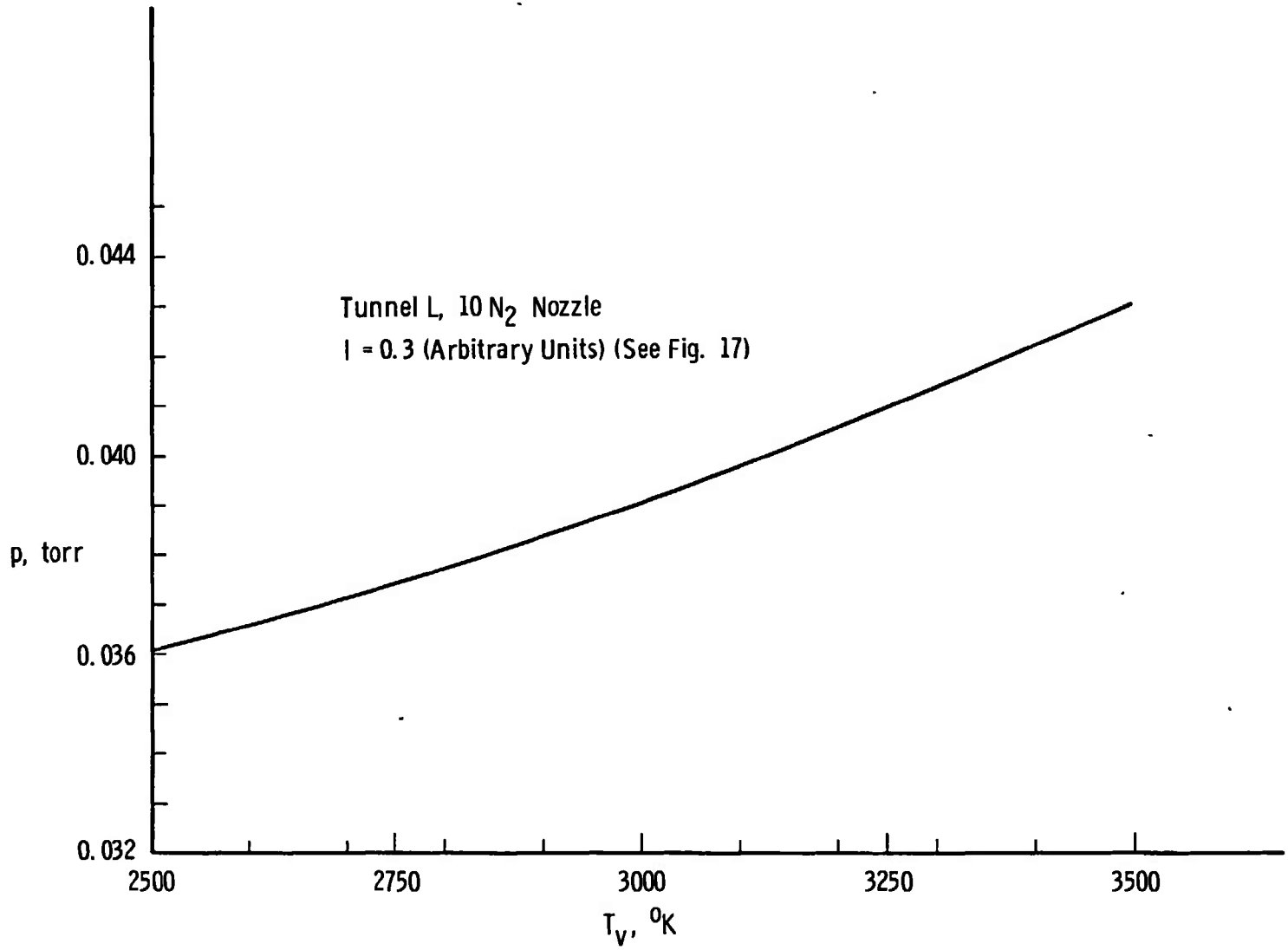

Fig. 47 T_v versus ρ for Tunnel L 10 N_2

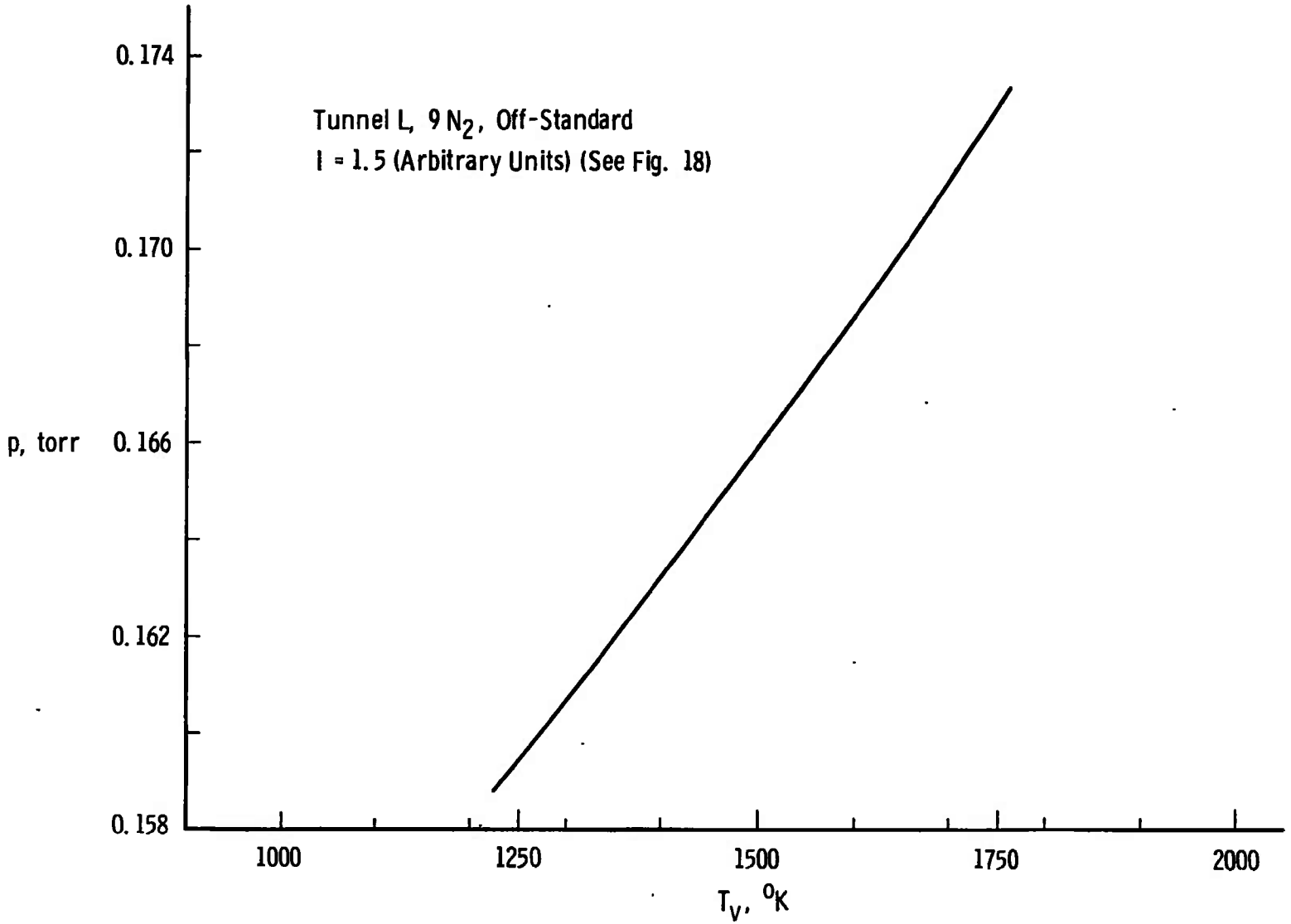

Fig. 48 T_v versus ρ for Tunnel L 9 N_2

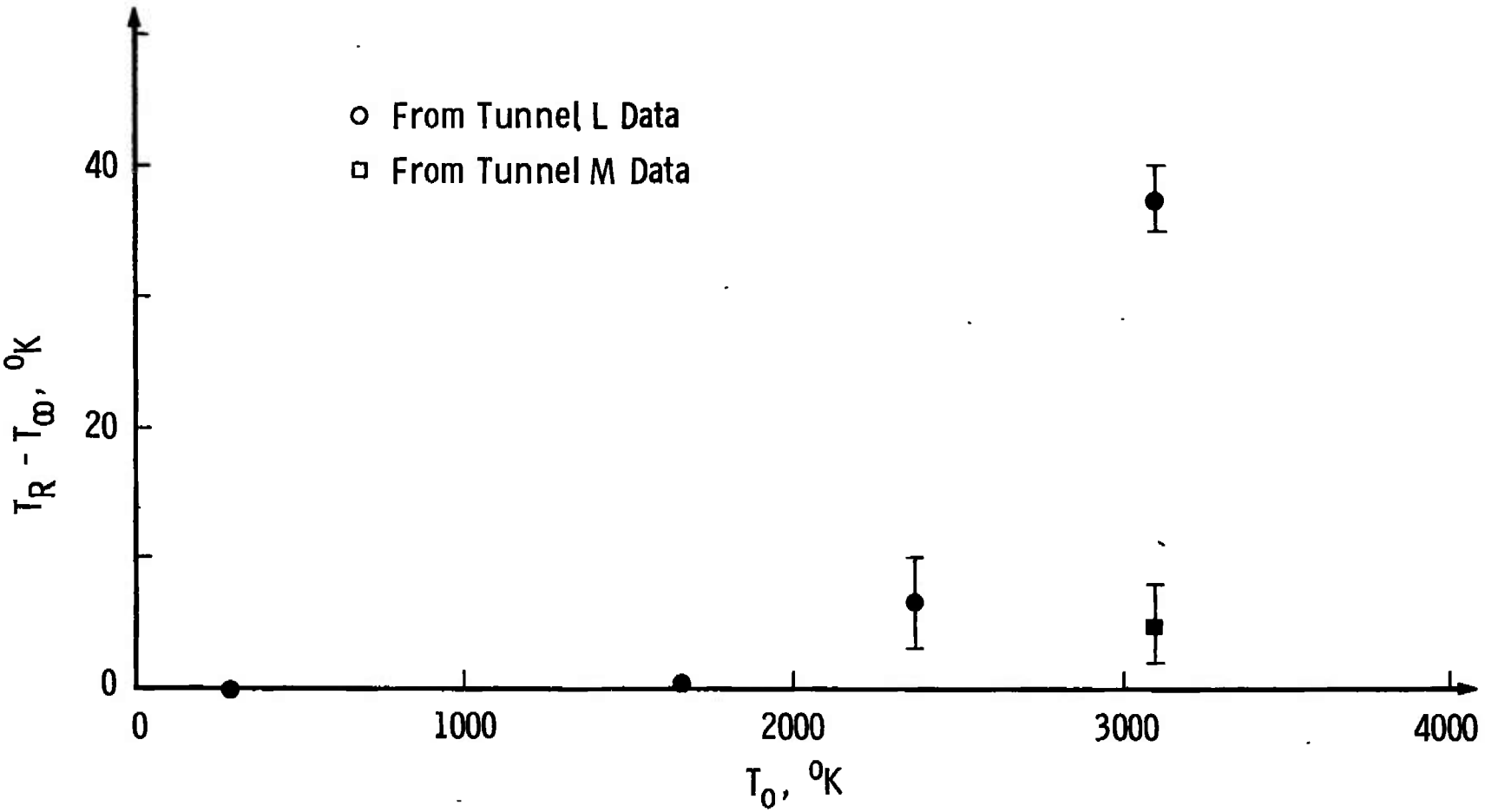

Fig. 49 Difference between Measured Rotational Temperature and Predicted Free-Stream Temperature versus T_o

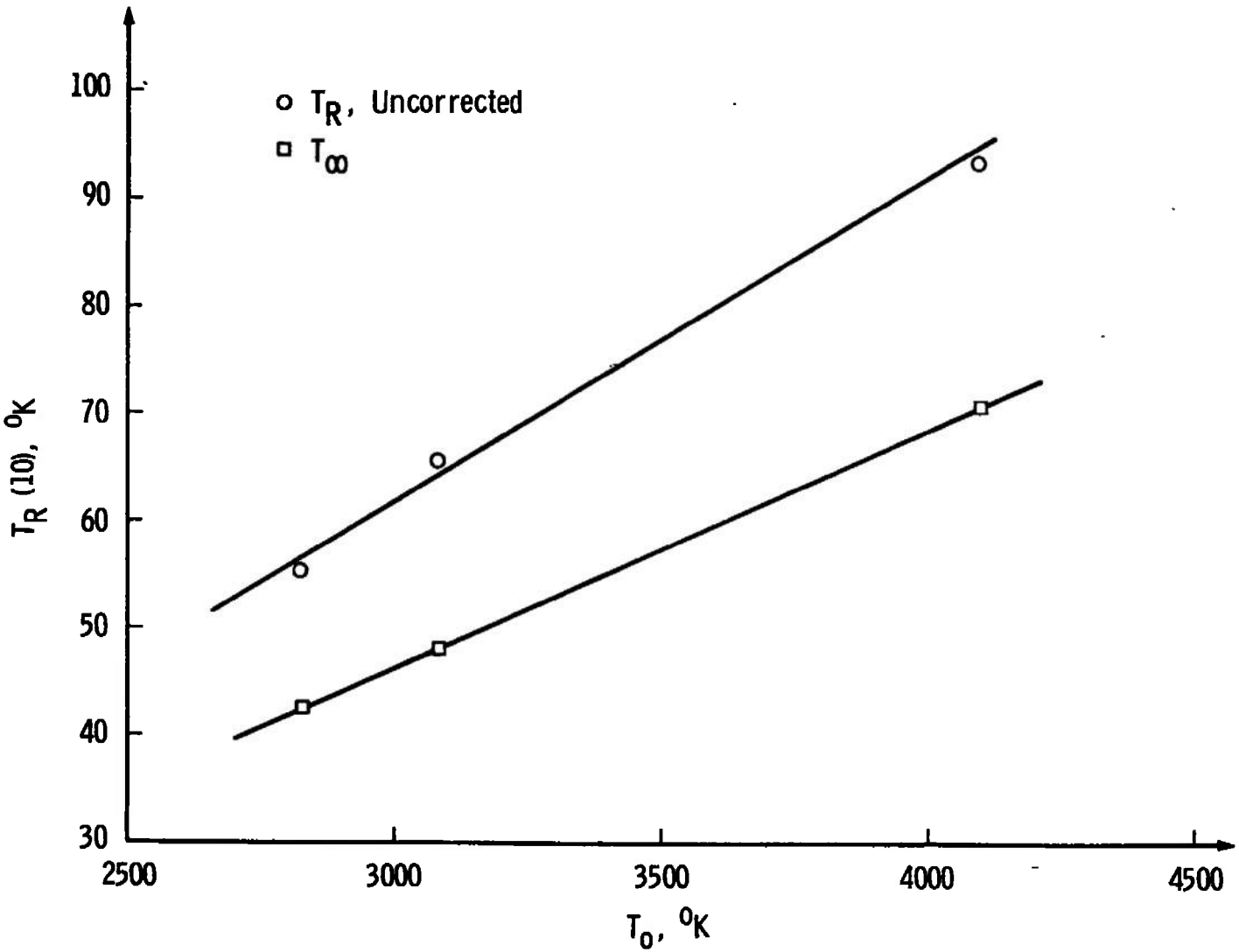

Fig. 50 Uncorrected Rotational Temperature Using 10 Lines versus T_o in Tunnel M

TABLE I
PROGRAM TROT

```
      PROGRAM TROT
      TYPE REAL NU,NUNORM,NSUMXY,NSUMXSQ
      TYPE INTEGER VU,VL
      DIMENSION I(22),G(22),      XY(22),XSQ(22),DELTAY(22),Y(22),
     *X(22),PER(22),WAVE(22),  TRR(10, 25),        SIGMATA(10, 25) ,
     *          TW(100), SIG(100), S(100), SS(100),   Y(100),
     1 YY(100), Z(100), W(100), WY(100), ID(10)
  30 READ 333, TWW, LILY
      IF (EOF,5 ) 331,332
  331 STOP
  332 LULU=
      DO 334 L=1,25
      TW(L) = TWW
  334 CONTINUE
      M = 0
    1 READ 200,RUN,VU,VL
      LULU= LULU + 1
      N= 0
      M = M + 1
      PRINT 100
      PRINT 101
      PRINT 102
      PRINT 103,RUN,VU,VL
      PRINT 104
      READ 201,KMAX
      KKK = KMAX
      DO 3 K=1,KMAX
    3 READ 202,I(K)
      TRG=200.
    4 SUMX=0.
      SUMY=0.
      SUMXY=0.
      SUMXSQ=0.
      BU=2.083-0.020*(VU+.5)
      BL=1.932-0.020*(VL+.5)
      DO 5 K=1,KMAX
      NU=2.997925E+10*(25461.5 + 2419.84*(VU+.5)-23.19*((VU+.5)**2)
     *-2207.19*(VL+.5) +16.14*((VL+.5)**2) + K*(K+1)*BU-K*(K-1)*BL)
        NUNORM=NU/(2.997925E+10*25566.0)
      WAVE(K)=2.997925E+10/NU*1.0E+08
      G(K)=(K*EXPF(5.7258*K/TRG)+(K+1)*EXPF(-5.7258*(K+1)/TRG))/(2.*K+1)
      Y(K)=LOGF(I(K)/((NUNORM**4)*G(K)*K))
      X(K)=1.*K*(K+1)
      XY(K)=X(K)*Y(K)
      XSQ(K)=X(K)*X(K)
      SUMX=SUMX+X(K)
      SUMY=SUMY+Y(K)
      SUMXY=SUMXY+XY(K)
    5 SUMXSQ=SUMXSQ+XSQ(K)
      SQSUMX=SUMX*SUMX
      PRODSUM=SUMX*SUMY
      NSUMXY=KMAX*SUMXY
      NSUMXSQ=KMAX*SUMXSQ
      SLOPE=(NSUMXY-PRODSUM)/(NSUMXSQ-SQSUMX)
      ORDCEP=(SUMXSQ*SUMY-SUMX*SUMXY)/(NSUMXSQ-SQSUMX)
      TR=-2.8629/SLOPE
```

TABLE I (Continued)

```
      SUMDELSQ=0.
      DO 6 K=1,KMAX
      YT(K)=SLOPE*X(K)+ORDCEP
      DELTAY(K)=Y(K)-YT(K)
      PER(K)=100.*DELTAY(K)/YT(K)
    6 SUMDELSQ=SUMDELSQ+DELTAY(K)*DELTAY(K)
      SIGMAY=(SUMDELSQ/(KMAX-2.))**.5
      SIGMAT=(2.8629*SIGMAY/(SLOPE*SLOPE))*((KMAX/(NSUMXSQ-SQSUMX))**.5)
      TESTTR=ABSF(TR-TRG)/TR
      IF (TESTTR.LT.1.E-04) 8,7
    7 TRG=TR
      GO TO
    8 N=N+1
      IF (N.GT.1) 11,9
    9 DO 10 K = 1, KMAX
   10 PRINT 105,K,I(K),G(K),Y(K),X(K),WAVE(K),PER(K)
      PRINT 106
      PRINT 107,PRODSUM,NSUMXY,SQSUMX,NSUMXSQ
      PRINT 108,SLOPE,ORDCEP
      PRINT 109
      PRINT 110,KMAX,TR,SIGMAT
      TRR(M,KMAX) = TR
      SIGMATA(M, KMAX) = SIGMAT
      KMAX=KMAX-1
      GO TO 4
   11 PRINT 111,KMAX,TR,SIGMAT
      TRR(M,KMAX) = TR
      SIGMATA(M, KMAX) = SIGMAT
      KMAX=KMAX-1
      IF (KMAX.GT.5) 4,400
  400 IF (LULU.LT.LILY) 1,12
   12 CONTINUE
      KM X = KKK
      PRINT 65
   65 FORMAT (1H1)
   19 CONTINUE
      IF (KMAX .GT. 5) 18, 300
   18 CONTINUE
      PRINT 7
      DO 13 J = 1, M
      PRINT 8 , TRR(J,KMAX), TW(J), SIGMATA(J, KMAX)
   13 CONTINUE
      DO 14 J = 1, M
      Y(J) = TRR(J, KM X)/TW(J)
      S(J) = SIGMATA(J, KMAX)/TW(J)
      SS(J) = S(J)**2.
      YY(J) = Y(J)/SS(J)
      Z(J) = 1./SS(J)
      W(J) = SS(1)/SS(J)
   14 WY(J) = W(J) * W(J) * SS(J)
      SUM1 = 0.0 $ SUM2 = 0.0 $ SUM3 = 0.0 $SUM4 = 0.0
      DO 15 J = 1, M
      SUM1 = SUM1 + YY(J)
      SUM2 = SUM2 + Z(J)
      SUM3 = SUM3 + WY(J)
   15 SUM4 = SUM4 + W(J)
```

TABLE I (Concluded)

```
      TRBAR = SUM17/SUM2
      SIGBAR = (SUM3/(SUM4 * SUM4)) ** 0.5
      PRINT 30, TRBAR, SIGBAR
      PRINT 210, KMAX, M
      KMAX = KMAX - 1
      PRINT 23
   23 FORMAT (1H0, ///)
      GO TO 19
  210 FORMAT (1H0, 5X, 5HUSING, I3, 18H LINES, AVERAGE OF, I2, 5H RUNS)
   30 FORMAT (1H0,15HAVERAGE TEMP = , F15.9, 5X, 16HAVERAGE SIGMA = ,
     1F11.5)
   70 FORMAT (1H , 20HMEASURED TEMPERATURE, 5X, 16HWALL TEMPERATURE,
     *10X, 18HSTANDARD DEVIATION //)
   80 FORMAT (1H , 3X, F15.9, 7X, F15.9, 13X, F10.5)
  100 FORMAT (1H1,/,47X,25HROTATIONAL BOLTZMANN PLOT)
  101 FORMAT (1H ,/,57X,5HUSING)
  102 FORMAT (1H ,/,52X,14H4UNTZ G-FACTOR)
  103 FORMAT (1H ,///,21X,12HRUN NUMBER =,1X,A8,5X,I1,1H,,I1,5H-BAND)
  104 FORMAT (1H ,///,6X,1HK,7X,4HI(K),11X,4HG(K),15X,4HY(K),15X,4HX(K),
     *13X,10HWAVELENGTH,9X,27H(DELTA Y(K))/YT(K), PERCENT)
  105 FORMAT (1H ,4X,I2,6X,I5,8X,E11.4,8X,E11.4,8X,E11.4,8X,E11.4,
     *12X,E11.4)
  106 FORMAT (1H ,///,5X,13HSUM(X)*SUM(Y),6X,9HN*SUM(XY),8X,
     *13HSUM(X)*SUM(X),6X,10HN*SUM(X*X))
  107 FORMAT (1H ,5X,E11.4,6X,E11.4,7X,E11.4,7X,E11.4)
  108 FORMAT (1H ,///,21X,7HSLOPE =,1X,E11.4,10X,11HINTERCEPT =,1X,E11.4)
  109 FORMAT (1H ,///)
  110 FORMAT (1H ,15X,I2,6H-LINES,5X,24HROTATIONAL TEMPERATURE =,
     *E11.4,5X,26HSTANDARD DEVIATION OF TR =,E11.4)
  111 FORMAT (1H ,15X,I2,6H-LINES,5X,24H                    =,
     *E11.4,5X,26H                              =,E11.4)
  200 FORMAT (A8,1X,I1,1X,I1)
  201 FORMAT (I2)
  202 FORMAT (I5)
  333 FORMAT (F10.3, I2)
      END TROT
```

TABLE II
VIBRATIONAL BAND STRENGTHS FOR EMISSION

v' \ v_2''	0	1	2	3	4
0	0.6348	0.2706	0.0784	0.0192	0.0042
1	0.2580	0.2179	0.2983	0.1472	0.0505
2	0.0319	0.3452	0.0501	0.2372	0.1836

TABLE III
FRANCK-CONDON FACTORS FOR EMISSION

v' \ v_2''	0	1	2	3	4
0	0.6570	0.2546	0.0686	0.0157	0.0329
1	0.2982	0.2316	0.2838	0.1299	0.0418
2	0.0482	0.4065	0.0561	0.2284	0.1635

TABLE IV
FRANCK-CONDON FACTORS FOR EXCITATION

v' \ v_1''	0	1	2
0	0.8794	0.1064	0.0127
1	0.1183	0.6876	0.1606
2	0.0022	0.2012	0.5587

TABLE V
SUMMARY OF TUNNEL M VIBRATIONAL BAND INTENSITY DATA

Band Pair	Raw Intensity Ratio	Corrected Intensity Ratio	T_V, °K
(0, 1)/(1, 2)	2.27	2.16	3140
(0, 2)/(1, 3)	1.25	1.22	3280
(0, 3)/(1, 4)	0.84	0.87	3221
(1, 3)/(2, 4)	1.77	1.91	3222

TABLE VI
SUMMARY OF TUNNEL L AND TUNNEL M ELECTRON BEAM DATA

Nozzle Flow Field	$T_{\infty calc.}$, °K	$T_{R_{meas.}}$, °K	$T_{R_{meas.\ Q.\ fit}}$, °K	$T_{V_{meas.}}$, °K	T_o, °K	$\rho_{\infty meas.}$, gm/cm^3	$\rho_{\infty calc.}$, gm/cm^3
4 N_2 Nozzle Standard Conditions	67	60 to 67 10 Lines 64 to 68 15 Lines	66.4	---	298	5.61×10^{-7}	4.8×10^{-7}
4 N_2 Nozzle Off-Standard Conditions	66	60 to 67 10 Lines 64 to 68 15 Lines	66.1	---	298	6.56×10^{-7}	5.6×10^{-7}
9 N_2 Nozzle Standard Conditions	135	140 to 145 10 Lines 138 to 143 15 Lines	141.7	2363	2365	---	2.02×10^{-7}
9 N_2 Nozzle Off-Standard Conditions	93	98 10 Lines 92 to 97 15 lines	93.4	1678	1662	2.64×10^{-7}	2.32×10^{-7}
10 N_2 Nozzle Standard Conditions	145	175 to 180 6 to 15 Lines	180.5	3458	3100	6.49×10^{-8}	6.16×10^{-8}
10 N_2 Nozzle Cold Flow	---	---	30	---	298	---	---
18 N_2 Nozzle x = 12.25 in.	51.2	59.4	59.1	3216	2800 to 3200 2825 For T_V Measured	---	5.45×10^{-8} to 6.25×10^{-8}
18 N_2 Nozzle x 6.0 in.	49.1 to 49.6	51.6 to 53.3	51.2 to 54.3	---	2800 to 3200	---	5.45×10^{-8} to 6.25×10^{-8}

TABLE VII
TUNNEL L 10 N_2 FLOW CONDITIONS FOR FOUR CASES†

Parameter	Units	Case I	Case II	Case III	Case IV
T^*	°K	2656	3121	2845	2448
p^*	psia	9.756	9.770	9.761	9.749
$T_o)_{real}$	°K	3050. (H_o known)	3573	3265	2813
M_∞	---	10.10	10.10	9.71	10.10
T_∞	°K	149	175 known	175 known	137
p_∞	μ Hg	21.1	21.1	26.8	21.0
ρ_∞	lbm/ft^3	3.968×10^{-6}	3.379×10^{-6}	4.1×10^{-6} known	4.1×10^{-6} known
U_∞	ft/sec	8248	8939	8594	7909
Re_∞	per inch	392	317	389	437
λ'_∞	in.	0.0389	0.0479	0.0377	0.0347
q_∞	psf	4.195	4.196	4.924	4.170
p'_o	μ Hg	2780 known	2780 known	3337	2780 known
d*	in.	0.148 known	0.154	0.151	0.145
$\rho_\infty U_\infty$	lbm/ft^2-sec	0.03273 known	0.03020	0.0369	0.03393
$\dot{m}$	lbm/hr	7.76 known	7.76 known	7.76 known	7.76 known
p_o	psia	18 known	18 known	18 known	18 known

Case I: Standard Measurements Used
Case II: Electron Beam Results (T_∞) and p'_o, $\dot{m}$, and p_o
Case III: Electron Beam Results and p_o and $\dot{m}$
Case IV: Electron Beam Results (ρ_∞) and p'_o, $\dot{m}$, and p_o

† All four calculations assume the flow is in equilibrium in the stilling chamber and becomes frozen at the sonic point which is assumed to be d*.

TABLE VIII
PROGRAM TROTQUAD

```
      PROGRAM TROTQUAD
      TYPE INTEGER  VU, VL, CODE
      TYPE DOUBLE  XL, Y, C, VARY, VC
      DIMENSION  PH(10), I(22), K(22), CODE(6), WN(22), G(22), XL(22,6),
     *  C(6), VC(6,6), X(22), Y(22)
    1 READ 2000, (PH(N),N=1,10)
      READ 2001, RUN, LINES, VU, VL
      DO 3 N=1,LINES
      READ 2002, I(N), K(N)
      IF (K(N).EQ.0) 2,3
    2 K(N)= N
    3 CONTINUE
      CALL WAVE  (WN, K, VU, VL, LINES)
    4 READ 2003, (CODE(N),N=1,6)
      IF (EOF,5) 5,6
    5 STOP
    6 IF (CODE(1).EQ.0) 1,7
    7 TRG= 200.0
    8 DO 9 N=1,LINES
      G(N)= ( K(N) * EXPF(5.725R * K(N) / TRG )  +
     *  ( K(N)+1 ) * EXPF( -5.725R * (K(N)+1) / TRG ) ) / ( 2*K(N)+1 )
      Y(N)= LOGF( I(N) / ( G(N)*K(N)*WN(N)**4 ) )
    9 X(N)= K(N) * (K(N)+1)
      CALL SETUP  (XL, MATRIX, X, LINES, CODE)
      CALL REGRESS  (C, VARY, VC, XL, Y, MATRIX, LINES)
      TR= -2.8629 / C(2)
      TESTTR= ABSF( (TR-TRG)/TR )
      IF (TESTTR.GT.1.0E-04) 10,11
   10 TRG= TR
      GO TO 8
   11 PRINT 1000, (PH(N),N=1,10)
      PRINT 1001, RUN, VU, VL
      PRINT 1002
      JMAX= MATRIX - 1
      DO 14 N=1,LINES
      YCAL= C(1)
      DO 13 J=1,JMAX
      IF (CODE(J+1).NE.0) 12,13
   12 YCAL= YCAL + C(J+1)*X(N)**J
   13 CONTINUE
      PER= 100.0  *  ( (Y(N)-YCAL)/Y(N) )
   14 PRINT 1003, K(N), I(N), X(N), Y(N), YCAL, PER
      PRINT 1004, (CODE(N),N=1,6)
      PRINT 1005, VARY
      PRINT 1006
      PRINT 1007, (C(N),N=1,MATRIX)
      PRINT 1008
      PRINT 1007, (VC(N,N),N=1,MATRIX)
      SDTR= 2.8629 * VC(2,2) / ( C(2)*C(2) )
      PRINT 1009, TR, SDTR
      GO TO 4
 1000 FORMAT (1H1, 10X, 10A8)
 1001 FORMAT (1H0, 20X, 6HRUN = , A8, 5X, I1, 1H,, I1, 5H-BAND)
 1002 FORMAT (1H0, 8X, 1HK, 4X, 1HI, 7X, 1HX, 9X, 1HY, 11X, 4HYCAL,
     *  7X, 6HYERROR)
 1003 FORMAT (1H , 7X, I2, 2X, I5, 2X, F6.1, 2X, E11.4, 2X, E11.4,
     *  2X, E9.2)
 1004 FORMAT (1H0, 10X, 6I2)
 1005 FORMAT (1H0, 10X, 25HSTANDARD DEVIATION IN Y =, E11.4)
 1006 FORMAT (1H0, 10X, 20HCOEFFICIENTS IN YCAL)
 1007 FORMAT (1H , 10X, 5(1X,E11.4))
 1008 FORMAT (1H0, 10X, 35HSTANDARD DEVIATIONS IN COEFFICIENTS)
 1009 FORMAT (1H0, 10X, 4HTR =, F11.4, 5X, 26HSTANDARD DEVIATION IN TR =
     *  , E11.4)
 2000 FORMAT ( 10A8 )
 2001 FORMAT (A8, 1X, I2, 1X, I1, 1X, I1)
 2002 FORMAT (I5, 1X, I2)
 2003 FORMAT ( 6I2 )
      END TROT
```

TABLE VIII (Continued)

```
      SUBROUTINE WAVE  (WN, K, VU, VL, LINES)
      DIMENSION  WN(22), K(22), CVU(10), CVL(4), CRU(7), CRL(5)
      TYPE INTEGER  VU, VL
      CVU(1)= 2.40991692E 03   $ CVU(2)=-4.44654495E 00
      CVU(3)=-1.22059335E 01   $ CVU(4)= 3.30935594E 00
      CVU(5)=-5.12501236E-01   $ CVU(6)= 4.41509795E-02
      CVU(7)=-2.20993070E-03   $ CVU(8)= 6.44444393E-05
      CVU(9)=-1.01930442E-06   $ CVU(10)= 6.77466456E-09
      CVL(1)= 2.20724710E 03   $ CVL(2)=-1.62009323E 01
      CVL(3)=-2.47417489E-02   $ CVL(4)=-9.90410591E-04
      CRU(1)= 2.08851196E 00   $ CRU(2)=-3.04846249E-02
      CRU(3)= 3.70926335E-03   $ CRU(4)=-8.88446139E-04
      CRU(5)= 6.17351017E-05   $ CRU(6)=-1.79358650E-06
      CRU(7)= 1.89381730E-08
      CRL(1)= 1.93192653E 00   $ CRL(2)=-2.09167196E-02
      CRL(3)= 3.27251558E-04   $ CRL(4)=-2.56908851E-05
      CRL(5)= 4.47731140E-07
      GU= 25461.50
      XU= 1.0*VU + 0.5
      XT= 1.0
      DO 1 N=1,10
      XT= XT * XU
    1 GU= GU  +  CVU(N) * XT
      GL= 0.0
      XL= 1.0*VL + 0.5
      XT= 1.0
      DO 2 N=1,4
      XT= XT * XL
    2 GL= GL  +  CVL(N) * XT
      BVU= CRU(1)
      XT= 1.0
      DO 3 N=2,7
      XT= XT * XU
    3 BVU= BVU  +  CRU(N) * XT
      BVL= CRL(1)
      XT= 1.0
      DO 4 N=2,5
      XT= XT * XL
    4 BVL= BVL  +  CRL(N) * XT
      DO 5 N=1,LINES
    5 WN(N)= GU + BVU*K(N)*(K(N)+1)  -  GL - BVL*K(N)*(K(N)-1)
      WNORM= WN(1)
      DO 6 N=1,LINES
    6 WN(N)= WN(N) / WNORM
      RETURN
      END WAVE
```

TABLE VIII (Continued)

```
      SUBROUTINE SETUP  (XL, MATRIX, X, LINES, CODE)
      TYPE INTEGER  CODE, TEMCODE
      TYPE DOUBLE  XL
      DIMENSION  XL(22,6), X(22), CODE(6), TEMCODE(6)
      DO 1 I=1,22
      DO 1 J=1,6
    1 XL(I,J)= 0.0
      MATRIX= 0
      DO 3 N=1,6
      IF (CODE(N).EQ.1) 2,3
    2 MATRIX= MATRIX + 1
    3 CONTINUE
      DO 8 I=1,LINES
      DO 4 N=1,6
    4 TEMCODE(N)= CODE(N)
      DO 8 J=1,MATRIX
      DO 7 N=1,6
      IF (TEMCODE(N).EQ.1) 5,7
    5 XT= 1.0
      KMAX= N-1
      DO 6 K=1,KMAX
    6 XT= XT * X(I)
      TEMCODE(N)= 0
      GO TO 8
    7 CONTINUE
    8 XL(I,J)= XT
      RETURN
      END SETUP
      SUBROUTINE REGRESS  (C, VARY, VC, XL, Y, MATRIX, LINES)
      TYPE DOUBLE  XL, Y, A, Z, C, VARY, VC
      DIMENSION  XL(22,6), Y(22), A(6,6), Z(6), C(6), VC(6,6)
      DO 2 I=1,MATRIX
      DO 2 J=I,MATRIX
      A(I,J)= 0.0
      DO 1 K=1,LINES
    1 A(I,J)= A(I,J)  +  XL(K,I) * XL(K,J)
    2 A(J,I)= A(I,J)
      DO 3 I=1,MATRIX
      Z(I)= 0.0
      DO 3 J=1,LINES
    3 Z(I)= Z(I)  +  XL(J,I) * Y(J)
      CALL MATINVRT  (A, MATRIX)
      DO 4 I=1,MATRIX
      C(I)= 0.0
      DO 4 J=1,MATRIX
    4 C(I)= C(I)  +  A(I,J) * Z(J)
      VARY= 0.0
      DO 5 I=1,LINES
    5 VARY= VARY  +  Y(I) * Y(I)
      DO 6 I=1,MATRIX
    6 VARY= VARY  -  C(I) * Z(I)
      VARY= ABSF( VARY/(LINES-MATRIX) )
      DO 8 I=1,MATRIX
      DO 7 J=1,MATRIX
    7 VC(I,J)= A(I,J) * VARY
    8 VC(I,I)= ( ABSF( VC(I,I) ) )**0.5
      RETURN
      END REGRESS
```

TABLE VIII (Concluded)

```
      SUBROUTINE MATINVRT  (A, NN)
      TYPE DOUBLE  A, AMAX, PIVOT, F
      DIMENSION  A(6,6), LOCATE(6,3)
      DO 1 N=1,NN
    1 LOCATE(N,3)= 0
      DO 14 N=1,NN
      AMAX= 0.0
      DO 6 I=1,NN
      IF ( LOCATE(I,3).EQ.0 ) 2,6
    2 DO 5 J=1,NN
      IF ( LOCATE(J,3).EQ.0 ) 3,5
    3 IF ( ABSF(A(I,J)).GT.AMAX ) 4,5
    4 AMAX= ABSF(A(I,J))
      IROW= I
      JCOL= J
    5 CONTINUE
    6 CONTINUE
      IF ( AMAX.GT.1.0E-15 ) 7,18
    7 LOCATE(N,1)= IROW
      LOCATE(N,2)= JCOL
      LOCATE(JCOL,3)= 1
      IF ( IROW.NE.JCOL ) 8,10
    8 DO 9 J=1,NN
      SWAP= A(IROW,J)
      A(IROW,J)= A(JCOL,J)
    9 A(JCOL,J)= SWAP
   10 PIVOT= A(JCOL,JCOL)
      A(JCOL,JCOL)= 1.0
      DO 11 J=1,NN
   11 A(JCOL,J)= A(JCOL,J) / PIVOT
      DO 14 I=1,NN
      IF ( I.NE.JCOL ) 12,14
   12 F= A(I,JCOL)
      A(I,JCOL)= 0.0
      DO 13 J=1,NN
   13 A(I,J)= A(I,J) - F*A(JCOL,J)
   14 CONTINUE
      DO 17 N=1,NN
      L= NN-N+1
      IF ( LOCATE(L,1).NE.LOCATE(L,2) ) 15,17
   15 IROW= LOCATE(L,1)
      JCOL= LOCATE(L,2)
      DO 16 K=1,NN
      SWAP= A(K,IROW)
      A(K,IROW)= A(K,JCOL)
      A(K,JCOL)= SWAP
   16 CONTINUE
   17 CONTINUE
      RETURN
   18 PRINT 1000
      RETURN
 1000 FORMAT (1H , 10X, 15HSINGULAR MATRIX)
      END MATINVRT
```

TABLE IX
PROGRAM TRADV

```
      PROGRAM TRADV
      DIMENSION TR(100), TW(100), SIG(100), S(100), SS(100), Y(100),
     1 YY(100), Z(100), W(100), WY(100), ID(10)
      PRINT 40
      READ 60, ID
      PRINT 90, ID
    3 READ 10,XLINES
      IF(EOF,50) 50,51
   50 STOP
   51 CONTINUE
      READ 10,IA1
      READ 20, (TR(I), TW(I), SIG(I), I=1,IA1)
      PRINT 70
      PRINT 80, (TR(I), TW(I), SIG(I), I=1,IA1)
   10 FORMAT (I3)
   20 FORMAT (2F15.9, F10.5)
   30 FORMAT (1H0,15HAVERAGE TEMP = , F15.9, 5X, 16HAVERAGE SIGMA = ,
     1F10.5)
   40 FORMAT (1H1)
   60 FORMAT (10A8)
   70 FORMAT (1H , 20HMEASURED TEMPERATURE, 5X, 16HWALL TEMPERATURE,
     *10X, 18HSTANDARD DEVIATION //)
   80 FORMAT (1H , 3X, F15.9, 7X, F15.9, 13X, F10.5)
   90 FORMAT (25X, 10A8)
      DO 1 J=1,IA1
      Y(J) = TR(J)/TW(J)
      S(J) = SIG(J)/TW(J)
      SS(J) = S(J)**2.
      YY(J) = Y(J)/SS(J)
      Z(J) = 1./SS(J)
      W(J) = SS(1)/SS(J)
    1 WY(J) = W(J) * W(J) * SS(J)
      SUM1 = 0.0
      SUM2 = 0.0
      SUM3 = 0.0
      SUM4 = 0.0
      DO 2 K=1,IA1
      SUM1 = SUM1 + YY(K)
      SUM2 = SUM2 + Z(K)
      SUM3 = SUM3 + WY(K)
    2 SUM4 = SUM4 + W(K)
      TRBAR = SUM1/SUM2
      SIGBAR = (SUM3/(SUM4 * SUM4)) ** 0.5
      PRINT 30, TRBAR, SIGBAR
      PRINT 10, XLINES
      PRINT 10, IA1
      GO TO 3
      END
```

APPENDIX III
ROTATIONAL TEMPERATURE CALCULATIONS USING A LEAST-SQUARES QUADRATIC FITTING PROCEDURE

Ashkenas (Ref. 8) and Williams (Ref. 7) have observed that as the number of spectral lines used to determine T_R is reduced the deduced T_R agrees increasingly better with the true gas temperature. For instance, using a typical rotational spectral scan obtained in nitrogen at a pressure of 0.005 torr at liquid nitrogen temperature (78°K), a linear fit through 13 rotational lines yields a T_R = 88.2°K with σ = 1.2°K, whereas a similar fit through only the first eight rotational lines yields T_R = 82.7°K and σ = 1.5°K. An inspection of the Boltzmann plot of the intensity values shows this variation of T_R with the number of spectral lines to be the result of curvature in the dependence of y on x, where y and x are as defined in Eqs. (5) and (6). For this case it now appears that y is at least a quadratic function of x instead of the linear relationship as predicted by the Muntz model, and this dependence can be written as

$$y = a_o + a_1 x + a_2 x^2 \qquad \text{(III-1)}$$

If one assumes that the causative agent for this nonlinearity does not affect the linear term in x, one sees that a_1, and thus T_R, is given by the first derivative of y with respect to x, the slope of y, evaluated at x equal to zero, or K = 0, where it is assumed that $a_1 = hcB_o/kT_R$ as before. It is emphasized that no a priori justification can be given for such an assumption. An iterative, least-squares quadratic fit of the spectral data to Eq. (III-1) was performed using Program TROTQUAD presented as Table VIII.

A least-squares quadratic fit through the 13 points of the preceding example yields T_R = 77.6°K and σ = 2.3°K, which is in excellent agreement with the true gas temperature.

For a given spectral scan a rotational temperature and standard deviation are obtained from Program TROTQUAD, and for a number of spectral scans at the same condition a weighted average rotational temperature and standard deviation are calculated using Program TRADV shown in Table IX. This program uses Eqs. (7) through (10) which were explained previously.

Applying this procedure to the laboratory data of Ref. 8, good agreement between average rotational temperature and test chamber wall

temperature is found provided that the nitrogen number density-electron beam current product, $N_T i_B$ (ma/cm^3) is greater than approximately 10^{15} ma/cm^3. Since all the free-stream conditions of Tunnels L and M which were investigated had number densities such that the product $N_T i_B$, where i_B is the measured electron beam current used for the measurement, was greater than 10^{15} ma/cm^3 and less than 10^{17} ma/cm^3, it was considered worthwhile to analyze the tunnel data using the empirical quadratic fitting method, and the results are shown in Table VI where it is seen that excellent agreement is obtained between the quadratic fitting results and the theoretically predicted values except for the 10 N_2 nozzle. For the 10 N_2 nozzle condition a total of 54 rotational scans were analyzed and averaged. An average rotational temperature of 180.5°K was determined, still approximately 35°K above the predicted value.

Using both laboratory and tunnel data the coefficient a_2 (Eq. (III-1)) is plotted in Fig. III-1 as a function of temperature, and it is seen that a_2 is a strong function of temperature and can be inferred to be only weakly dependent on N_2 density over this temperature range, assuming $N_T i_B \geq 10^{15}$ ma/cm^3.

It can, therefore, be concluded that for nitrogen over the temperature, density, and beam current ranges investigated, the quadratic form of y as a function of x is a more accurate representation than the linear for all cases except the 10 N_2 flow, and, additionally, this functional relationship yields values of a_1, the functional form of which is hcB_o/hT_R, which are independent of N_2 density. However, caution must be exercised for applications to any data lying outside the investigated regions and for which the gaseous composition is other than pure N_2.

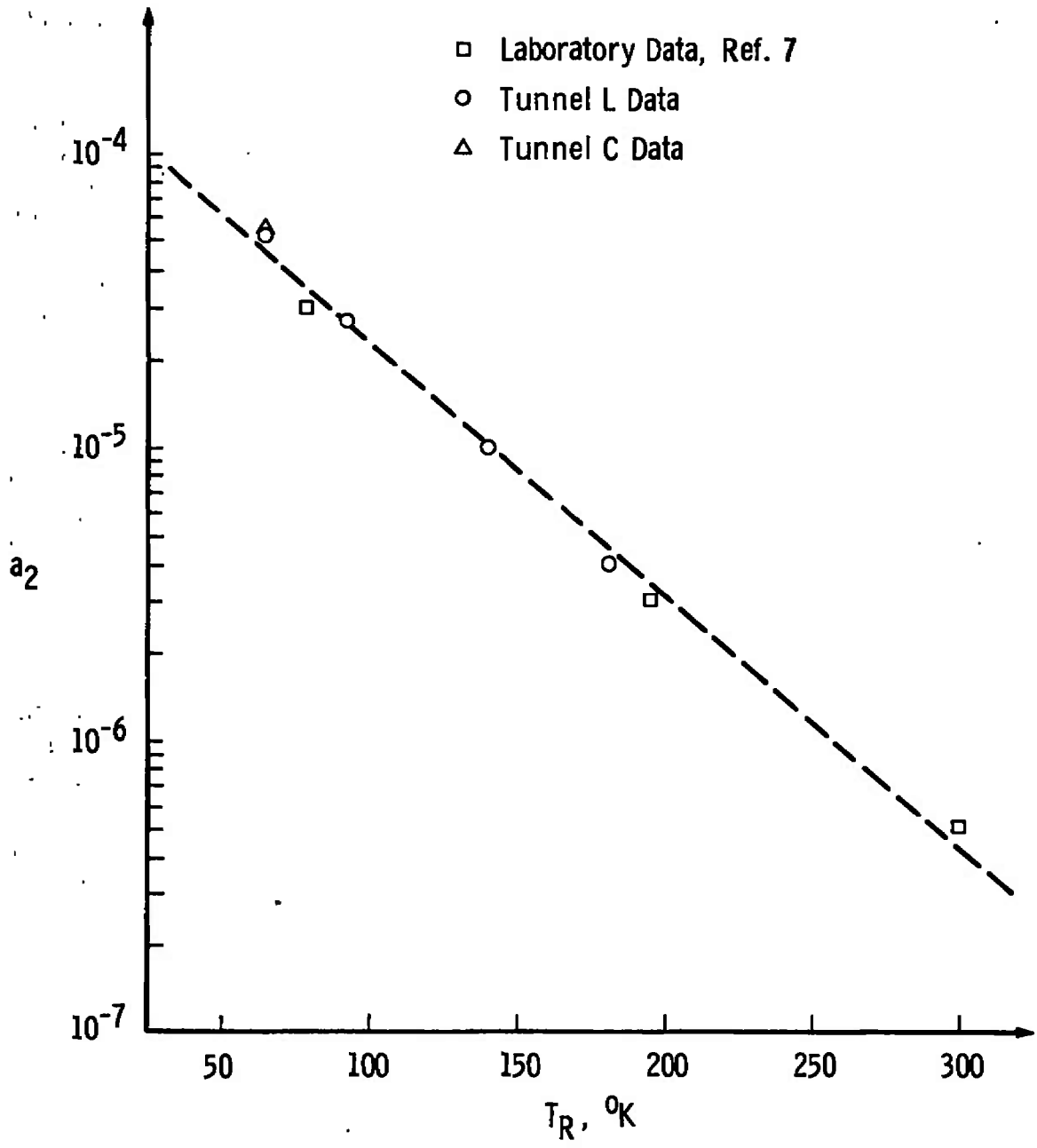
Laboratory Data, Ref. 7
Tunnel L Data
Tunnel C Data
10^{-4}
10^{-5}
10^{-6}
10^{-7}
a_2
50
100
150
200
250
300
T_R, °K

Fig. III-1

UNCLASSIFIED

Security Classification

DOCUMENT CONTROL DATA - R & D

(Security classification of title, body of abstract and indexing annotation must be entered when the overall report is classified)

1 ORIGINATING ACTIVITY (Corporate author)	2a. REPORT SECURITY CLASSIFICATION
Arnold Engineering Development Center ARO, Inc., Operating Contractor Arnold Air Force Station, Tennessee 37389	UNCLASSIFIED
	2b. GROUP N/A

3 REPORT TITLE

ELECTRON BEAM PROBE FOR A LOW DENSITY HYPERSONIC WIND TUNNEL

4. DESCRIPTIVE NOTES (Type of report and inclusive dates)

Final Report - December 1, 1968 to June 30, 1970

5 AUTHOR(S) (First name, middle initial, last name)

W. D. Williams, J. O. Hornkohl, and J. W. L. Lewis, ARO, Inc.

6 REPORT DATE	7a. TOTAL NO OF PAGES	7b. NO. OF REFS
July 1971	106	15

8a. CONTRACT OR GRANT NO	9a. ORIGINATOR'S REPORT NUMBER(S)
F40600-72-C-0003 b. PROJECT NO	AEDC-TR-71-61
c. Program Element 64719F d.	9b. OTHER REPORT NO(S) (Any other numbers that may be assigned this report) ARO-VKF-TR-70-313

10 DISTRIBUTION STATEMENT

Approved for public release; distribution unlimited.

11. SUPPLEMENTARY NOTES	12 SPONSORING MILITARY ACTIVITY
Available in DDC	Arnold Engineering Development Center, Air Force Systems Command, Arnold Air Force Station, Tenn.37389

13 ABSTRACT

The purpose of the experiments and calculations reported herein was to use the electron beam technique for rotational and vibrational temperature and density measurements in the free stream of low density, hypersonic flows of nitrogen. Beam energy was varied from 10 to 20 kev with currents of 1.0 to 4.0 ma. Free-stream rotational temperatures were in the range from 30 to 200°K, and vibrational temperatures varied from 300 to 3100°K, and free-stream densities were on the order of 10^{-8} to 10^{-7} gm/cm^3. The variation in the flow parameters was obtained through the use of four different nozzles; each was operated at two different conditions. The electron beam was injected through the flow, and the resulting spontaneous emission of light was spectroscopically analyzed. Light intensity measurements were made photoelectrically, and signal amplification and averaging were accomplished with a lock-in amplifier.

DD FORM 1 NOV 65 1473

UNCLASSIFIED

Security Classification

14. KEY WORDS	LINK A		LINK B		LINK C	
	ROLE	WT	ROLE	WT	ROLE	WT
electron beams						
plasma diagnostics						
electron density (concentration)						
electron energy						
hypersonic wind tunnels						

AFSC
Arnold AFS Tenn